



Chemical Synthesis of Peptides and Their Biological Applications as Mitochondria-Targeting Chemotherapeutics

A thesis submitted in accordance with the conditions governing candidates for the degree of

Philosophiae Doctor at Cardiff University

Davide Cardella

Under the supervision of

Dr. Louis Luk

Dr. Yu-Hsuan Tsai

Prof. Arwyn Tomos Jones

17.06.2022

Cardiff School of Chemistry

Cardiff University

Ai miei genitori

e ai miei fratelli

ACKNOWLEDGEMENTS

First and foremost, I thank my supervisors Dr. Louis Luk, Dr. Yu-Hsuan Tsai and Prof. Arwyn Jones, for allowing me to pursue my PhD studies in Cardiff University and for the training offered.

I am immensely grateful to have shared my working environment with very inspiring people such as Davide, Emily, Gareth, Heather, Helen, Luke, Mia, Muge, Patrick, Simon and Victoria, from whom I had the luck to learn a lot. Special mention goes to Alex L., Alex N., Antonio, Gilda, Giulia, Irene, Jon, Luca, Martin, Margherita, Mauro, Nicolò, Riccardo, Tom and Victor for the constant support at work and in everyday life, for all the fun and for making me a better person.

Thanks to all the other friends I made in Cardiff, in particular to Alberto, Dave, Kim, Mike and Sylvester for the great time spent together.

I thank all my other friends as Agostino, Antimo, Antonio, Arcangelo, Dario, Francesco R., Francesco S., Gennaro, Giovanni C., Giovanni D., Michele, Nando, Pippo, Roberta, Salvatore, and many others who made me feel loved and supported despite the physical distance during my doctoral studies.

A special thank goes to my beloved Agnes, whom I cannot thank enough. The days together have been the happiest of my years as a PhD student.

Conclusively, I am most grateful to my family for the unconditional love and support provided throughout my whole time in Cardiff.

SUMMARY

Synthetic peptides are of great use in many areas of chemical biology and drug discovery. This PhD thesis details new synthetic approaches for the preparation of peptide molecules, along with applications of synthetic peptide derivatives as chemotherapeutics agents.

In this work, I give an overview on peptides and their applications in the chemical biology research area (Chapter 1).

Then, I start illustrating my experimental work by exploring a new method for the total synthesis of peptides and proteins on solid phase (Chapter 2).

Next, I investigate the effect of conjugating a mitochondria- and a cancer cell-targeting motif to reported proapoptotic peptides, to enhance their potency and selectivity profiles (Chapter 3 and 4).

Finally, I give a brief review and outline the future directions towards addressing the limitations of the presented projects (Chapter 5).

Table of contents

1. CHAPTER 1 - INTRODUCTION - Overview of peptides in chemical biology	1
1.1 Chemical properties	1
1.2 Biological properties of Peptides	4
1.3 Peptide Synthesis	5
1.3.1 Chemical Synthesis of Peptides	5
1.3.1.1 Solid-Phase Peptide Synthesis	6
1.3.1.2 Native Chemical Ligation	17
1.3.2 Peptide biosynthesis	20
1.3.3 Recombinant gene expression vs total chemical synthesis	21
1.3.4 Solid-Phase Chemical Ligation	22
1.3.4.1 Overview of the <i>N</i> -to- <i>C</i> method	23
1.3.4.2 Overview of the <i>C</i> -to- <i>N</i> method	27
1.3.4.3 Limitations of SPCL	29
1.4 Biological applications of chemically synthesised peptides	30
1.4.1 Anticancer applications of chemically synthesised antimicrobial peptides	30
1.5 Research aim and objectives	33
CHAPTER 2 - Solid-Phase Chemical Synthesis of Peptides and Proteins via Nickel-Assisted Cleavage	35
2.1 Abstract	35
2.2 Introduction	35
2.2.1 Nickel (II) as trigger of sequence-specific protein cleavage	35
2.2.2 Potential of SNAC in solid-phase synthesis of peptides and proteins ..	36
2.3 Aim and Objectives	37
2.4 Results and Discussion	37
2.4.1 SNAC of a model peptide from a solid support	37

2.4.2 SPCL of a model polypeptide.....	39
2.4.3 Proof of Concept: SPCL of a ubiquitin derivative using SNAC	40
2.5 Conclusion and Perspectives.....	43
2.6 Experimental Section	44
2.6.1 SPPS procedure for peptide 1.....	45
2.6.2 SPPS procedure for polypeptide H-LFKAGCFKAGCFKGAG-NH ₂ for calibration curve	46
2.6.3 SPPS procedure for peptide 4a.....	47
2.6.4 SPPS procedure for peptide 4b	49
2.6.5 SPPS procedure for peptide 4c.....	50
2.6.6 SPPS procedure for peptide 5a.....	51
2.6.7 SPPS procedure for peptide 5b	54
2.6.8 SPPS procedure for peptide 5c.....	55
2.6.9 Supplementary figures	57
CHAPTER 3 - Synthesis and biological evaluation of trimethine cyanine dye-mitochondriolytic peptide conjugates.....	60
3.1 Abstract	60
3.2 Introduction.....	60
3.3 Aim and Objectives.....	62
3.4 Results and discussion.....	63
3.4.1 Synthesis of the cyanine dye scaffold.....	63
3.4.2 Solid-Phase Peptide Synthesis of mitochondriolytic peptides	65
3.4.3 Cell viability assay	68
3.4.4 Subcellular localisation and cellular uptake of folate conjugates.....	70
3.5 Conclusions and perspectives	71
3.6 Experimental section.....	72
3.6.1 Organic chemical synthesis of the cyanine scaffold.....	72

3.6.1.1 Synthesis of 1,2,3,3-tetramethyl-3H-indolium iodide	72
3.6.1.2 Synthesis of 1-(5-carboxypentyl)-2,3,3-trimethyl-3H-indolium bromide.....	73
3.6.1.3 Synthesis of Cy3-COOH (1-(5-carboxypentyl)-3,3-dimethyl-2- [(1E,3Z)-3-(1,3,3-trimethyl-1,3-dihydro-2H-indol-2-ylidene)-1-propen-1-yl]- 3H-indolium iodide)	74
3.6.2 Solid Phase Peptide Synthesis	75
3.6.2.1 Determination of Rink Amide resin loading	76
3.6.2.2 General procedure for the synthesis of KLA, kla and kXa	77
3.6.2.3 General procedure for the synthesis of cyanine dye-labelled peptides	80
3.6.3 Biological evaluation	82
3.6.3.1 Cell culture	82
3.6.3.2 Cell viability assay	83
3.6.3.3 Confocal microscopy.....	87
3.6.3.4 Flow cytometry	88
3.6.3.5 Statistical analysis	88
CHAPTER 4 - Enhancing the selectivity of Cy3-labelled mitochondriolytic peptides towards cancer cells	90
4.1 Abstract	90
4.2 Introduction	90
4.3 Aim and Objectives	91
4.4 Results and discussion	93
4.4.1 Solid-Phase Peptide Synthesis of folate-conjugated peptides.....	93
4.4.2 Cell viability assay	96
4.4.3 Subcellular localisation and cellular uptake of folate conjugates.....	97
4.5 Conclusions and perspectives	99
4.6 Experimental procedure	100

4.6.1 Solid Phase Peptide Synthesis	100
4.6.1.1 Synthesis of Cy3-K(FA)-KLA and Cy3-K(FA)-kla	101
4.6.1.2 Synthesis of Cy3-K(FA)-kXa	103
4.6.1.3 General procedure for the synthesis of Ac-K(FA)-KLA, Ac-K(FA)-kla and Ac-K(FA)-kXa	106
4.6.2 Biological Evaluation.....	109
4.6.2.1 Cell Culture.....	109
4.6.2.2 Cell viability assay	109
4.6.2.3 Confocal Microscopy.....	112
4.6.2.4 Flow cytometry	112
4.6.2.5 Statistical analysis	112
CHAPTER 5 - Conclusions and future work	115
CHAPTER 6 - References	118
CHAPTER 7 – Appendix	126
7.1 SPPS MW cycle and method descriptions of CEM Liberty Blue™ Automated Microwave Peptide Synthesizer	126
7.2 Publications in peer-reviewed journals.....	137

List of figures

Figure 1.1. General structure of α -amino acids in their (left) L and (right) D configurations, represented as zwitterion species. R refers to the side-chain moiety.....	2
Figure 1.2. Geometrical description of peptide bonds; bonds defining the dihedral angle ω are highlighted in orange	2
Figure 1.3. a) Bond lengths of O=C-N. b) Resonance structures of a peptide bond.	3
Figure 1.4. Cartoon (above) and ribbon-stick (below) representations of a) an α -helix and b) an antiparallel β -sheet. Hydrogen bonds are shown as dotted lines. Blue, black and white colours are used to denote nitrogen, oxygen and carbon atoms in the ribbon-stick representation.....	4
Figure 1.5. Total chemical synthesis by stepwise assembling of peptidyl segments (a) in solution or (b) solid phase	6
Figure 1.6. Molecular structure of some of the most employed a) α -amine protecting groups, b) coupling reagents and (c) additives.....	9
Figure 1.7. a) Molecular structure of a polystyrene polymer, cross-linked with divinylbenzene. b) before the swelling procedure, the polymeric support is shrunk, and the reaction sites cannot be reached. c) after being swollen, the resin can accommodate the SPPS reactants in its matrix.....	12
Figure 1.8. CEM Liberty Blue™ Automated Microwave Peptide Synthesiser.	15
Figure 1.9. Common laboratory setup for manual SPPS.....	16
Figure 1.10. Section of a mammalian mitochondrion. The main components are highlighted: outer mitochondrial membrane, intermembrane space, inner mitochondrial membrane, matrix and the electron transport chain, a protein complex anchored to the inner membrane responsible for the mitochondrial membrane potential. Cytochrome c is a main player in the apoptosis triggering. Figure template provided by smart.servier.com.....	31
Figure 1.11. Folate receptor α -mediated endocytosis of a folate-conjugated drug. Figure template provided by smart.servier.com.....	32

Figure 2.1. The proposed mechanism of SNAC and release of the target protein (in red).....	36
Figure 2.2. A) Model peptide-hydrazide 1 conversion into peptide-azide, its attachment to a solid support by NCL, to yield peptide 2 . SNAC afforded desired cleaved peptide 3 . a) 0.2 M K_2HPO_4 , 6 M GdmCl, $NaNO_2$ (10 eq), pH 3, -20 °C, 15 min; b) MPAA (40 eq), TCEP 50 mM, pH 6.9, 16 h; c) $NiCl_2 \cdot 6H_2O$ (1 eq), 0.1 M CHES, 0.1 M NaCl, 0.1 M acetone oxyma, pH 8.6, 24 h, rt or 40 °C; d) TFA/ H_2O /TIS/DODT 92.5:2.5:2.5:2.5, 1 h. B) Release of model peptide 3 from the resin via SNAC, quantified by integrating the peak area corresponding to peptide 3 from the 214 nm LC chromatogram trace of the cleavage at different time points. C) LC chromatograms recorded at 280 nm of TFA cleavages of model peptide before and after SNAC. * oxidised product.	38
Figure 2.3. Sequence of model polypeptide 4 (left). Model polypeptide 4 was split in three peptide blocks 4a-c (right), which are then assembled via SPCL.	39
Figure 2.4. Sequence of ubiquitin derivative 5 (left). Ubiquitin derivative 5 was split in three peptide blocks 5a-c (right), which are then assembled on a solid support via SPCL.	41
Figure 2.5. LC chromatogram recorded at 214 nm (+ mass spectrum of the indicated peak) of peptide 1 . Column: <i>ACE 3 C18</i> , 2.1 x 100 mm, 3 μm particle size, 300 Å pore size; Method: flow rate = 0.5 mL · min ⁻¹ , H_2O : CH_3CN , 0.1% $HCOOH$, 95:5 for 2 min → 95:5 to 43:57 over 13 min → 5:95 for 7 min.	46
Figure 2.6. LC chromatogram recorded at 214 nm (+ mass spectrum of the indicated peak) of polypeptide H-LFKAGCFKAGCFKGAG-NH₂ . Column: <i>ACE 3 C18</i> , 2.1 x 100 mm, 3 μm particle size, 300 Å pore size; Method: flow rate = 0.5 mL · min ⁻¹ , H_2O : CH_3CN , 0.1% $HCOOH$, 95:5 for 2 min → 95:5 to 43:57 over 13 min → 5:95 for 7 min.	47
Figure 2.7. LC chromatogram recorded at 214 nm (+ mass spectrum of the indicated peak) of peptide 4a . Column: <i>ACE 3 C18</i> , 2.1 x 100 mm, 3 μm particle size, 300 Å pore size; Method: flow rate = 0.5 mL · min ⁻¹ , H_2O : CH_3CN , 0.1% $HCOOH$, 95:5 for 2 min → 95:5 to 43:57 over 13 min → 5:95 for 7 min.	49

Figure 2.8. LC chromatogram recorded at 214 nm (+ mass spectrum of the indicated peak) of peptide **4b**. Column: *ACE 3 C18*, 2.1 x 100 mm, 3 µm particle size, 300 Å pore size; Method: flow rate = 0.5 mL · min⁻¹, H₂O: CH₃CN, 0.1% HCOOH, 95:5 for 2 min → 95:5 to 43:57 over 13 min → 5:95 for 7 min. 50

Figure 2.9. LC chromatogram recorded at 214 nm (+ mass spectrum of the indicated peak) of peptide **4c**. Column: *ACE 3 C18*, 2.1 x 100 mm, 3 µm particle size, 300 Å pore size; Method: flow rate = 0.5 mL · min⁻¹, H₂O: CH₃CN, 0.1% HCOOH, 95:5 for 2 min → 95:5 to 43:57 over 13 min → 5:95 for 7 min. 51

Figure 2.10. LC chromatogram recorded at 214 nm (+ mass spectrum of the indicated peak) of peptide **5a**. Column: *ACE 3 C18*, 2.1 x 100 mm, 3 µm particle size, 300 Å pore size; Method: flow rate = 0.5 mL · min⁻¹, H₂O: CH₃CN, 0.1% HCOOH, 95:5 for 2 min → 95:5 to 55:45 over 10 min → 5:95 for 5 min. 53

Figure 2.11. LC chromatogram recorded at 214 nm (+ mass spectrum of the indicated peak) of peptide **5b**. Column: *ACE 3 C18*, 2.1 x 100 mm, 3 µm particle size, 300 Å pore size; Method: flow rate = 0.5 mL · min⁻¹, H₂O: CH₃CN, 0.1% HCOOH, 95:5 for 2 min → 95:5 to 43:57 over 13 min → 5:95 for 7 min. 55

Figure 2.12. LC chromatogram recorded at 214 nm (+ mass spectrum of the indicated peak) of peptide **5c**. Column: *ACE 3 C18*, 2.1 x 100 mm, 3 µm particle size, 300 Å pore size; Method: flow rate = 0.5 mL · min⁻¹, H₂O: CH₃CN, 0.1% HCOOH, 95:5 for 2 min → 95:5 to 55:45 over 10 min → 5:95 for 5 min. 57

Supplementary figure 2.1. LC chromatogram recorded at 280 nm of TFA cleavages of polypeptide **4** before (a) and after (b) SNAC. Percentage of cleavage is worked out by integrating the areas of the peak corresponding to the cleaved linker and to the peptide remained on the resin. Column: *ACE 3 C18*, 2.1 x 100 mm, 3 µm particle size, 300 Å pore size; Method: flow rate = 0.5 mL · min⁻¹, H₂O: CH₃CN, 0.1% HCOOH, 95:5 for 2 min → 95:5 to 43:57 over 13 min → 5:95 for 7 min. 57

Supplementary figure 2.2. Calibration curve for polypeptide H-LFKAGCFKAGCFKGAG-NH₂. The plot was obtained by plotting the absorbance obtained at the LC/MS of a stock solution of H-LFKAGCFKAGCFKGAG-NH₂. For each quantity point, LC/MS run was repeated three times. The calibration curve was obtained by fitting the data points using Origin, version 2019b, OriginLab Corporation, Northampton, MA, USA. 58

Supplementary figure 2.3. LC chromatogram recorded at 214 nm of TFA cleavages after SNAC for the synthesis of compound 5 . * denotes uncleaved intermediate 5c* , ** denotes cleaved product 5	58
Figure 3.1. Molecular structures of some of the carriers that have been conjugated to kla thus far. R7, TAT, TCTP and RGD-4C have been covalently linked via an amide bond to the <i>N</i> -terminus of kla through a diglycyl spacer (r7 , TAT , TCTP , RDG-4C) or a six-carbon chain (TPP).	61
Figure 3.2. Mechanism of apoptosis induction of Cy3 -conjugated peptides. Figure template provided by smart.servier.com.	63
Figure 3.3. Molecular structures of compounds Cy3-COOH	63
Figure 3.4. Peptide sequences synthesised and tested in this chapter. Lower-case letters denote D-configuration.....	66
Figure 3.5. TIC chromatograms of the crude of KLA synthesis a) before and b) after optimising the SPPS protocol.....	67
Figure 3.6. Confocal microscopy images of SK-OV-3 and MCF7 cells treated with Cy3-COOH , Cy3-KLA , Cy3-kla and Cy3-kXa . Cells were treated with 10 μ M of the indicated conjugate for 10 min at 37 °C, washed, stained with 50 nM MitoTracker Green and 10 μ g/ml Hoechst33258 for 10 min at 37 °C, washed and imaged at 63X. Excitation wavelengths for Hoechst 33258, MitoTracker Green and Cy3 were set as 405, 488 and 561 nm, respectively. Pearson's correlation coefficients of MitoTracker Green FM and Cy3 fluorescence for compounds Cy3-COOH , Cy3-KLA , Cy3-kla and Cy3-kXa in SK-OV-3 and MCF cells are 0.75/0.64, 0.73/0.81, 0.91/0.61, and 0.78/0.63, respectively. Scale bars denote 25 μ m.	71
Figure 3.7. TIC chromatogram (+ mass spectrum at 13.181:13.509 min) of KLA . Column: <i>Poroshell 120 EC-C18</i> , 2.1 x 100 mm, 4 μ m particle size, 120 Å pore size; Method: flow rate = 0.5 mL \cdot min ⁻¹ , H ₂ O: CH ₃ CN, 0.1% HCOOH, 95:5 for 2 min → 95:5 to 70:30 over 25 min → 5:95 for 5 min.	78
Figure 3.8. TIC chromatogram (+ mass spectrum at 9.439:9.639 min) of kla . Column: <i>Poroshell 120 EC-C18</i> , 2.1 x 100 mm, 4 μ m particle size, 120 Å pore size; Method: flow rate = 0.5 mL \cdot min ⁻¹ , H ₂ O: CH ₃ CN, 0.1% HCOOH, 95:5 for 2 min → 95:5 to 40:60 over 23 min → 5:95 for 5 min.	79

Figure 3.9. TIC chromatogram (+ mass spectrum at 12.562:12.853 min) of **kxa**. Column: *Poroshell 120 EC-C18*, 2.1 x 100 mm, 4 µm particle size, 120 Å pore size; Method: flow rate = 0.5 mL · min⁻¹, H₂O: CH₃CN, 0.1% HCOOH, 95:5 for 2 min → 95:5 to 40:60 over 23 min → 5:95 for 5 min. 79

Figure 3.10. TIC chromatogram (+ mass spectrum at 16.042:16.771 min) of **Cy3-KLA**. Column: *Poroshell 120 EC-C18*, 2.1 x 100 mm, 4 µm particle size, 120 Å pore size; Method: flow rate = 0.5 mL · min⁻¹, H₂O: CH₃CN, 0.1% HCOOH, 95:5 for 2 min → 95:5 to 40:60 over 23 min → 5:95 for 5 min..... 81

Figure 3.11. TIC chromatogram (+ mass spectrum at 16.188:16.680 min) of **Cy3-kla**. Column: *Poroshell 120 EC-C18*, 2.1 x 100 mm, 4 µm particle size, 120 Å pore size; Method: flow rate = 0.5 mL · min⁻¹, H₂O: CH₃CN, 0.1% HCOOH, 95:5 for 2 min → 95:5 to 40:60 over 23 min → 5:95 for 5 min..... 82

Figure 3.12. TIC chromatogram (+ mass spectrum at 19.056:19.256 min) of **Cy3-kXa**. Column: *ACE 3 C18*, 2.1 x 100 mm, 3 µm particle size, 100 Å pore size; Method: flow rate = 0.3 mL · min⁻¹, H₂O: CH₃CN, 0.1% HCOOH, 85:15 to 5:95 over 35 min → 5:95 for 2 min. 82

Figure 3.13. Cytotoxicity of tested compounds towards KB cell lines. Fitting curves are shown as solid black lines. Dots and error bars represent the mean and the standard deviation from a minimum of nine values resulted from three biological replicates (i.e. cells split from three different passages); each biological replicate is calculated from three technical replicates (i.e. cells split from the same passage). 84

Figure 3.14. Cytotoxicity of tested compounds towards SK-OV-3 cell lines. Fitting curves are shown as solid black lines. Data for compounds **KLA** and **kla** were not fitted. Dots and error bars represent the mean and the standard deviation from a minimum of nine values resulted from three biological replicates (i.e. cells split from three different passages); each biological replicate is calculated from three technical replicates (i.e. cells split from the same passage). 85

Figure 3.15. Cytotoxicity of tested compounds towards MCF7 cell lines. Fitting curves are shown as solid black lines. Dots and error bars represent the mean and the standard deviation from a minimum of nine values resulted from three biological replicates (i.e. cells split from three different passages); each biological

replicate is calculated from three technical replicates (i.e. cells split from the same passage).	86
Figure 3.16. Cytotoxicity of tested compounds towards HEK293 cell lines. Fitting curves are shown as solid black lines. Dots and error bars represent the mean and the standard deviation from a minimum of nine values resulted from three biological replicates (i.e. cells split from three different passages); each biological replicate is calculated from three technical replicates (i.e. cells split from the same passage).	87
Figure 4.1. Folate receptor α -mediated endocytosis of a folic acid-conjugated drug. Figure template provided by smart.servier.com.....	91
Figure 4.2. Increasing selectivity towards cancer cells via folate labelling. Figure template provided by smart.servier.com.	92
Figure 4.3. Molecular structures of the compounds synthesised and tested in this chapter.	93
Figure 4.4. TIC chromatogram of the crude of Cy3-K(FA)-KLA synthesis after coupling folic acid to the ϵ -amino group of the <i>N</i> -terminal lysine. Mass spectrum shows the same <i>m/z</i> peaks for two different chromatogram peaks, indicating the formation of two folate-labelled isomers.....	94
Figure 4.5. TIC chromatogram of the crude of synthesis for Cy3-K(FA)-kXa after coupling and deprotection of glutamic acid to the ϵ -amino group of the <i>N</i> -terminal lysine. Mass spectrum shows the desired <i>m/z</i> for the mono-labelled glutamic acid intermediate (on the left) along with the bi-labelled glutamic acid intermediate (on the right). This led to an inseparable mixture of the desired product and bi-labelled folate side product.	96
Figure 4.6. Confocal microscopy images of SK-OV-3 and MCF7 cells treated with dual-labelled conjugates. Cells were treated with 10 μ M of the indicated conjugate for 10 min at 37 $^{\circ}$ C, washed, stained with 50 nM MitoTracker Green and 10 μ g/ml Hoechst33258 for 10 min at 37 $^{\circ}$ C, washed and imaged at 63X. Excitation wavelengths for Hoechst 33258, MitoTracker Green and Cy3 were set as 405, 488 and 561 nm, respectively. Pearson's correlation coefficients of MitoTracker Green FM and Cy3 fluorescence for Cy3-K(FA)-KLA , Cy3-K(FA)-kla and Cy3-K(FA)-kXa in	

SK-OV-3 and MCF cells are 0.85/0.69, 0.43/0.82, and 0.78/0.60, respectively. Scale bars denote 25 μm 98

Figure 4.7. Flow cytometry analysis of cyanine dye- and dual-labelled conjugates uptakes by SK-OV-3 and MCF7 cells. Cells were treated with 10 μM of the indicated conjugate for 10 min at 37 $^{\circ}\text{C}$, washed, stained with 50 nM MitoTracker Green for 10 min at 37 $^{\circ}\text{C}$, washed, trypsinized and subjected to flow cytometry analysis. Cellular uptakes are shown as the ratios of Cy3 and MitoTracker fluorescence. Mean ratios \pm standard deviations are calculated from three biological replicates and plotted in arbitrary unit (A.U.) The negative control (-) refers to cells only stained with MitoTracker Green. Statistical analysis was performed by applying the extra sum-of-squares F test, performed using GraphPad Prism version 6 for Windows, GraphPad Software, La Jolla California USA, www.graphpad.com. ns = non statistically significant, * = $p < 0.05$ 99

Figure 4.8. TIC chromatogram (+ mass spectrum at 11.300:11.719 min) of **Cy3-K(FA)-KLA**. Column: *ACE 3 C18*, 2.1 x 100 mm, 3 μm particle size, 100 \AA pore size; Method: flow rate = 0.3 $\text{mL} \cdot \text{min}^{-1}$, H_2O : CH_3CN , 0.1% HCOOH , 85:15 for 2 min \rightarrow 85:15 to 40:60 over 13 min \rightarrow 5:95 for 7 min \rightarrow 5:95 to 85:15 over 0.5 min \rightarrow 85:15 for 7 min..... 102

Figure 4.9. TIC chromatogram (+ mass spectrum at 11.956:12.667 min) of **Cy3-K(FA)-kla**. Column: *ACE 3 C18*, 2.1 x 100 mm, 3 μm particle size, 100 \AA pore size; Method: flow rate = 0.3 $\text{mL} \cdot \text{min}^{-1}$, H_2O : CH_3CN , 0.1% HCOOH , 85:15 for 2 min \rightarrow 85:15 to 40:60 over 13 min \rightarrow 5:95 for 7 min \rightarrow 5:95 to 85:15 over 0.5 min \rightarrow 85:15 for 7 min..... 103

Figure 4.10. TIC chromatogram (+ mass spectrum at 11.985:12.654 min) of **Cy3-K(FA)-kXa**. Column: *ACE 3 C18*, 2.1 x 100 mm, 3 μm particle size, 100 \AA pore size; Method: flow rate = 0.3 $\text{mL} \cdot \text{min}^{-1}$, H_2O : CH_3CN , 0.1% HCOOH , 85:15 for 2 min \rightarrow 85:15 to 40:60 over 13 min \rightarrow 5:95 for 7 min \rightarrow 5:95 to 85:15 over 0.5 min \rightarrow 85:15 for 7 min..... 105

Figure 4.11. TIC chromatogram (+ mass spectrum at 13.721:13.940 min) of **Ac-K(FA)-KLA**. Column: *Poroshell 120 EC-C18*, 2.1 x 100 mm, 4 μm particle size, 120 \AA pore size; Method: flow rate = 0.5 $\text{mL} \cdot \text{min}^{-1}$, H_2O : CH_3CN , 0.1% HCOOH , 95:5 for 2 min \rightarrow 95:5 to 40:60 over 23 min \rightarrow 5:95 for 5 min..... 107

Figure 4.12. TIC chromatogram (+ mass spectrum at 8.684:9.012 min) of **Ac-K(FA)-kla**. Column: *Poroshell 120 EC-C18*, 2.1 x 100 mm, 4 μ m particle size, 120 Å pore size; Method: flow rate = 0.5 mL · min⁻¹, H₂O: CH₃CN, 0.1% HCOOH, 95:5 for 1 min → 95:5 to 45:65 over 15 min → 5:95 for 5 min.108

Figure 4.13. TIC chromatogram (+ mass spectrum at 10.097:10.735 min) of **Ac-K(FA)-kXa**. Column: *ACE 3 C18*, 2.1 x 100 mm, 3 μ m particle size, 100 Å pore size; Method: flow rate = 0.3 mL · min⁻¹, H₂O: CH₃CN, 0.1% HCOOH, 85:15 for 2 min → 85:15 to 40:60 over 13 min → 5:95 for 7 min → 5:95 to 85:15 over 0.5 min → 85:15 for 7 min.108

Figure 4.14. Cytotoxicity of tested compounds towards KB cell lines. Fitting curves are shown as solid black lines. Dots and error bars represent the mean and the standard deviation from a minimum of nine values resulted from three biological replicates (i.e. cells split from three different passages); each biological replicate is calculated from three technical replicates (i.e. cells split from the same passage).110

Figure 4.15. Cytotoxicity of tested compounds towards SK-OV-3 cell lines. Fitting curves are shown as solid black lines. Dots and error bars represent the mean and the standard deviation from a minimum of nine values resulted from three biological replicates (i.e. cells split from three different passages); each biological replicate is calculated from three technical replicates (i.e. cells split from the same passage).110

Figure 4.16. Cytotoxicity of tested compounds towards MCF7 cell lines. Fitting curves are shown as solid black lines. Data for **Ac-K(FA)-KLA** and **Ac-K(FA)-kla** were not fitted. Dots and error bars represent the mean and the standard deviation from a minimum of nine values resulted from three biological replicates (i.e. cells split from three different passages); each biological replicate is calculated from three technical replicates (i.e. cells split from the same passage).111

Figure 4.17. Cytotoxicity of tested compounds towards HEK293 cell lines. Fitting curves are shown as solid black lines. Data for **Ac-K(FA)-KLA** were not fitted. Dots and error bars represent the mean and the standard deviation from a minimum of nine values resulted from three biological replicates (i.e. cells split from three

different passages); each biological replicate is calculated from three technical replicates (i.e. cells split from the same passage). 111

List of schemes

Scheme 1.1. a) general synthetic scheme for SPPS. X = linker reactive group for the first amino acid loading, Aa = amino acid residue (with protected side chain, if needed), PG = protecting group on the α -amine. b) first report of SPPS, synthetic scheme for the tetrapeptide H-LAGA-OH. TEA: triethylamine, DCC: <i>N,N'</i> -dicyclohexylcarbodiimide, Cbz: carboxybenzyl.	8
Scheme 1.2. Proposed racemisation scheme of amino acid mediated by 2-(1H-benzotriazol-1-yl)-1,1,3,3-tetramethyluronium hexafluorophosphate (HBTU) and proposed racemisation minimisation mechanism by 1-hydroxybenzotriazole (HOBt)	10
Scheme 1.3. Preparation of thiodipeptides by employment of a) 2-Chlorotrityl hydrazine linker and b) MeDbz linker	14
Scheme 1.4. NCL reaction mechanism between the C-terminal thioester moiety of a thiodipeptide (in pink) and an <i>N</i> -terminal cysteine of a peptide (in blue) in aqueous buffer at neutral pH	18
Scheme 1.5. a) When carrying out sequential ligations by NCL, the cysteine residue must be hidden to avoid side reactions. Usually, an HPLC purification is needed for each ligation step b) In the kinetically controlled ligation approach, the reaction kinetics is dictated by the reactivity of the aminothiol group.....	19
Scheme 1.6. In the expressed protein ligation approach, the thiodipeptide involved in the NCL is obtained by thiol exchange between a peptide expressed by recombinant gene expression and an aryl or alkyl thiol.....	20
Scheme 1.7. SPCL in C-to-N direction	22
Scheme 1.8. SPCL in N-to-C direction	23
Scheme 1.9. Cleavage mechanism for the release of the peptide from Esoc linker	25
Scheme 2.1. Synthetic scheme for the preparation of model polypeptide 4 with LC/MS traces of the intermediates recorded at 280 nm of the analytical TFA cleavages. LC/MS trace recorded at 214 nm of the crude cleavage mixture was	

obtained after incubation of the resin with SNAC buffer for 24 h at 40 °C. a) 0.2 M K_2HPO_4 , 6 M GdnHCl, 0.2 M MPAA, 50 mM TCEP, pH 6.9, 16 h; b) TFA/H₂O/TIS/DODT 92.5:2.5:2.5:2.5, 1 h; c) 0.4 M MeONH₂, 25 mM TCEP, 40 °C, 16 h; d) i. NiCl₂·6H₂O (4 eq), 0.1 M CHES, 0.1 M NaCl, 0.1 M acetone oxyma, pH 8.6, 24 h, 40 °C; ii. 0.1 M TCEP, 30 min, 40 °C. 40

Scheme 2.2. Synthetic scheme for the preparation of ubiquitin derivative **5** with LC/MS traces of the intermediates recorded at 280 nm of the analytical TFA cleavages. LC/MS trace for the cleaved product **5** was obtained after incubation of the resin with SNAC buffer for 24 h at 40 °C, followed by HPLC purification. a) 0.2 M K_2HPO_4 , 6 M GdmCl, 0.2 M MPAA, 50 mM TCEP, pH 6.9, 16 h (SPCL is repeated twice); b) 0.4 M MeONH₂, 25 mM TCEP, 40 °C, 16 h; c) TFA/H₂O/TIS/DODT 92.5:2.5:2.5:2.5, 1 h; d) i. NiCl₂·6H₂O (1 eq), 0.1 M CHES, 0.1 M NaCl, 0.1 M acetone oxyma, pH 8.6, 24 h, 40 °C; ii. 0.1 M TCEP, 30 min, 40 °C. * denotes unreacted intermediate **5b***. 42

Scheme 3.1. Synthetic route for **Cy3-COOH**. *Reagents and conditions:* (a) iodomethane, MeNO₂, 60 h, rt, 92%; (b) 6-bromohexanoic acid, MeNO₂, 16 h, rt, 54%; (c) *N,N*-diphenylformamidine, pyridine, Ac₂O, 16 h, 120 °C → rt, 40%. 64

List of Tables

Table 1.1. Some of the commercially available linkers for Fmoc/SPPS	11
Table 1.2. Cleavable linkers in <i>N</i> -to- <i>C</i> SPCL	24
Table 1.3. Latent thioesters in <i>N</i> -to- <i>C</i> SPCL	25
Table 1.4. Cleavable linkers in <i>C</i> -to- <i>N</i> SPCL	27
Table 1.5. Cysteine protection strategies in <i>C</i> -to- <i>N</i> SPCL	29
Table 3.1. The EC ₅₀ values (expressed in μ M) on different cell lines of different molecules and their cyanine dye conjugates were quantified using cell viability assays. The values in brackets represent the standard error of the curve fitting using Origin, version 2019b, OriginLab Corporation, Northampton, MA, USA.	69
Table 3.2 Calculated and expected molecular weight for the synthesised compounds	78
Table 4.1. The EC ₅₀ values (expressed in μ M) on different cell lines of different molecules and their cyanine dye conjugates were quantified using cell viability assays. The values in brackets represent the standard error of the curve fitting using Origin, version 2019b, OriginLab Corporation, Northampton, MA, USA.	96
Table 4.2. Calculated and expected molecular weight for the folate conjugates synthesised in this chapter	100

List of abbreviations

¹³ C-NMR	carbon-13 nuclear magnetic resonance
¹ H-NMR	proton nuclear magnetic resonance
Abs	absorbance
Boc	tert-butyloxycarbonyl
CAPS	<i>N</i> -cyclohexyl-3-aminopropanesulfonic acid
Cbz	carboxybenzyl
CHES	<i>N</i> -cyclohexyl-2-aminoethanesulfonic acid
CuAAC	Cu ^I -catalyzed azide/alkyne cycloaddition
DCM	dichloromethane
DIC	<i>N</i> , <i>N'</i> -diisopropylcarbodiimide
DIPEA	<i>N</i> , <i>N</i> -diisopropylethylamine
DMEM	Dulbecco's modified eagle medium
DMF	<i>N</i> , <i>N</i> -dimethylformamide
DMSO	dimethylsulfoxide
DMSO-d6	deuterated dimethylsulfoxide
DNA	deoxyribonucleic acid
DODT	3,6-dioxa-1,8-octanedithiol
DTT	1,4-dithiothreitol
EC ₅₀	half maximal effective concentration
FA	folic acid (when conjugated to a peptide)
FBS	fetal bovine serum
Fmoc	fluorenylmethoxycarbonyl
GdmCl	guanidine hydrochloride
HEPES	<i>N</i> -2-hydroxyethylpiperazine- <i>N'</i> -2-ethanesulfonic acid
HPLC	high-pressure liquid chromatography
LC/MS	liquid chromatography/mass spectrometry
MBHA	4-methylbenzhydrylamine
MeDbz	<i>o</i> -amino(methyl)aniline
MeNbz	<i>N</i> -acyl- <i>N'</i> -methyl-benzimidazolinone
MPA	3-mercaptopropionic acid
MPAA	4-mercaptophenylacetic acid
mRNA	messenger ribonucleic acid
Mtt	4-methyltrityl
NCL	native chemical ligation

NMP	<i>N</i> -methyl-2-pyrrolidone
PBS	phosphate-buffered saline
PEG	polyethylene glycol
PMP	protein metallo phosphatases
PyBOP	benzotriazol-1-yl-oxytripyrrolidinophosphonium hexafluorophosphate
RMPI-1640	Roswell Park memorial institute 1640
RNA	ribonucleic acid
rt	room temperature
SEA	bis(2-sulfanylethyl)amino
SNAC	spontaneous nickel (II)-assisted cleavage
SPCL	solid-phase chemical ligation
SPPS	solid-phase peptide synthesis
TCEP	tris(2-carboxyethyl)phosphine hydrochloride
TFA	trifluoroacetic acid
TIC	total ion current
TIS	triisopropylsilane
tRNA	transfer ribonucleic acid

CHAPTER 1

INTRODUCTION

Overview of peptides in chemical biology

1. CHAPTER 1 - INTRODUCTION - Overview of peptides in chemical biology

Historical hints. A peptide (from Greek *πεπτός*, "digested") is a short chain of amino acids linked together through amide (or peptide) bonds. Both peptides and proteins are linear chains of amino acids. Generally, peptides refer to those with less than 50 amino acid residues, whereas longer amino acid chains are regarded as proteins.

The first peptide with biological functions in humans to ever be discovered was secretin, in 1902.¹ Secretin is a hormone produced by the S cells of the duodenum and activated by the gastric acid arrival to the intestine.² Its role is to inhibit gastric acid secretion and trigger the production of sodium bicarbonate by the pancreas. Secretin was also the first peptide hormone to be discovered: as to highlight the importance and potential of peptides in endocrinology, its discovery was worth the Nobel Prize in Physiology to Starling and Bayliss.

Following the discovery of secretin, many other peptides were identified and reported to have biological activity in humans, such as substance P, oxytocin, nerve growth factor and so on.^{3, 4}

On the chemistry side, a breakthrough happened in the 1963 when a seminal paper describing the chemical synthesis of peptides using a solid support was published by Robert Merrifield.⁵ This new synthetic procedure considerably improved the yield and time for the synthesis of peptides compared to previous methodologies (the topic of the chemical synthesis of peptides in solid phase will be discussed in detail later in this chapter).

1.1 Chemical properties

Amino acids as building blocks. Amino acids, as the building blocks of peptides, are defined as molecules bearing both an amino and a carboxylic acid functionality. Amino acids are zwitterionic molecules under physiological pH, because they carry a basic (amine) and an acidic (carboxyl) group. In the case of peptides and proteins, α -amino acids are the most common type of building blocks, where the amino and carboxylic functionalities are both covalently bonded to the α -carbon. Overall, there are 20 amino acids in the genetic code (22 if pyrrolysine and selenocysteine are also taken into account), although more than 500 have been identified in nature.⁶ Apart from glycine, naturally occurring α -

amino acids are chiral molecules. Depending on the chirality of α -carbon, chiral α -amino acids can exist in either D or L configuration. Except for cysteine (where the sulphur changes the priority of the sidechain in the configuration assignment), the absolute configuration of the α -carbon is (*S*) in L-amino acids. In vice versa, the α -carbon absolute configuration in D-amino acids is (*R*) (Figure 1.1).



Figure 1.1. General structure of α -amino acids in their (left) L and (right) D configurations, represented as zwitterion species. R refers to the side-chain moiety

Peptide bond. The type of chemical bond holding amino acid units together in a peptide is known as an amide or peptide bond. The peptide bond is a covalent bond joining the nitrogen of an amine group to a carbonyl carbon. In peptides, the peptide bond links the nitrogen of the α -amine of an amino acid to the carbonyl carbon of the α -carboxyl group of another amino acid. The angles of the bonds between the α -carbon and the carbonyl carbon and between the α -nitrogen and the α -carbon are known as ψ and ϕ . The dihedral angle of the peptide bond is indicated with ω and can assume the value of $\approx 180^\circ$ when the bond is in the *trans* (most common) configuration, while its value is $\approx 0^\circ$ for *cis* peptide bonds; consequently, the carbonyl oxygen, the carbonyl carbon, the α -nitrogen and the hydrogen linked to it all lie on the same plane (Figure 1.2).

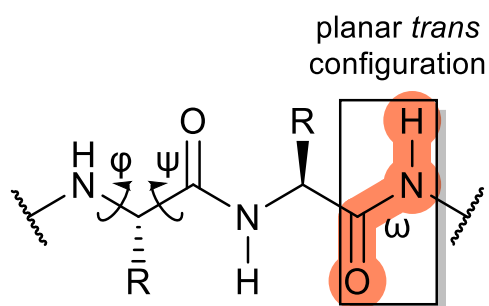


Figure 1.2. Geometrical description of peptide bonds; bonds defining the dihedral angle ω are highlighted in orange

In a peptide bond, the C-N bond is shorter (1.32 Å) than in an amine (typically of 1.47 Å) (Figure 1.3a). This partial double bond character of the C-N bond can be explained by considering the contribution of the C=N⁺ bond in the resonance structure given by the electron delocalisation shown in Figure 1.3b.

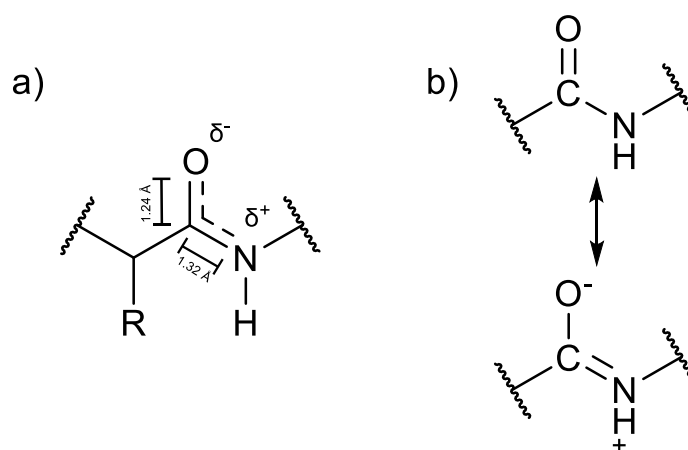


Figure 1.3. a) Bond lengths of O=C-N. b) Resonance structures of a peptide bond.

The resonance, provided by the delocalisation of four electrons in π cloud generated by the alignment of the three $2p_z$ orbitals of the oxygen, the carbonyl carbon and the nitrogen, confers great stability to the peptide bond.

The two most significant electronic transitions of a peptide bond, namely $\pi \rightarrow \pi^*$ and $n \rightarrow \pi^*$, both absorb in the far-UV region (180-230 nm). Furthermore, the $\pi \rightarrow \pi^*$ transition in the tryptophan, histidine, tyrosine and phenylalanine sidechains absorb in the near-UV region (240-295 nm). These spectral properties make easy the detection of peptides by instruments relying on UV absorption, such as HPLC or LC/MS if equipped with an UV lamp.

Peptide structure. All peptides have a primary structure, made up of the amino acid sequence; depending on the sequence, peptides can possess a secondary and a tertiary structure, as well. A secondary structure is the disposition of amino acid residues to form distinct spatial arrangements such as α -helices (Figure 1.4a) and β -sheets (Figure 1.4b).

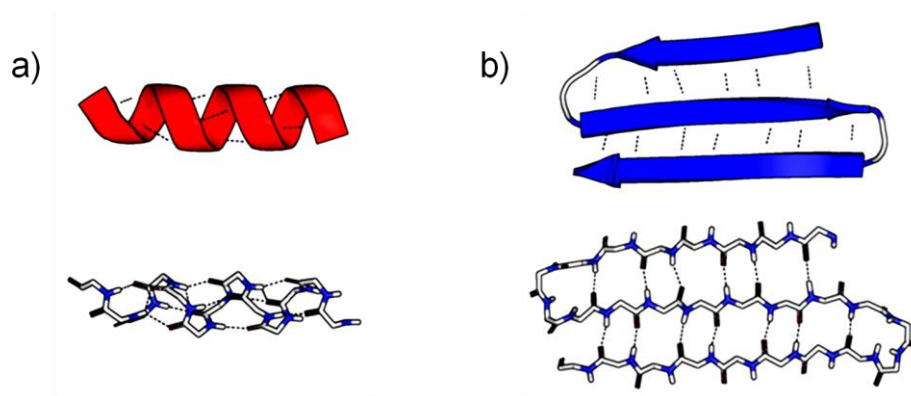


Figure 1.4. Cartoon (above) and ribbon-stick (below) representations of a) an α -helix and b) an antiparallel β -sheet. Hydrogen bonds are shown as dotted lines. Blue, black and white colours are used to denote nitrogen, oxygen and carbon atoms in the ribbon-stick representation.

α -helical structures are stabilised by hydrogen bonds between the CO and NH groups of a peptide backbone in the same strand: these interactions happen between amino acids distant 4 residues to each other.

β -sheets, instead, are stabilised by hydrogen bonds between the CO and NH groups of a peptide backbone in different strands: if the strands have the same direction, the β -sheet is called parallel; if the strands have opposite directions, the β -sheet is anti-parallel.

The propensity of a peptide to assume a secondary structure depends on the amino acid residues involved: while, for example, alanine, leucine and lysine favour an α -helical structure, valine, isoleucine and threonine tend to form β -sheets.

Finally, a tertiary structure is the arrangement of a peptide chain in the three-dimensional space.

1.2 Biological properties of Peptides

Peptides have a plethora of biological functions.^{7, 8} In biological systems, peptides serve as immunity mediators, opioids, antioxidant, and antihypertensive molecules and so on.^{7, 8} For example, glutathione is an endogenous antioxidant tripeptide.⁹ Its cysteine residue sidechain is able to keep thiol groups in proteins in the functional redox state. On the other hand, oxytocin is a peptide hormone involved in the contraction of the uterine myometrium and in social and cognitive behaviour.

Membranolytic peptides. Amongst biologically active peptides, those with membranolytic properties have been drawing a lot of attention, owing a great potential in drug discovery.¹⁰

Membranolytic peptides can be of different origins (i.e. animal, plant, bacterial) and bear the ability to interact with and disrupt biological membranes. Antimicrobial peptides stand out as a class of membranolytic peptides. Because they do not usually interact with any protein to carry out their biological activity, resistance is not easily developed by the targeted cell.¹¹ Therefore, antimicrobial peptides are seen as promising candidates in the fight against antibiotic resistance.

1.3 Peptide Synthesis

1.3.1 Chemical Synthesis of Peptides

One of the currently available methods to prepare a peptide molecule is via total chemical synthesis, by stepwise connecting amino acid residues in organic solvents or peptidyl segments in aqueous buffer.

The assembly of peptidyl segments, for instance, can either occur in solution or onto a solid support and, after a certain number of assembly cycles, yields the desired peptide (Figure 1.5).

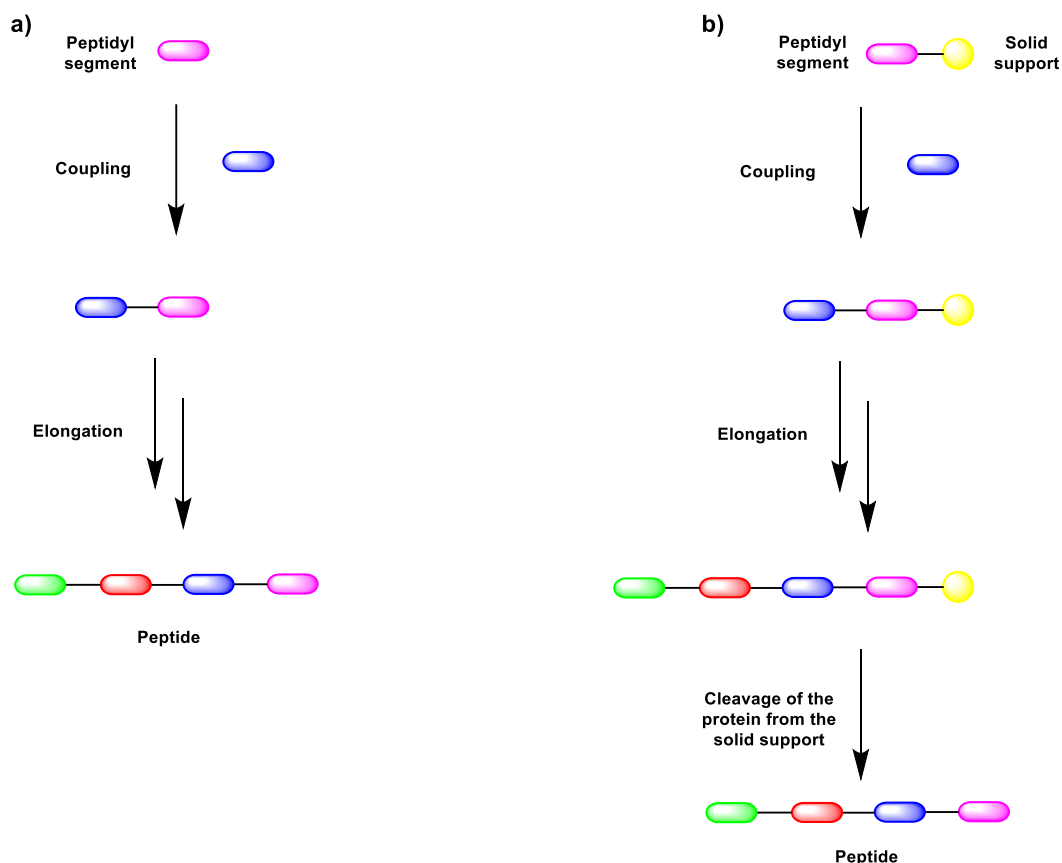


Figure 1.5. Total chemical synthesis by stepwise assembling of peptidyl segments (a) in solution or (b) solid phase

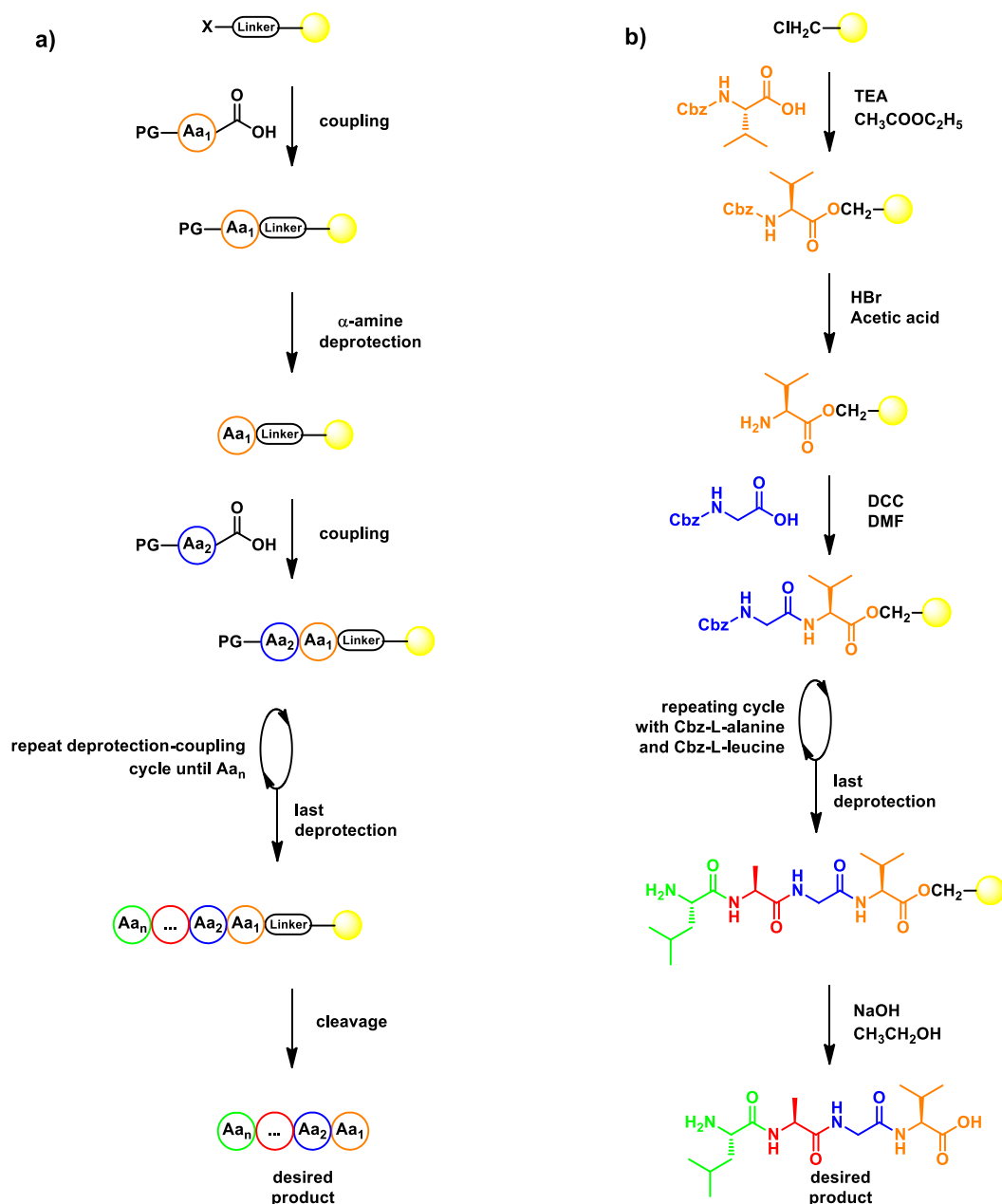
The field of total chemical synthesis of peptides is dominated by solid-phase peptide synthesis (SPPS) and native chemical ligation (NCL).¹² Through these techniques, the peptide of interest is prepared in a synthetic organic chemistry fashion by a solid or a solution phase approach.

1.3.1.1 Solid-Phase Peptide Synthesis

In a classic SPPS protocol, the peptide chain is anchored at its C-terminus to the resin and the elongation occurs from the C-to-N terminus. The resin is usually equipped with a linker, which bears a reactive functionality needed for loading the first amino acid residue onto the solid support. The amino acid residues are coupled as α -amino protected amino acid. Furthermore, residues that carry reactive side chains are also protected with orthogonal groups. The protection strategy allows the α -carboxylic functionality of the residue to selectively react with the free α -amine of the elongating chain on the solid

support. To enable sequential coupling, the α -amino protecting group on the peptidyl resin is cleaved, freeing the amino functionality for reaction. The described α -amino deprotection/coupling cycle enables the building of the peptide onto the solid support. All reactions occur in an organic solvent, such as *N,N*-dimethylformamide (DMF) or *N*-methyl-2-pyrrolidone (NMP), which solubilises the chemical components needed for the coupling and the deprotection whilst remaining chemically inert. After the α -amino deprotection of the last amino acid residue, a final cleavage from the solid support yields the crude mixture containing the desired peptide (Scheme 1.1a). This is usually precipitated from the cleavage mixture and isolated via chromatographic procedures.

The first application of a SPPS protocol, published in 1963 by Merrifield,⁵ was the preparation of a tetrapeptide. The solid support employed was a chloromethylated polymer of nitrostyrene, cross-linked by divinylbenzene, which is very similar to the resins used today. The amino acid residues were chemically joined by using *N,N'*-dicyclohexylcarbodiimide as the coupling reagent, which activates the carboxylic functionality of the incoming α -amine carboxybenzyl (Cbz) protected amino acid (Scheme 1.1b). To enable the coupling of the next residue, the peptide on the resin was first treated with HBr, which deprotects the Cbz group, thereby freeing the α -amino group. After the last residue was coupled and deprotected, the tetrapeptide was cleaved from the resin by NaOH treatment. This work laid the foundation for SPPS. However, as Cbz deprotection conditions can lead to premature peptide detachment from the resin, other types of coupling approaches have been investigated.



Scheme 1.1. a) general synthetic scheme for SPPS. X = linker reactive group for the first amino acid loading, Aa = amino acid residue (with protected side chain, if needed), PG = protecting group on the α -amine. b) first report of SPPS, synthetic scheme for the tetrapeptide H-LAGA-OH. TEA: triethylamine, DCC: *N,N'*-dicyclohexylcarbodiimide, Cbz: carboxybenzyl.

α -amine protecting groups. Presently, *tert*-butoxycarbonyl (Boc) and fluorenylmethoxycarbonyl (Fmoc) are the most employed α -amine protecting groups (Figure 1.6a). In the Boc strategy, trifluoroacetic acid (TFA)-resistant linkers and side chain protecting groups are used, such as benzyl or benzyloxycarbonyl groups, which are cleaved by final treatment with HF. The Boc-protected *N*-terminal α -amine of the growing peptidyl chain is freed by TFA to allow the coupling of the upcoming residue. This strategy is preferred when base labile

moieties are present in the sequence during the elongation, like ester or thioester groups. However, the Boc strategy normally requires the use of HF, which is very hazardous requiring special equipment along with specialised and well-trained users.

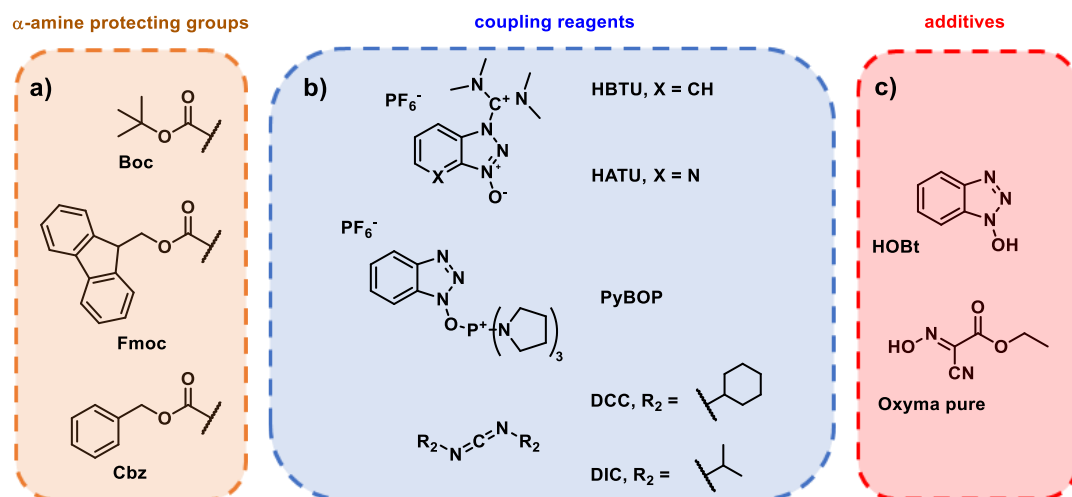
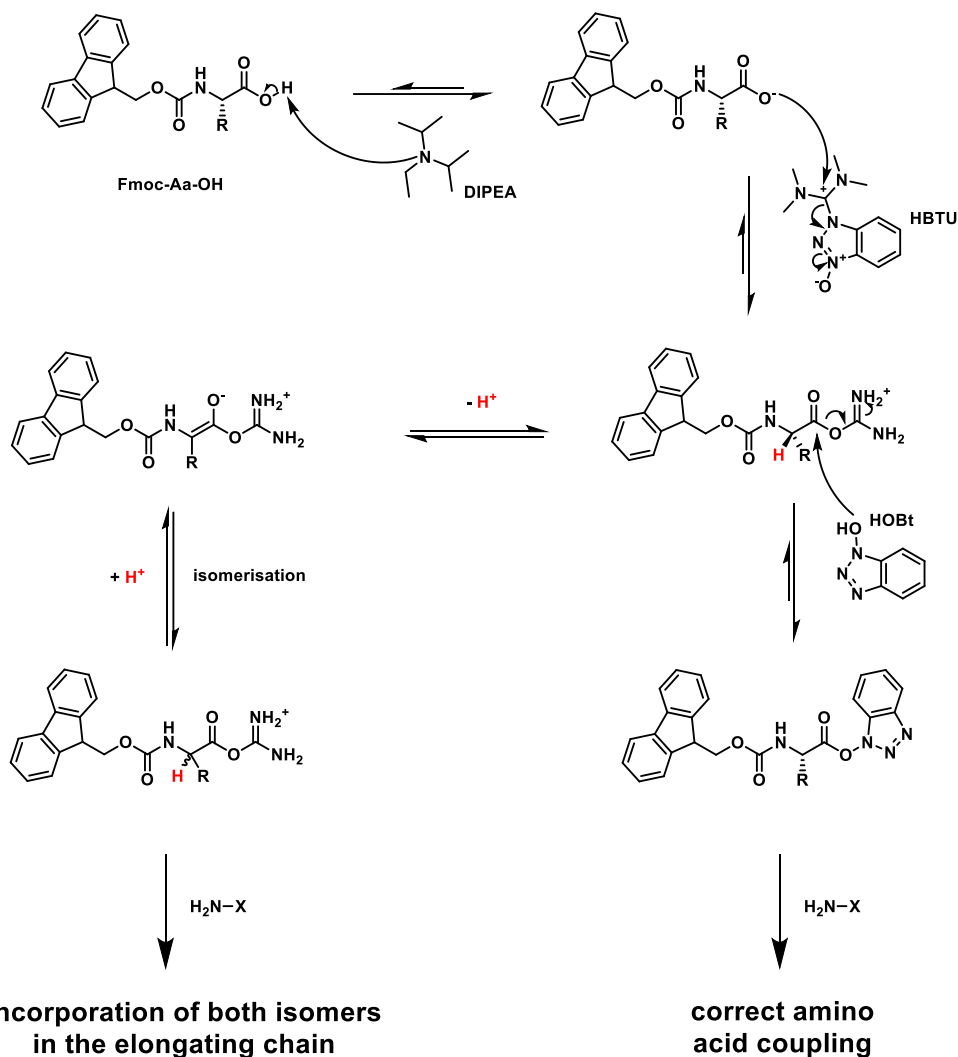


Figure 1.6. Molecular structure of some of the most employed a) α-amine protecting groups, b) coupling reagents and (c) additives

As a safer alternative, most of the more recent protocols use Fmoc strategy, where the Fmoc group protects the α-amine of the residue to be attached during the coupling step. After the coupling, the peptidyl resin is treated with a basic deprotection cocktail (usually a solution of piperazine or piperidine in DMF) to deprotect the α-amine group and to make it available for the following coupling step. In this strategy, the amino acid residue side chains are protected with TFA-labile protecting groups, such as *tert*-butyl, Boc, pentamethylbenzofuranyl and trityl. The orthogonal stability between Fmoc, side chain protecting groups and linker (which is often TFA labile as well) enables the SPPS. As mentioned above, the main advantage of the Fmoc strategy is the bypass of using HF. Nevertheless, base-labile peptides such as thiodipeptides cannot be directly synthesised by Fmoc/SPPS, unless some changes are made to the common protocol (i.e. post SPPS modifications of C-terminus, employment of special linkers).^{13, 14}



Scheme 1.2. Proposed racemisation scheme of amino acid mediated by 2-(1H-benzotriazol-1-yl)-1,1,3,3-tetramethyluronium hexafluorophosphate (HBTU) and proposed racemisation minimisation mechanism by 1-hydroxybenzotriazole (HOBT)

Coupling reagents. For the coupling step, peptide bond formation usually takes advantage of reagents that activate the carboxyl group of the incoming residue. This requires the use of coupling reagents, such as carbodiimide derivatives, phosphonium or uronium/guanidinium salts (Figure 1.6b).¹⁵ The main requirements for a good coupling reagent are:

- high reactivity
- minimal interference on amino acid stereochemistry (i.e. no racemisation)
- no side reactions (amino acid side chain reacting with the activated carboxylic functionality).

To suppress or minimise racemisation and side reactions that may occur during the activation step, additives like 1-hydroxybenzotriazole (HOBt) and oxyma pure (Figure 1.6c) are usually present along with the coupling reagent. For example, HOBt can inhibit racemisation by forming a benzotriazole ester, which is less prone to undergo to racemisation or side reactions (Scheme 1.2).¹⁶

Table 1.1. Some of the commercially available linkers for Fmoc/SPPS

Linker	Cleavage conditions	C-terminus
2-Chlorotrityl chloride	1% TFA in DCM	-COOH
Rink Amide	95% TFA	-CONH ₂
2-Chlorotrityl hydrazine	1% TFA in DCM	-CONHNH ₂
MeDbz	i) <i>p</i> -NO ₂ PhOCOCi ii) DIPEA iii) TFA iv) RSH	-COMeNbz -COSR

Resins and linkers. At the start of the synthesis, the first amino acid residue is coupled to the linker, whose choice dictates the C-terminal functionality of the peptide, once submitted to the cleavage treatment. As the field of peptide chemistry has continued to advance, different types and sizes of peptides have been designed and developed,¹⁵ including thioester peptides used for native chemical ligation (NCL) (see below). Consequently, there are several types of linkers (Table 1.1) available to meet the demands for different needs. For instance, because of the acidic conditions employed throughout the synthetic protocol, thiodipeptide synthesis in solid phase was classically carried out by Boc/SPPS. As mentioned above, this approach needs HF handling. Fmoc/SPPS would be an ideal alternative. Unfortunately, the thioester moiety does not survive the basic conditions employed during the deprotection step and thiodipeptides cannot be directly synthesised by Fmoc/SPPS. Consequently, different linkers were designed to enable the preparation of thiodipeptides via Fmoc/SPPS.¹³

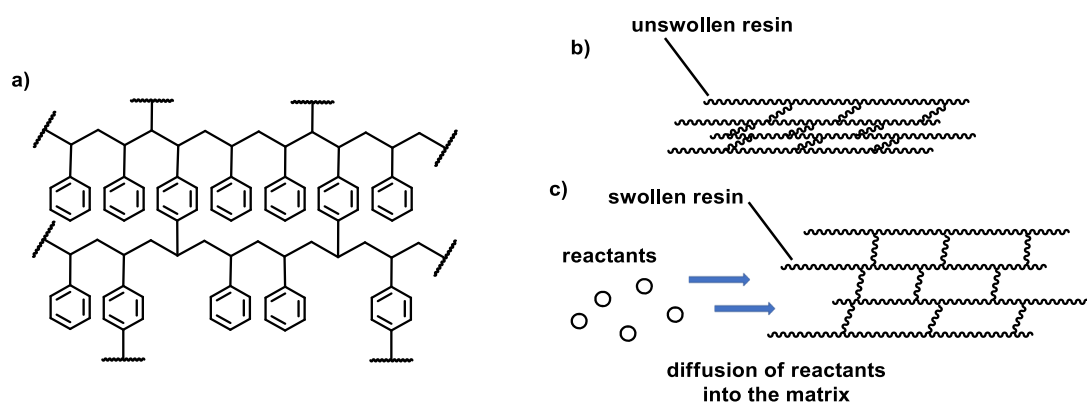
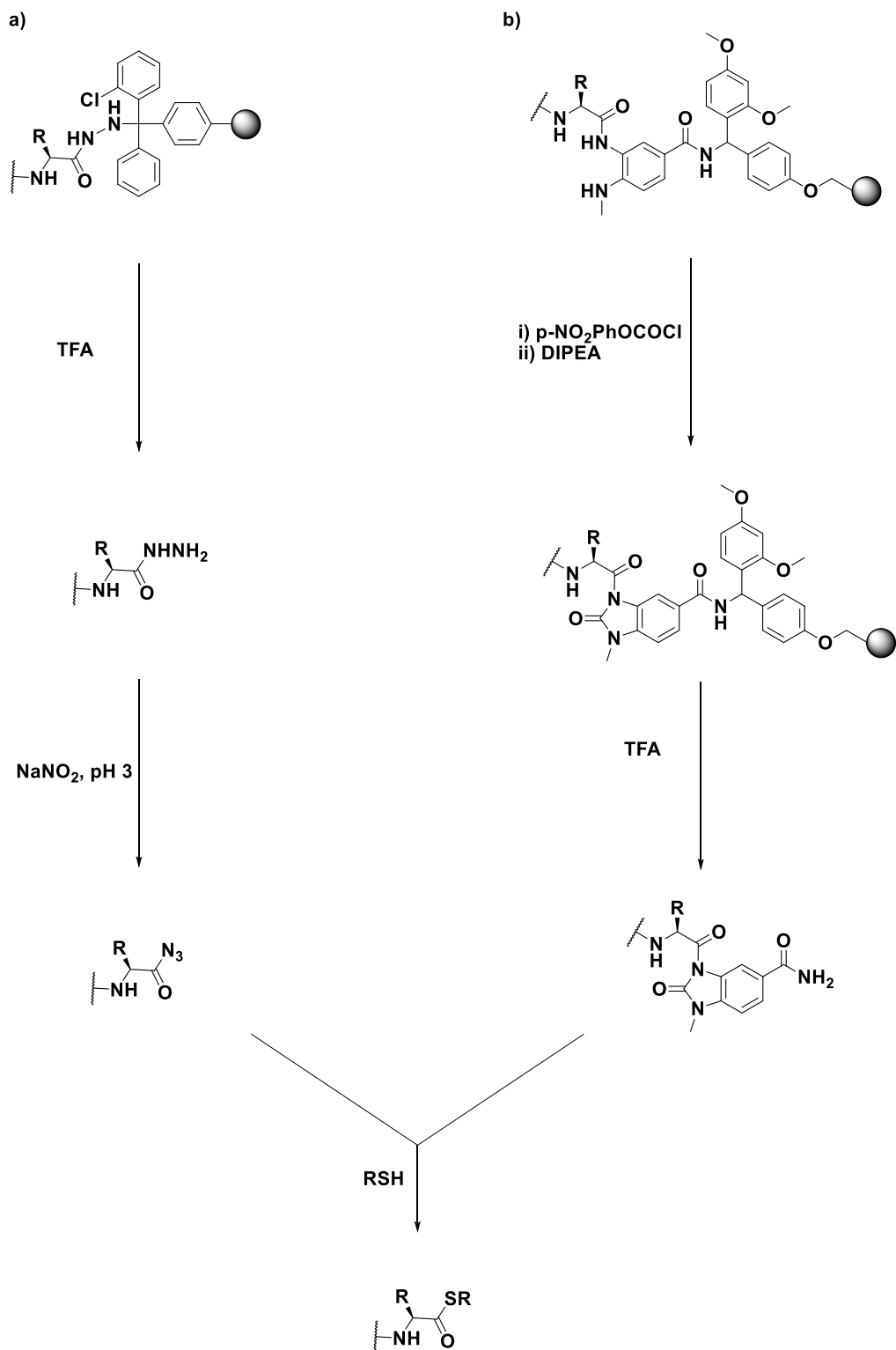


Figure 1.7. a) Molecular structure of a polystyrene polymer, cross-linked with divinylbenzene. b) before the swelling procedure, the polymeric support is shrunk, and the reaction sites cannot be reached. c) after being swollen, the resin can accommodate the SPPS reactants in its matrix.

Nowadays, some of the most employed solid phase supports are very similar to that used by Merrifield in his first SPPS report.¹⁵ In fact, the most popular SPPS resin is usually a divinylbenzene cross-linked styrene polymer (Figure 1.7a), which can be equipped with several linkers. Furthermore, to reduce problems of

yield and purity related to the aggregation of the peptide chain on the solid support, different types of resins were made available. In fact, resins like TentaGel, ChemMatrix and CLEAR, bear more hydrophilic cores, mainly comprised of polyethylene glycol (PEG) units, which were found to reduce aggregation of the elongating chain onto the solid support for some peptide sequences.¹⁵

Prior to the start of the synthesis, the solid support needs to be swollen (Figure 1.7b) such that the reactants can diffuse into the matrix of the resin (Figure 1.7c), thereby enabling protein chain elongation during the SPPS. Some of the most employed resins for routine Fmoc/SPPS are reported in the Table 1.1. The Cl-Trt resin (Table 1.1, entry 1) is used to obtain peptides/proteins with a C-terminal carboxylic functionality, but it is extremely acid sensitive (the peptide is cleaved from the resin at 1% TFA) and usually more susceptible to polymer degradation (leaching). The Rink Amide linker (Table 1.1, entry 2) yields a C-terminal amide moiety, and it is probably the most used resin, given its superior stability. Nonetheless, this resin does not afford a native C-terminus carboxylic group but an amide group, which can be undesirable when studying peptides/proteins whose C-terminal carboxylic group plays an important role.¹⁷ Moreover, it is worth mentioning the 2-Cl-Trt hydrazine and the *o*-amino(methyl)aniline (MeDbz) resins (Table 1.1, entry 3 and 4) for their great significance in NCL when doing iterative ligations. In fact, the earlier enables the synthesis of peptide hydrazides (Scheme 1.3a), which can be converted into thiodipeptides *in situ* (see section 1.3.4.1 for a more detailed discussion); the latter resin yields an *N*-acyl-*N'*-methylbenzimidazolinone (MeNbz) peptide when treated with *p*-NO₂PhOCOCl and *N,N*-diisopropylethylamine (DIPEA) before the cleavage, and directly affords a thiodipeptide by further reacting the MeNbz peptide with a thiol (Scheme 1.3b).



Scheme 1.3. Preparation of thiopeptides by employment of a) 2-Chlorotrityl hydrazine linker and b) MeDbz linker

Automated SPPS systems. Currently, several automated systems are available for the total chemical synthesis of peptides via SPPS. These instruments automate the SPPS protocol and couple to microwave-assisted (Figure 1.8) or flow-synthesis technology to allow the synthetic steps to proceed at higher

temperatures.¹⁸ These methods drastically reduce the coupling and the deprotection time per residue, thereby enabling the synthesis of the target molecule in significantly shorter time. Additionally, the automation of the synthesis leads to highly reproducible yields and purity.¹⁹



Figure 1.8. CEM Liberty Blue™ Automated Microwave Peptide Synthesiser.

Recently, automated flow systems in peptide synthesis have gained great interest in the scientific community.^{20, 21} This technology relies on the use of HPLC pumps to continuously deliver the reagents to the reactor, where the elongating polypeptide-resin stands. Temperature and pressure are both controlled to create reaction conditions which greatly facilitate the synthesis of peptides and even proteins in high yields and short time. In fact, automated flow synthesis technology has recently enabled the preparation of proteins comprised of up to 164 amino acid residues in a few hours.²²

Pros and cons. One of the key advantages of SPPS is that the excess reagents and the by-products can be promptly washed out by filtration of the resin with solvent,⁵ while the elongating polypeptide remains attached to the resin. This passage avoids time-consuming intermediate purification, which is often encountered during solution-phase synthesis. In fact, the common container for SPPS reactions is a plastic or glass vessel equipped with a filter and a tap. When the tap is opened, the solvent is drained off through the filter and the peptidyl resin stays on the vessel (Figure 1.9).

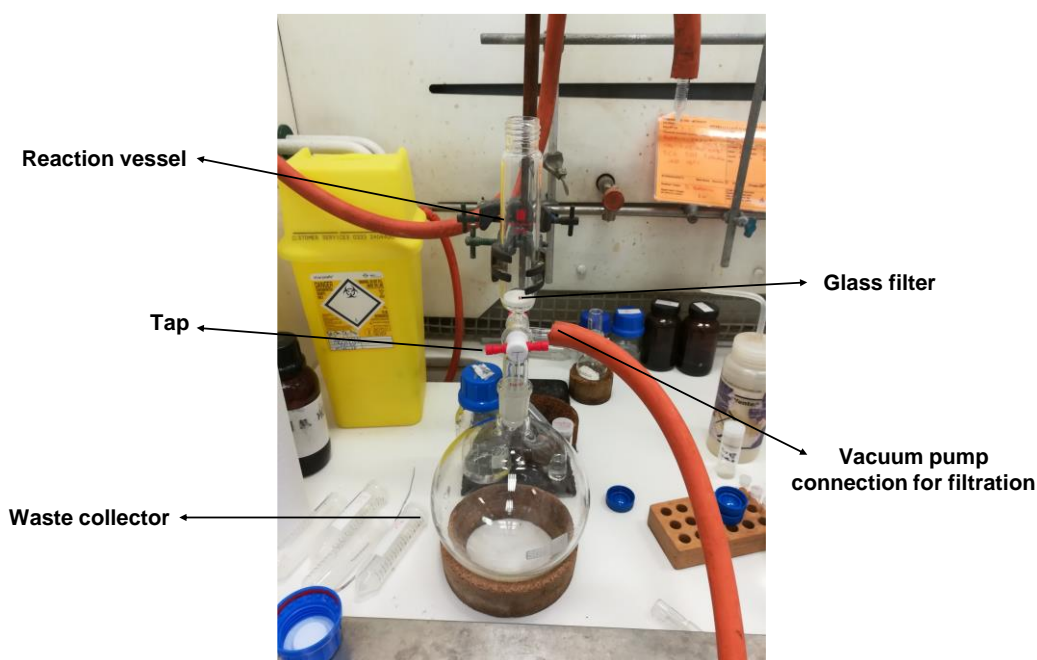


Figure 1.9. Common laboratory setup for manual SPPS

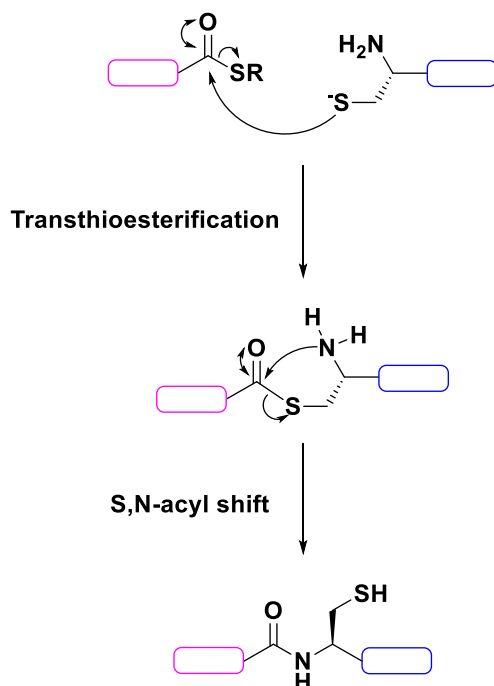
Unlike other molecular biology techniques which relies on the protein synthesis machinery of the host cell and hence specific building blocks (i.e. L-amino acids commonly found in nature), SPPS confers atomistic control on the peptide sequence. In fact, there is no theoretical limitation on the kind of functionalities on the amino acid side chain to be inserted by SPPS. Moreover, D-amino acids can be used as building blocks, enabling the synthesis of enantiomeric peptides. Lastly, isotopic-labelled amino acid residues can be specifically incorporated into the peptide sequence at any position.

The main limitation of the SPPS technique is currently the size of the target molecule. In fact, the upper limit for SPPS is empirically around 50-70 residues, because as the number of couplings increases the yield becomes very low and the elongating chain undergoes aggregation, making the *N*-terminal α -amine less accessible for further couplings.¹⁵ On the other hand, automated flow peptide synthesis has been shown to be an highly efficient technique;²² today, its usage unfortunately remains not easily accessible. In fact, no automated flow peptide synthesis system is currently available on the market and setting it up in a research lab requires highly trained personnel.

1.3.1.2 Native Chemical Ligation

History and overview. NCL is a chemoselective reaction between the C-terminus of a thiopeptide and the *N*-terminal cysteine of another peptide occurring in aqueous buffer at neutral pH (Scheme 1.4), and it has become a well-established and very promising tool in the field of total synthesis of peptide and proteins. The ligation reaction between a thioester of an amino acid and a cysteine, to afford a dipeptide, was first discovered in the early 1950s.²³ Only almost 40 years later this reaction was exploited independently by two research groups for the total synthesis of proteins.^{24, 25}

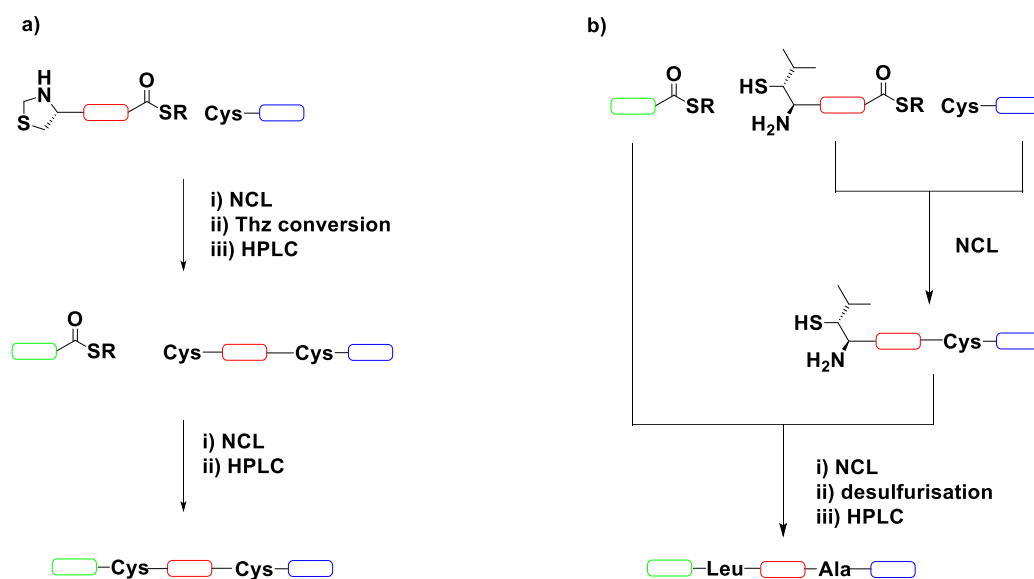
Having shown its effectiveness for the synthesis of proteins comprised of up to 427 amino acid residues,²⁶ NCL largely exceeds the size limitation of SPPS. The huge impact of this reaction is given by the fact that more unprotected peptide segments can be joined to yield a full-length sequence, either in its native or mutated form. Moreover, these segments can be synthesised by SPPS, which confers atomistic control on the peptide sequences, overcoming different limitations of other molecular biology techniques occurring in cells (i.e. post-translational modifications, isotopic-labelled residues, isopeptide bonds and an unlimited number of unnatural amino acids in the sequence).



Scheme 1.4. NCL reaction mechanism between the C-terminal thioester moiety of a thiopeptide (in pink) and an N-terminal cysteine of a peptide (in blue) in aqueous buffer at neutral pH

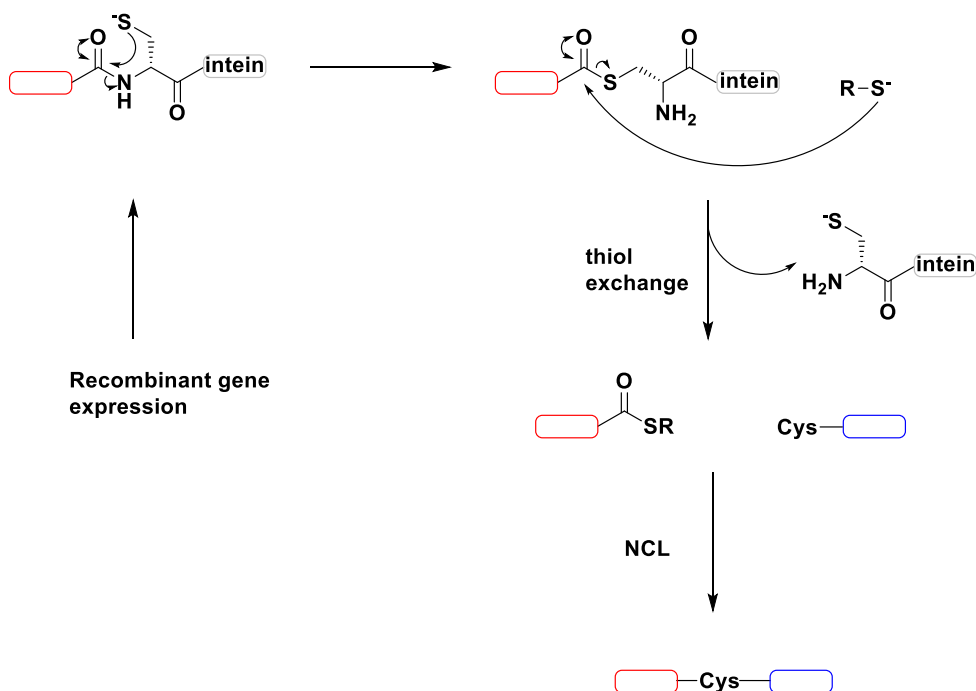
One-pot NCL. Since its first application for the synthesis of the human interleukin 8,²⁷ where it was used for the ligation of two unprotected peptides in solution, NCL has been implemented for sequential ligations. To allow more than one ligation, the “internal” thiopeptide must bear either a protected or a masked cysteine, to avoid side reactions as cyclisation or oligomerisation of the thiopeptide. One of the most employed strategies for this purpose is the use of the thiazolidine residue as a cysteine surrogate. In presence of *o*-methylhydroxylamine, the thiazolidine residue is converted into a cysteine at slightly acidic pH, thereby allowing the next ligation (Scheme 1.5a). To ligate three segments by NCL in solution, more than one purification step is required. In fact, after ligating the first two segments (assuming the direction of the elongation is C-to-N), the protecting group on the α -amine of the cysteine of the N-terminal segment must be deprotected, to allow the next ligation. Although it has been reported that the side product may not be present in a significant amount,²⁸ the deprotection conditions can lead to side reactions involving the thioester moiety.²⁹ Thereby, the intermediate usually needs to be isolated by a purification step which is often time consuming and can lead to loss of material. To skip this process, kinetically controlled ligation was developed. One of the reports

exploiting this strategy relies on the different reactivity of the *N*-terminal thiol functionalities to allow one-pot three segment ligation in solution (Scheme 1.5b).³⁰



Scheme 1.5. a) When carrying out sequential ligations by NCL, the cysteine residue must be hidden to avoid side reactions. Usually, an HPLC purification is needed for each ligation step b) In the kinetically controlled ligation approach, the reaction kinetics is dictated by the reactivity of the aminothiol group

Expressed protein ligation. A hybrid approach combining SPPS, NCL and recombinant gene expression is known as expressed protein ligation. In the majorities of the NCL protocols, the peptidyl segments are still obtained by SPPS. Consequently, the preparation of these segments is still restricted to the SPPS limitations. To access larger thiodepsipeptides, the *N*-terminal peptidyl segment can be obtained by recombinant gene expression as an *N*-terminal extein fused to a C-terminal intein domain. The cysteine residue of the intein domain can cleave the amide bond between the extein and the intein, thus generating a thioester bond. In the presence of a thiol, this thioester bond will react and, by thiol exchange, the target thiodepsipeptide will be afforded. This peptidyl segment can now react via NCL (Scheme 1.6).³¹



Scheme 1.6. In the expressed protein ligation approach, the thiopeptide involved in the NCL is obtained by thiol exchange between a peptide expressed by recombinant gene expression and an aryl or alkyl thiol

1.3.2 Peptide biosynthesis

Another way to access peptide/protein preparation is to leverage the main biosynthetic route in eukaryotic and prokaryotic cells: the ribosomal pathway.

The ribosomal biosynthesis of peptides follows the same steps of protein biosynthesis: a strand of mRNA is synthesised by an RNA polymerase that uses a DNA region as a template; then, the mRNA strand interacts with the ribosome, which assembles the amino acids carried by the tRNA (according to the information coded in the mRNA), to biosynthesise a peptide chain. Oftentimes, the newly biosynthesised peptide undergoes further modifications (known as post-translational modifications) such as proteolytic cleavage, site-specific phosphorylation, glycosylation, hydroxylation and so on, finally yielding the peptide in its biologically active form.³²

The most exploited and routinely used method for the preparation of peptides and proteins that profits from the protein biosynthetic machinery of cells is the recombinant gene expression technique.

1.3.3 Recombinant gene expression vs total chemical synthesis

Although the methods described thus far in this chapter have shown to be powerful tools in peptide and protein synthesis, they still present significant limitations. Recombinant gene expression in a host cell is limited by the biological components of the host carrying out the biosynthesis. For instance, excluding few exceptions,³³ only amino acids compatible with the aminoacyl-tRNA synthetases of the host can be inserted into the sequence of interest and only by the canonical genetic code. Additionally, recombinant gene expression can be very challenging in the preparation of short peptide sequences. In fact, this technique usually relies on fusion tags that cannot be always readily cleaved from the peptide of interest,³⁴ moreover, small peptides are difficult to isolate via size-exclusion chromatography. Finally, small peptide sequences are often target of endogenous cellular proteases:³⁴ this leads to their preparation in very low yields.

Notwithstanding the atomic-level control on the sequence of the peptide or protein and the high efficiency reached nowadays by automated microwave devices, SPPS is severely limited by the short number of residues per peptide/protein allowed. In fact, as already mentioned previously, after a certain number of couplings depending on the target sequence, the fully protected elongating chain starts folding and rearranges into secondary structures.¹⁵ This event ultimately leads to the inaccessibility of the *N*-terminal α -amine group, which is needed for further couplings.

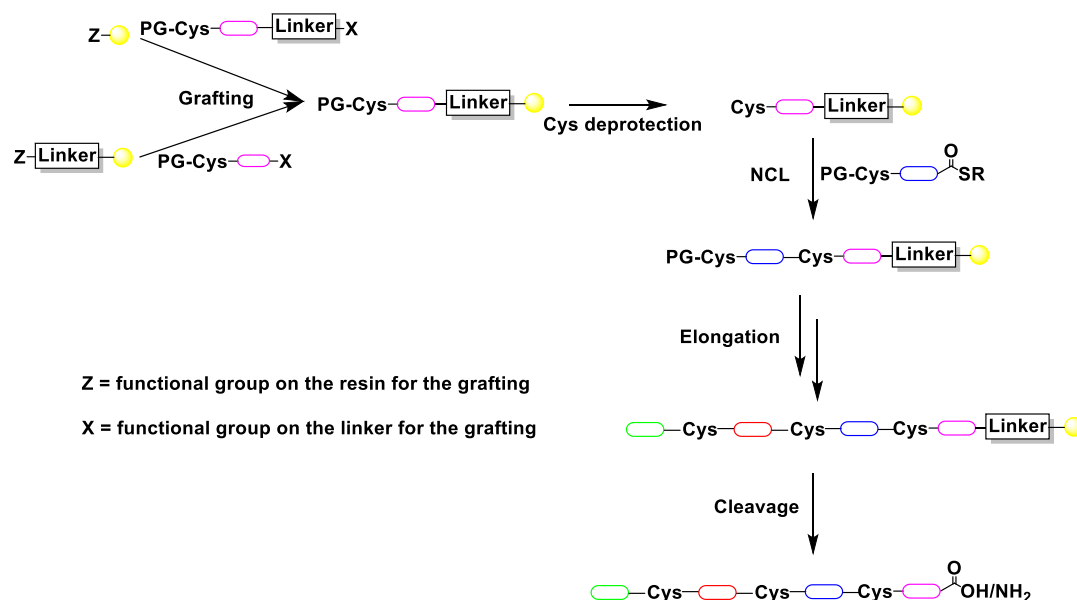
The bottleneck of the synthesis by NCL carried out in solution is the need for purification steps which are time consuming and lead to inevitable loss of material, resulting in diminished yield as the number of ligations increases. Consequently, one-pot methods were fostered, like the kinetically controlled ligation approach, where the purification only occurs as a final step.³⁵ Unfortunately, NCL by kinetically controlled ligation has only been shown for the ligation of three segments.

Finally, for the synthesis of the thiopeptide, expressed protein ligation still relies on recombinant gene expression, which carries a series of limitations. Amongst others, these include the lack of atomistic control on the thiopeptide sequence and the difficult insertion of post-translational

modifications. Moreover, after the thiol exchange reaction, another purification step is required before initiating the NCL reaction.

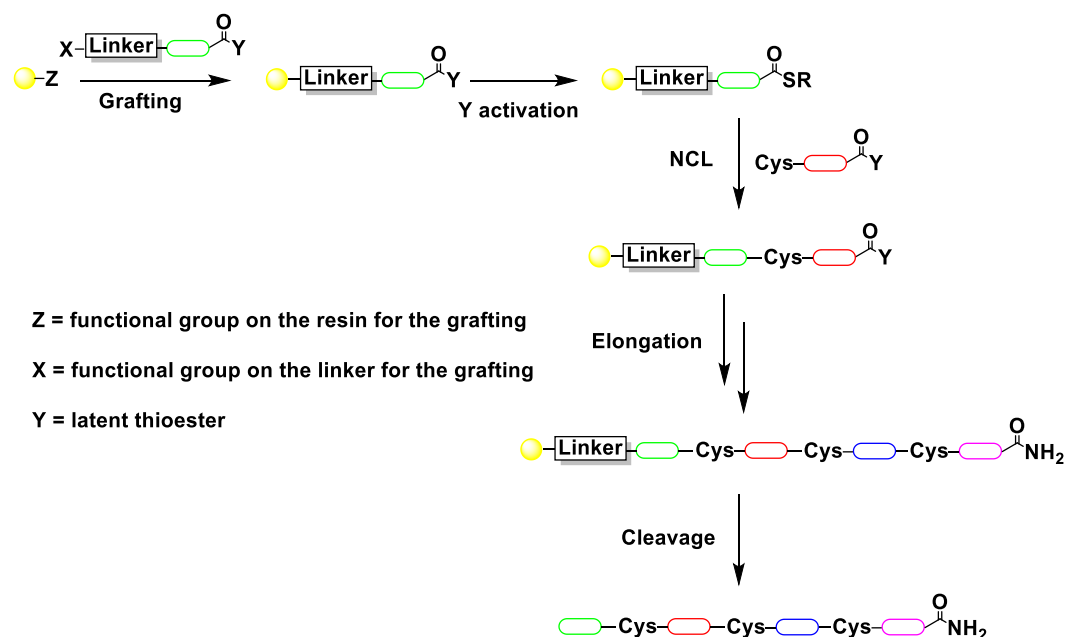
1.3.4 Solid-Phase Chemical Ligation

One section of this thesis (Chapter 2) will explore solid-phase chemical ligation (SPCL), a powerful method used in protein synthesis. This strategy combines the idea from SPPS of carrying out the synthesis with the aid of a solid support and the NCL reaction to ligate peptide segments. In fact, shortly after the NCL reaction was reported, this total protein synthesis method was implemented for the use on a solid support, described as SPCL.^{36, 37} The clear advantage of the SPCL over the NCL in solution is the avoidance of time-consuming isolations of the ligation products by HPLC, which additionally lead to the loss of material.³⁸ In fact, in the SPCL approach, the elongating peptide/protein chain is anchored to a resin, thereby allowing the removal of unreacted peptide segments, other reagents and by-products by simple washing and filtration.



Scheme 1.7. SPCL in C-to-N direction

Protein chain elongation can proceed in two directions, C-to-N (Scheme 1.7) or N-to-C (Scheme 1.8).



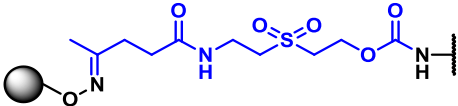
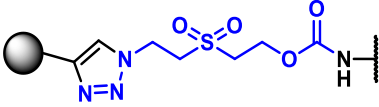
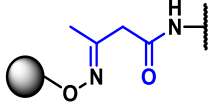
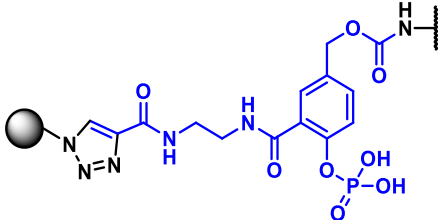
Scheme 1.8. SPCL in *N*-to-*C* direction

1.3.4.1 Overview of the *N*-to-*C* method

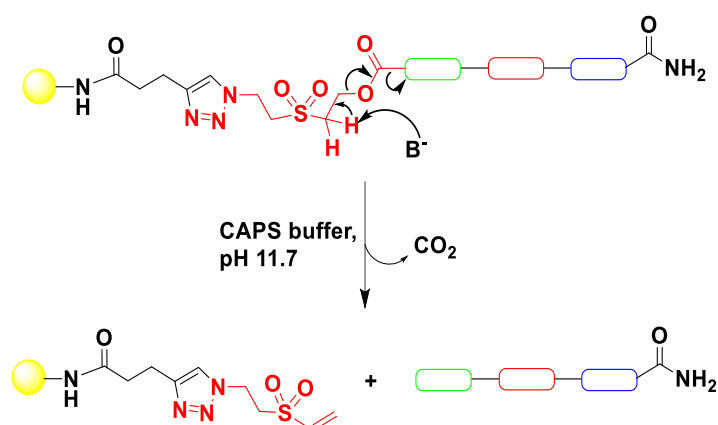
The major problems of the *N*-to-*C* method are the choice of the cleavable linker and of the latent thioester.

Cleavable linkers – grafting and cleavage. The cleavable linker, usually attached on the peptide directly during its SPPS, determines both the conditions for the grafting of the linker-peptide onto the resin and the cleavage conditions for the final release of the protein from the solid support (Table 1.2).

Table 1.2. Cleavable linkers in *N*-to-*C* SPCL

Entry ^{ref}	Cleavable linker	Grafting conditions	Cleavage conditions
1 ³⁷		Oxymation (GdmCl in phosphate buffer, pH 4.6)	GdmCl in phosphate buffer + 200 mM hydrazine, pH 14
2 ³⁸		CuAAC (HEPES, MeOH, Ascorbic acid, CuSO ₄ , pH 7)	CAPS buffer, pH 11.7
3 ³⁹		Oxymation (Sodium acetate, pH 4.6)	20% AcOH, 0.1 M H ₂ NOH and 1 M aniline, pH 4.3
4 ⁴⁰		CuAAC	PMP buffer, lambda phosphatase

The grafting of the linker-peptide requires an additional reaction to be added in the protocol. In fact, reported methods rely on the use oximation,^{37, 39} copper(I)-catalysed azide-alkyne cycloaddition³⁸ or strain-promoted azide-alkyne cycloaddition³⁸ for the anchoring of the linker to the resin. The linkers in question are cleaved either in basic conditions,^{37, 38} as in the case of the Esoc linker (Scheme 1.9),⁴¹ by transoxymation,³⁹ or by an enzymatic reaction.⁴⁰ Furthermore, Esoc and the phosphorylated linkers require time-consuming organic chemical synthesis.^{40, 41}



Scheme 1.9. Cleavage mechanism for the release of the peptide from **Esoc** linker

Most importantly, the conditions used throughout the synthesis must guarantee the stability of the components of the system, such as the peptide segment, the latent thioester moiety, and the cleavable linker.

Table 1.3. Latent thioesters in *N*-to-*C* SPCL

Entry ^{ref}	Latent thioester	Activation conditions
1 ³⁷		Bromoacetic acid, pH 4.6
2 ³⁸		TCEP, MPA, pH 4

Latent thioesters. The first *N*-to-*C* strategy to be reported was employing a thiocarboxylate group as a latent thioester (Table 1.3, entry 1), which is thus turned into a thioester by alkylation with bromoacetic acid at pH 4.³⁷

Currently, the thiocarboxylate as a thioester surrogate has been replaced by the bis(2-sulfanylethyl)amino (SEA) group (Table 1.3, entry 2). In its oxidised form, this moiety is stable under the ligation conditions. When reacted with a reducing agent like tris(2-carboxyethyl)phosphine, the SEA group rearranges into a thioester, which can then undergo a NCL reaction.³⁸

The bottleneck of this strategy is the synthesis of the peptide-SEA, which requires two HPLC purifications. In fact, being synthesised in its reduced form, the peptide-SEA needs to be made inert before its use in the SPCL. Therefore, after its SPPS and its isolation, the peptide-SEA is oxidised and then purified again. Additionally, some cautions might be needed during its oxidation. For instance, the cysteine residues are usually protected with the *tert*-butylsulphenyl group, to prevent side reactions.^{38, 39}

When synthesising a protein/peptide in *N*-to-*C* direction on a solid support via NCL, the latent thioester at the *C*-terminus of the peptide segment plays the crucial role, when activated, to allow sequential ligations.

As already mentioned in the previous section, the first *N*-to-*C* system relied on the thiocarboxylate as latent thioester. The major problem of this moiety was its only partial inertness in the ligation conditions. In fact, during the ligation step, the peptide segment in solution bearing an *N*-terminal cysteine and the thiocarboxylic function at its *C*-terminus can also cyclise.³⁷ This problem was overcome by the introduction of SEA as the latent thioester.³⁸ Nonetheless, SEA-peptides synthesis is time-consuming.³⁸

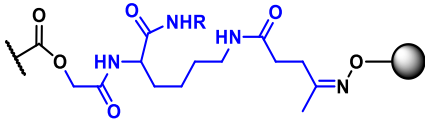
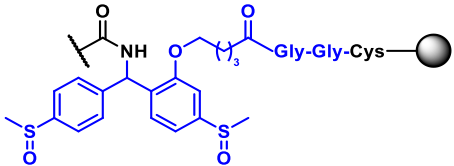
Alternative strategies to obtain latent thioesters include the use of peptide-hydrazides⁴² or peptide-*o*-aminoanilides,⁴³ which are both inert to ligation conditions. In fact, the *C*-terminal hydrazide group can either be oxidised to an acyl-azide by NaNO₂,³³ or turned into an acyl-imidazole by reacting with acetylacetone.³⁶ Both intermediates can then be converted into a thioester in presence of a thiol. Peptide-*o*-aminoanilides are afforded by SPPS via the Dawson linker.⁴³ They are activated to thiopeptides with NaNO₂ and have been

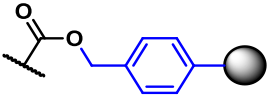
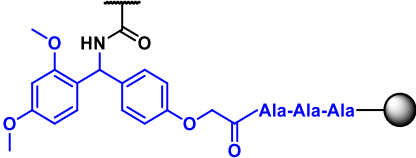
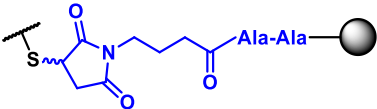
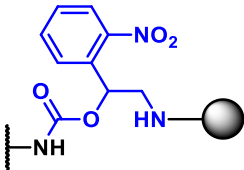
recently used for the synthesis on a solid support of a 212-residue linker histone H1.2.⁴⁴

1.3.4.2 Overview of the C-to-N method

Linkers. The most exploited direction in the SPCL literature is C-to-N.⁴⁵ In fact, this direction does not require the use of latent thioesters – which need a pre-ligation activation step – and the first peptide segment or the linker is generally attached to the resin by NCL. As shown in Table 1.4, all linkers reported so far in literature rely on either TFA or NaOH for the release of the synthesised polypeptide/protein.^{17, 37, 46, 47} Two exceptions are shown in entry 5, where the peptide/protein is released in presence of PdCl₂,⁴⁸ and in entry 6, where the linker is cleaved by UV light irradiation.⁴⁹

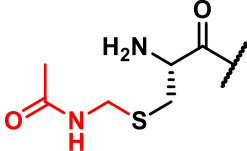
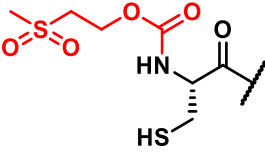
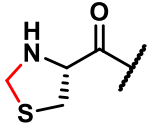
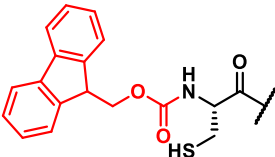
Table 1.4. Cleavable linkers in C-to-N SPCL

Entry ^{ref}	Cleavable linker	Grafting conditions	Cleavage conditions
1 ³⁷		Oxylation (GdmCl in phosphate buffer, pH 4.6)	8 M urea in phosphate buffer, 0.25 M NaOH
2 ⁴⁷		NCL (GdmCl in phosphate buffer, pH 7)	1 M SiCl ₄ , 10% thioanisol, 6% EDT, and 10% <i>m</i> -cresol in TFA at 0 °C

3 ¹⁷		Commercially available HMBA/PHB resin	TFA/NaOH
4 ⁴⁶		SPPS	95% TFA, 2.5% TIS, 2.5% H ₂ O
5 ⁴⁸		SPPS	1. PdCl ₂ , MgCl ₂ 2. DTT
6 ⁴⁹		Biotin-Streptavidin interaction	λ= 297 nm

Cysteine protection. Nonetheless, the C-to-N direction requires a strategy to protect the N-terminal cysteine (or other thiol derivatives) residue of the peptide segment, so that it does not take part in the ligation reaction. N-terminal cysteine protection can occur at either the thiol component, as in the case of acetamidomethyl protecting group, or the α-amine, using Fmoc or methylsulfonyl ethoxycarbonyl groups (Table 1.5). While the aforementioned protecting groups require basic conditions (that might be unwanted) or hazardous reagents for their cleavage, the use of the thiazolidine as a cysteine surrogate entails a mild deprotection with methoxyamine hydrochloride at pH 4,⁵⁰ or treatment with [PdCl(allyl)]₂,⁴⁸ affording the desired amino thiol residue.

Table 1.5. Cysteine protection strategies in C-to-N SPCL

Entry ^{ref}	Protecting strategy	Deprotection conditions
1 ³⁷		(AcO) ₂ Hg, AcOH, pH 4
2 ⁴⁷		Ligation buffer added with NaOH, pH 13
3 ^{48, 49}		H ₂ NOH, TCEP, pH 4 or [PdCl(allyl)] ₂ , 6 M GdmCl, 0.2 M phosphate buffer, pH 7.3
4 ⁵¹		Ligation buffer added with 20% piperidine, pH 11

1.3.4.3 Limitations of SPCL

Thus far, SPCL has been underemployed because of different reasons such as the lack of knowledge on the diffusion of the peptide segments within the matrix of the solid support, the unavailability of methods for reaction progress monitoring, the paucity of available SPCL strategies and the absence of resins purposely designed for protein synthesis.¹⁴ Furthermore, the scarcity of linkers that can be cleaved in mild conditions hinders the preparation of sensitive protein constructs.⁴⁰

1.4 Biological applications of chemically synthesised peptides

As previously mentioned in section 1.2, antimicrobial peptides are considered of great pharmacological potential both to overcome the antibiotic resistance plague and to develop next-generation cancer therapeutics.¹⁰ Furthermore, antimicrobial peptides can be chemically engineered to yield more effective drugs.

Chemically synthesised antimicrobial peptides. In 1996, a peptide library was synthesised with the general sequence [(BZZ)(BZZ)B]_n and [(BZZ)B(BZZ)]_n (where B = polar residue; Z = non-polar residue; n = 1 - 3) with the aim of obtaining new antimicrobial peptides.⁵² The rational *de novo* design of antimicrobial peptides with positive charged amphipathic α -helix as only structural starting point has been widely reported in literature.⁵³⁻⁵⁵ This approach derives from the fact that the majority of antimicrobial peptides possesses an amphipathic α -helix as the common motif and an overall positive charge at neutral pH.^{56, 57} The repetitive heptads approach was followed to formulate the general sequence of the library members.^{58, 59} Following cytotoxicity screening towards *E. coli*, *P. aeruginosa*, *S. aureus*, 3T3 (mouse fibroblasts) and human erythrocytes, the peptide sequence KLAKLAKKLAKLAK (**KLA**) was found to have the best activity against bacterial cells and the lowest activity against mammalian cells.

1.4.1 Anticancer applications of chemically synthesised antimicrobial peptides

In another section of this thesis, I will focus on testing new peptides conjugates targeting the mitochondria. In particular, in chapter 3 I will investigate the effect of conjugating a common fluorophore to existing mitochondriolytic peptides for improved potency. In chapter 4, I will explore the effect of adding a cancer targeting motif to the newly synthesised peptide conjugates.

Amongst the cellular organelles, the mitochondrion (Figure 1.10) probably stands out as the most appealing target for cancer therapies.⁶⁰ The mitochondrion hosts several putative drug targets for cancer therapy as the organelle plays key functions in various physiological and pathological cellular processes, such as programmed cellular death (i.e. apoptosis).⁶¹

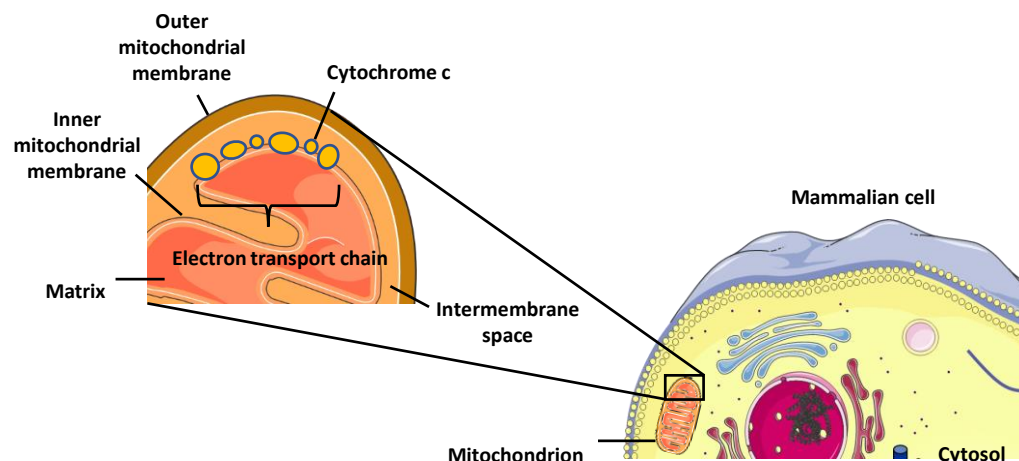


Figure 1.10. Section of a mammalian mitochondrion. The main components are highlighted: outer mitochondrial membrane, intermembrane space, inner mitochondrial membrane, matrix and the electron transport chain, a protein complex anchored to the inner membrane responsible for the mitochondrial membrane potential. Cytochrome c is a main player in the apoptosis triggering. Figure template provided by smart.servier.com.

Mitochondriolytic peptides. It was postulated that **KLA** would selectively interact with and destroy the mitochondrial membrane instead of mammalian cell membrane, in virtue of the overall positive charge of the peptide and the anionic nature of the mitochondrial membrane.⁶² Thus, the enantiomer of the peptide **KLA**, synthesised by using D-amino acids only (**kla**), was conjugated with tumour-homing peptide sequences CNRGC- or the RGD-4C sequence. The D-peptide and the tumour-homing peptide sequences were linked through a Gly-Gly spacer, to confer flexibility to the molecule. Both the constructs were able to kill KS1767 cells within 48 h at micromolar concentrations. Besides, the D-peptide without tumour-homing sequences was found to induce mitochondrial swelling and caspase-3 (a protein involved in apoptosis initiation) activation when incubated with isolated mitochondria.⁶²

In a later study,⁶³ the peptide was engineered by mutating its leucine residues to phenylalanine, (either D- or L-) cyclohexylalanine and 2-aminooctanoic acid. As a result, all the new constructs were found to be more cytotoxic than the parent sequence in the tested cell.

Other interesting efforts of chemical conjugation to mitochondriolytic peptides encompass the use of delocalised lipophilic cations⁶³⁻⁶⁷ and receptor-mediated molecules.^{68, 69}

Mitochondria delivery systems. Delocalised lipophilic cations are cationic molecules with a relatively high degree of lipophilicity; they exhibit specific mitochondrial targeting due to the unique negative membrane potential of the organelle (about -90 to -150 mV).⁶⁴ Therefore, these molecules can be exploited to deliver cargoes to mitochondria. Successful examples include triphenylphosphonium,⁶⁵ mitochondria-penetrating peptides⁷⁰ and cyanine dyes.^{66, 67} The latter case is worth a special mention. Because of their spectral properties, many cyanine dyes can report their subcellular localisation. This feature makes cyanine dyes very appealing in the chemical biology area as mitochondria-targeting molecules whose position can easily be tracked inside cells.

Folate-mediated delivery. Another effective way to enhance the biological potential of mitochondriolytic peptides is by selective delivery to cancer cells. This can be achieved via conjugation to receptor-mediated tumour-targeted drug delivery molecules.^{68, 69} One of the most reported examples of this class of molecules is folate. Since its discovery as a tumour-selective ligand,⁷¹ folate has been extensively used as a tumour-targeting moiety in drug delivery systems.⁷²⁻⁷⁴ This strategy takes advantage of the paucity or absence of the folate receptor from normal tissues to deliver chemotherapeutics to cancer cells via folate receptor α -mediated endocytosis.⁷⁵

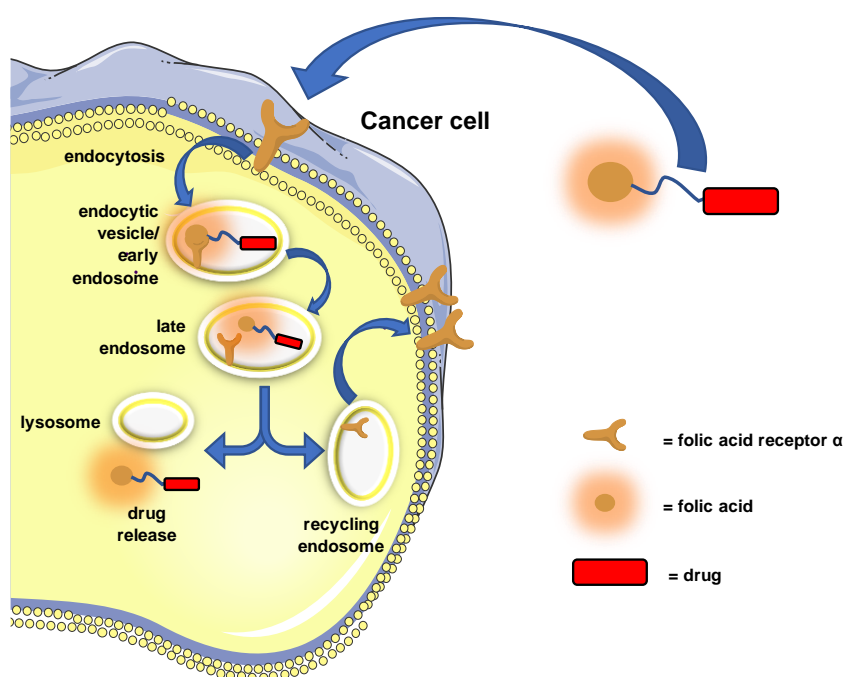


Figure 1.11. Folate receptor α -mediated endocytosis of a folate-conjugated drug. Figure template provided by smart.servier.com.

By this approach, the drug is usually covalently attached to folate by one of its two carboxylic groups. Once approached the cell expressing the folate receptor α on its membrane, the conjugate interacts with the receptor, triggering the invagination of the cell membrane. This event leads to the formation inside the cell of an early endosome, within which the receptor is still anchored to the membrane and tightly interacts with the drug conjugate. When the early endosome evolves into a late endosome, the pH inside the organelle reaches slightly lower values, which brings to the detachment of the drug conjugate from the receptor. Finally, the late endosome merges with the lysosome, where the drug can be released, and the recycling endosome brings the receptor back onto the cell surface (Figure 1.11).⁷²

1.5 Research aim and objectives

The aim of the present work is to give a contribution towards advancing the field of total chemical synthesis and biological applications of peptides.

Specific objectives are:

- developing a mild cleavage method for SPCL in C-to-N direction;
- synthesising and testing a new class of mitochondriolytic peptides;
- enhancing the tumour specificity of the newly prepared peptide conjugates.

CHAPTER 2

Solid-Phase Chemical Synthesis of Peptides and Proteins via Nickel-Assisted Cleavage

CHAPTER 2 - Solid-Phase Chemical Synthesis of Peptides and Proteins via Nickel-Assisted Cleavage

2.1 Abstract

The synthesis of proteins by solid-phase chemical ligation suffers from paucity of linkers that can be cleaved under mild conditions. Here, I deploy a peptide sequence, known to undergo spontaneous cleavage in presence of nickel (II), as a linker for the *C*-to-*N* synthesis of peptides/proteins on a solid-support.

2.2 Introduction

2.2.1 Nickel (II) as trigger of sequence-specific protein cleavage

During recombinant gene expression, proteins are often biosynthesised with different *C*- or *N*-terminal tags (i.e., His-tag, Ubiquitin-tag) to enhance solubility, facilitate their purification, improve expression yield, etc.⁷⁶ In certain cases, it is desirable to remove these tags to obtain the desired protein construct. The removal of the tags is often mediated by an enzyme,⁷⁷ or by chemical means such as BrCN,⁷⁸ or metal ions;⁷⁹⁻⁸¹ yet all these methods may be inconvenient. Enzymes sometimes fail to access the cleavage site between the protein and the tag, whereas chemical cleavages often involve harsh conditions, low sequence specificity and low expression yields.⁸²

To overcome these obstacles, the peptide sequence **-GSHHW-** was identified (following sequence optimisation from a phage display screening) and found to undergo spontaneous cleavage at the Gly-Ser junction, in presence of Ni²⁺ in aqueous buffer (Figure 2.1).⁸² When inserted before the protein of interest, this sequence, namely Spontaneous Nickel (II)-Assisted Cleavage (SNAC)-tag, was effective in removing different tags from proteins, even when enzymatic cleavages were unsuccessful.⁸²

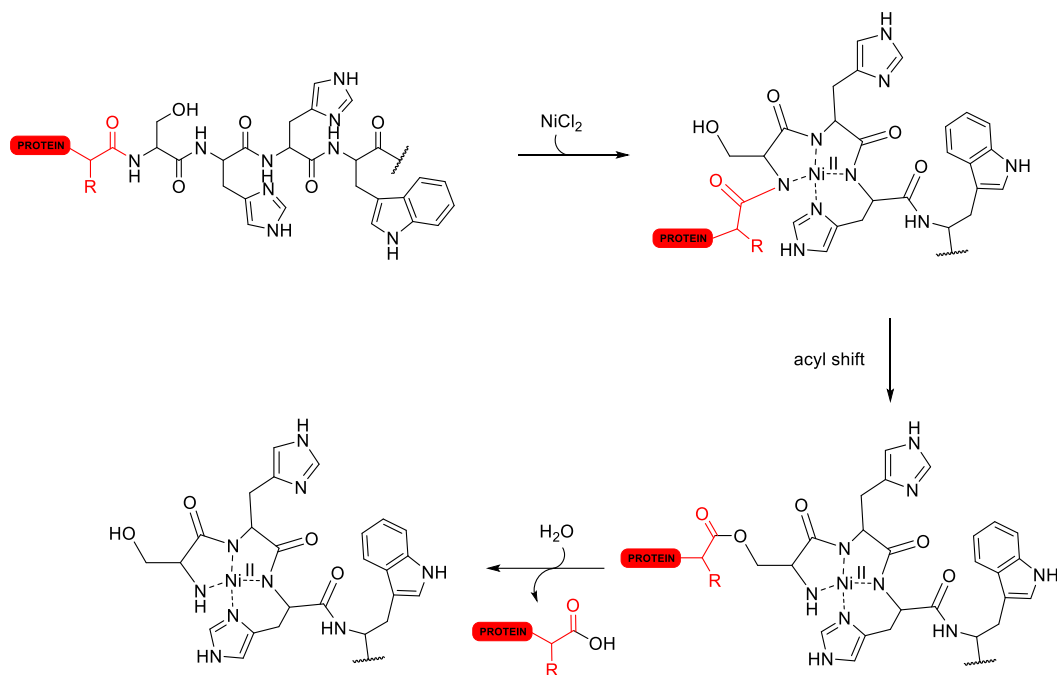


Figure 2.1. The proposed mechanism of SNAC and release of the target protein (in red).

2.2.2 Potential of SNAC in solid-phase synthesis of peptides and proteins

As already discussed in section 1.3.4, the desirability of SPCL derives from the necessity of avoiding time-consuming purification of the intermediates, which can also lead to poor yields.³⁸ Nonetheless, the choice of linkers that can be cleaved under mild conditions is very narrow.⁴⁵

The available methods reported for the cleavage of peptides/proteins from a solid support involve the use of TFA, NaOH, basic buffers with pH > 11 or nucleophiles such as NH_2OH and hydrazine (see section 1.3.4.1). Exceptions to these harsh cleavage conditions are represented by the phosphatase-labile linker (table 1.2, entry 4), which releases the protein from the solid support in PMP buffer (50 mM HEPES, 100 mM NaCl, 2 mM DTT, 0.01% Brij 35, 1 mM MnCl_2 , pH 7.5), at 30 °C, by the succinimide linker (Table 1.4, entry 5) and the photolabile 2-nitrobenzyl linker (Table 1.4, entry 6). Yet, the phosphatase-labile linker led to slow protein release over 6 days,⁸² and the succinimide linker involves the presence of a cysteine in the target protein.⁴⁸ Furthermore, both the phosphatase-labile linker and the photolabile linker require laborious organic chemical synthesis for their preparation.^{40, 49}

Being comprised of amino acid residues only, the SNAC-tag bears a great potential in solid-phase synthesis of peptides/proteins as a linker cleavable under mild conditions. In fact, it does not require organic chemical synthesis (it can be directly inserted into the sequence of the peptide segment by SPPS), nor does it release a protein containing a cysteine residue, which can often be undesirable.

2.3 Aim and Objectives

I aim to deploy the SNAC-tag as a linker cleavable under mild conditions for the release of peptides and proteins from a solid support.

Specific objectives are:

- Cleavage of a model peptide from a PEG-based resin;
- Assessment of the kinetics and efficiency of the SNAC for the model peptide;
- Synthesis of a model polypeptide and a ubiquitin derivative on a PEG-based resin by SPCL and cleavage of the target compound via SNAC.

2.4 Results and Discussion

2.4.1 SNAC of a model peptide from a solid support

To investigate the feasibility of the SNAC on a solid-support, a model peptide **1** bearing the SNAC-tag was synthesised via SPPS (see section 2.6.2) and ligated onto a PEG-based resin through SPCL (Figure 2.2A). The resin was equipped with a Rink Amide linker, to allow rapid cleavages and quantification of SNAC, and functionalised with a trialanine spacer, to allocate more space between the resin and the SNAC site. A thiazolidine residue was then coupled to the resin and converted into a cysteine, following the attachment of the peptide onto the solid support by SPCL. To assess the successful grafting of the model peptide on the resin, an analytical TFA cleavage was performed. LC/MS analysis of the TFA cleavage crude confirmed the desired ligation product **2**. The SNAC was then tested in the same buffer previously reported,⁸² at either room temperature or 40 °C for 24 h.

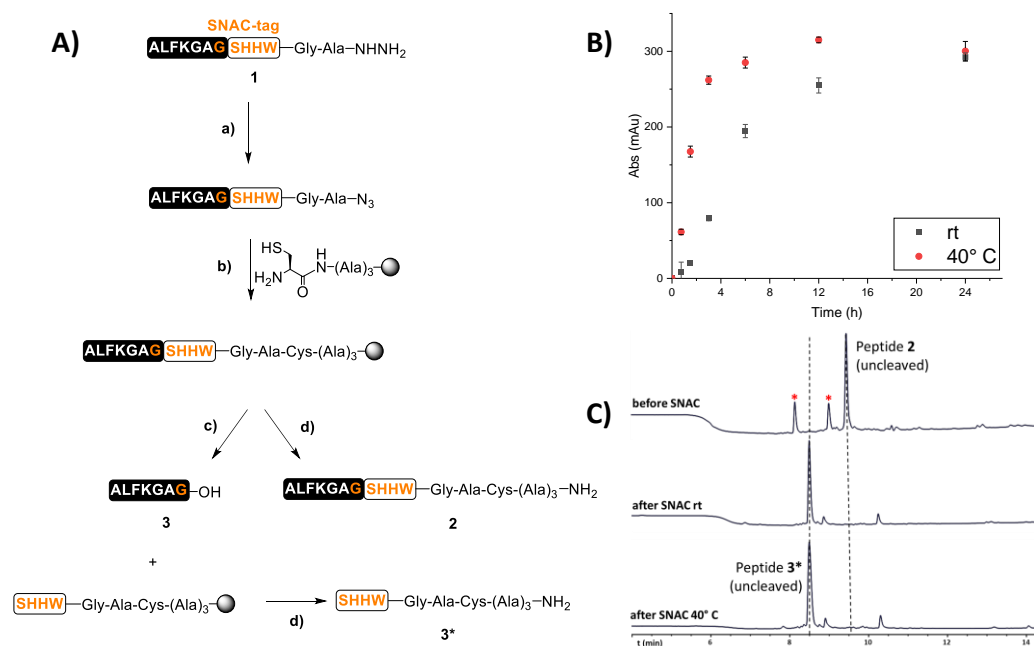


Figure 2.2. A) Model peptide-hydrazide **1** conversion into peptide-azide, its attachment to a solid support by NCL, to yield peptide **2**. SNAC afforded desired cleaved peptide **3**. a) 0.2 M K₂HPO₄, 6 M GdmCl, NaNO₂ (10 eq), pH 3, -20 °C, 15 min; b) MPAA (40 eq), TCEP 50 mM, pH 6.9, 16 h; c) NiCl₂·6H₂O (1 eq), 0.1 M CHES, 0.1 M NaCl, 0.1 M acetone oxyma, pH 8.6, 24 h, rt or 40 °C; d) TFA/H₂O/TIS/DODT 92.5:2.5:2.5:2.5, 1 h. B) Release of model peptide **3** from the resin via SNAC, quantified by integrating the peak area corresponding to peptide **3** from the 214 nm LC chromatogram trace of the cleavage at different time points. C) LC chromatograms recorded at 280 nm of TFA cleavages of model peptide before and after SNAC. * oxidised product.

The release of peptide **3** was monitored by LC/MS and its UV absorbance at 214 nm was recorded after 0, 0.75, 1.5, 3, 6, 12 and 24 hours from the start of the SNAC (Figure 2.2B). As a result, the same amount of peptide was released, but the rate of the cleavage performed at 40 °C was higher than the one at room temperature.

After 24 h, a TFA cleavage was performed to check for cleaved or uncleaved peptide still on the resin after the SNAC. Gratifyingly, while a peak corresponding to the cleaved peptide **3*** was found, no uncleaved peptide **2** could be detected (Figure 2.2C).

2.4.2 SPCL of a model polypeptide

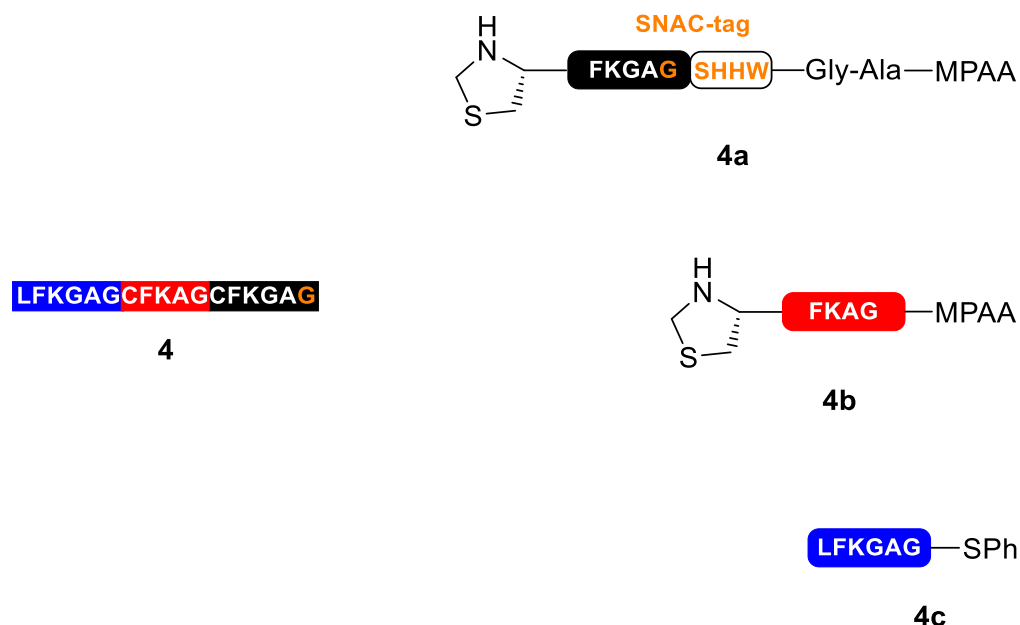
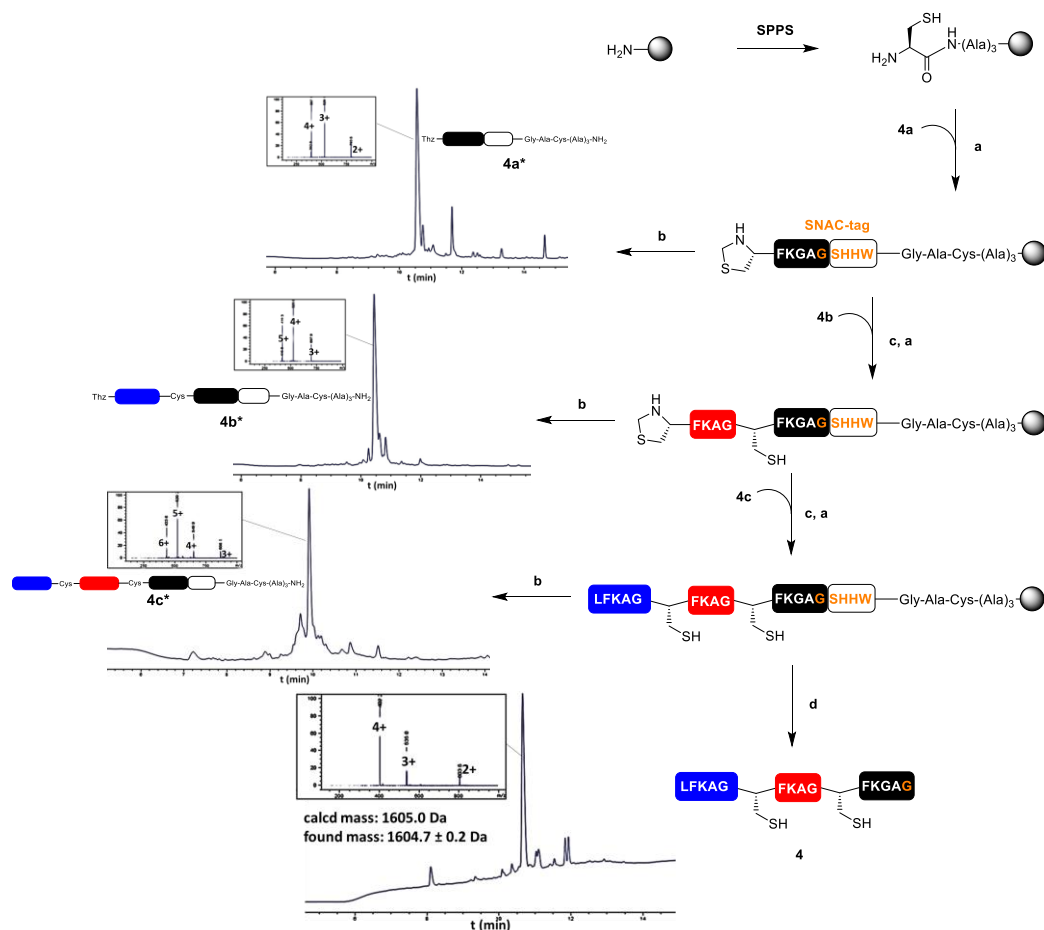


Figure 2.3. Sequence of model polypeptide **4** (left). Model polypeptide **4** was split in three peptide blocks **4a-c** (right), which are then assembled via SPCL.

For the preparation of compound **4**, peptide blocks **4a-c** (Figure 2.3) were synthesised by SPPS (see sections 2.6.4-6). Rink Amide ChemMatrix resin was chosen as water-compatible support and functionalised with a trialanine spacer and a thiazolidine residue, to allow SPCL of the first peptide block **4a** to the resin (Scheme 2.1). Following unmasking of the N-terminal cysteine residue, blocks **4b** and **4c** were sequentially ligated in the same fashion. Then, SNAC was carried out for 24 h at 40 °C, followed by addition of TCEP. The reaction resulted in 97% of cleavage of the peptide from the resin (see supplementary figure 2.1 in section 2.6.10) and afforded peptide **4** in 34% yield (not isolated, calculated via integration of the corresponding peak at the LC/MS chromatogram recorded at 214 nm. See supplementary figure 2.2 in section 2.6.10 for calibration curve.).



Scheme 2.1. Synthetic scheme for the preparation of model polypeptide **4** with LC/MS traces of the intermediates recorded at 280 nm of the analytical TFA cleavages. LC/MS trace recorded at 214 nm of the crude cleavage mixture was obtained after incubation of the resin with SNAC buffer for 24 h at 40 °C. a) 0.2 M K₂HPO₄, 6 M GdnHCl, 0.2 M MPAA, 50 mM TCEP, pH 6.9, 16 h; b) TFA/H₂O/TIS/DODT 92.5:2.5:2.5:2.5, 1 h; c) 0.4 M MeONH₂, 25 mM TCEP, 40 °C, 16 h; d) i. NiCl₂·6H₂O (4 eq), 0.1 M CHES, 0.1 M NaCl, 0.1 M acetone oxyma, pH 8.6, 24 h, 40 °C; ii. 0.1 M TCEP, 30 min, 40 °C.

2.4.3 Proof of Concept: SPCL of a ubiquitin derivative using SNAC

Towards assessing the use of the SNAC-tag for the cleavage of proteins from a solid-support, I sought to synthesise ubiquitin by SPCL.

Ubiquitin is a 8.6 kDa protein which is found “*ubiquitously*” in eukaryotic cells, where carries out regulatory tasks in several processes.⁸³ Its most well-known function is the regulation of protein degradation: when one or more ubiquitin molecules is enzymatically attached to a protein, the protein is delivered to the proteasome complex, where it is degraded and recycled.⁸³

As a small protein whose synthesis is well established, ubiquitin is often used as a model for the development of new synthetic procedures.^{48, 84-86}

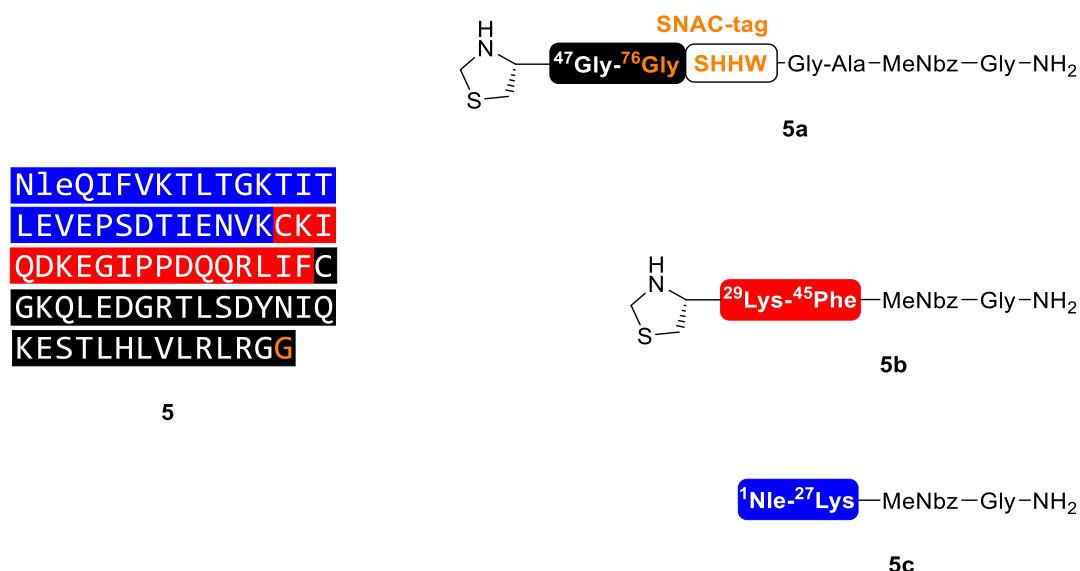
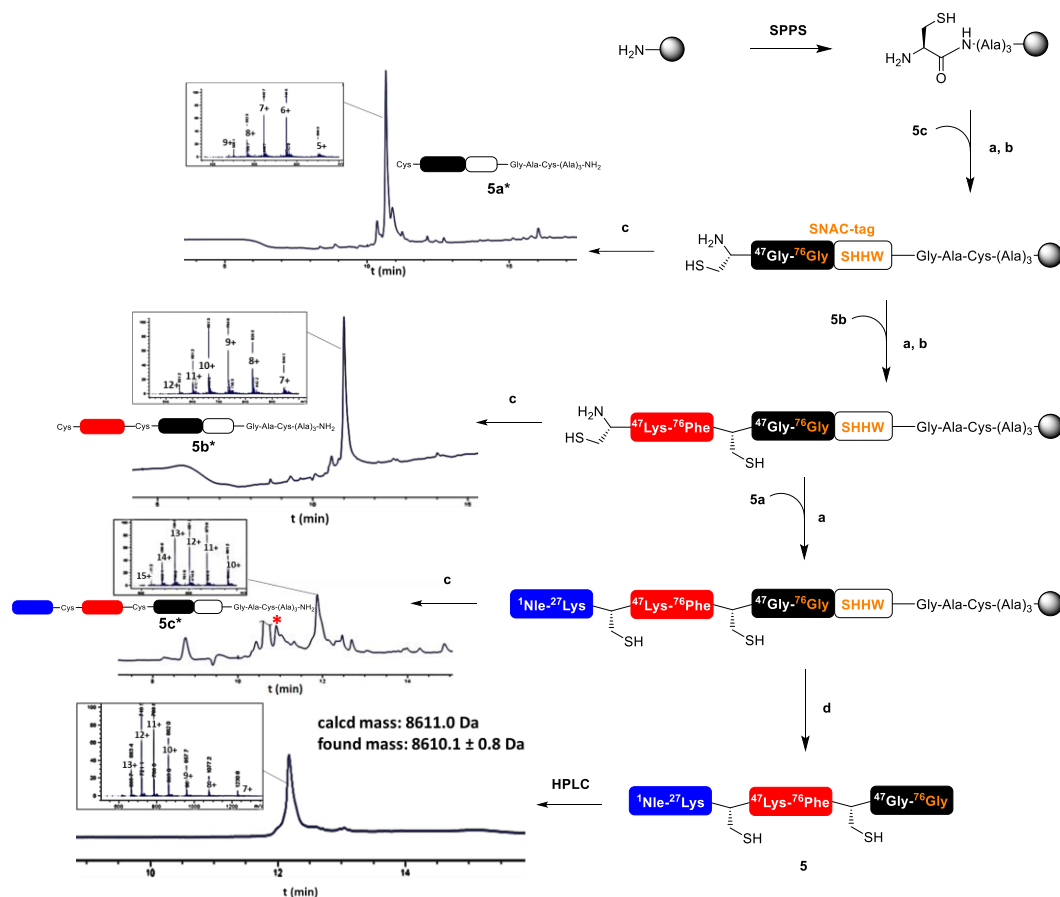


Figure 2.4. Sequence of ubiquitin derivative **5** (left). Ubiquitin derivative **5** was split in three peptide blocks **5a-c** (right), which are then assembled on a solid support via SPCL.

For its preparation, ubiquitin sequence was mutated by replacing Met1 with norleucine (to avoid oxidative side-reactions at the methionine sulphur) and Ala28 and Ala46 with cysteine residues (to provide reaction sites for NCL). Peptides **5a-c** were synthesised by SPPS (see sections 2.6.7-9) and served as building blocks for the synthesis of the target protein (Figure 2.4). Rink Amide PEGA resin was chosen as water-compatible support and functionalised with a trialanine spacer and a thiazolidine residue, to allow attachment of the first peptide block **5a** to the resin (Scheme 2.2). Following unmasking of the *N*-terminal cysteine residue, blocks **5b** and **5c** were sequentially ligated in the same fashion. Then, SNAC was carried out for 24 h at 40 °C, followed by addition of TCEP to afford ubiquitin derivative **5** in 7% isolated yield.



Scheme 2.2. Synthetic scheme for the preparation of ubiquitin derivative **5** with LC/MS traces of the intermediates recorded at 280 nm of the analytical TFA cleavages. LC/MS trace for the cleaved product **5** was obtained after incubation of the resin with SNAC buffer for 24 h at 40 °C, followed by HPLC purification. a) 0.2 M K₂HPO₄, 6 M GdmCl, 0.2 M MPAA, 50 mM TCEP, pH 6.9, 16 h (SPCL is repeated twice); b) 0.4 M MeONH₂, 25 mM TCEP, 40 °C, 16 h; c) TFA/H₂O/TIS/DODT 92.5:2.5:2.5:2.5, 1 h; d) i. NiCl₂·6H₂O (1 eq), 0.1 M CHES, 0.1 M NaCl, 0.1 M acetone oxyma, pH 8.6, 24 h, 40 °C; ii. 0.1 M TCEP, 30 min, 40 °C. * denotes unreacted intermediate **5b***.

One reason for the lower yield when compared to the other reported SPCL protocols is attributed to partial conversion of **5b*** to **5c***, as unreacted intermediate **5b*** was detected by the LC/MS of the analytical cleavage after the ligation reaction (scheme 2.3). The decreased ligation performance, when the size of the immobilised protein or peptide intermediate increases, is in fact a well-known limitation of SPCL syntheses.^{17, 37, 44, 45} Furthermore, after the SNAC, cleavage was not complete, as uncleaved protein could be detected by the LC/MS following an analytical TFA cleavage (see supplementary figure 2.3 in section 2.6.10). Interestingly, along with the uncleaved protein, product **5** was also found (see supplementary figure 2.3 in section 2.6.10). The presence of the ubiquitin derivative **5** in the TFA cleavage is probably due to the interaction between the

PEG-based resin and the target compound. After the SNAC, the protein could be extracted by the organic acid, rather than cleaved. Protein-resin interaction, broken by TFA after total synthesis of a protein by SPCL is in fact already reported in the literature.¹⁷

2.5 Conclusion and Perspectives

SPCL emerges from the idea to allow NCL reaction on solid supports like those used in SPPS, thus overcoming some of the hurdles of protein synthesis in solution.³⁷ As for SPPS, SPCL relies on cleavable linkers to release the desired product from the resin, and to allow its isolation. Thus far, most of the cleavable linkers require harsh conditions for the release of the product from the solid support:^{37-39, 41, 46} this hampers the preparation of constructs bearing labile chemical motifs, or of proteins in their native conformations. Here, we began to explore the suitability of the SNAC-tag⁸² as a linker that can be cleaved in relatively mild conditions, without the need for chemical synthesis for its preparation and of a cysteine residue in the target sequence. Constructs of different length were synthesised on PEG-based resins, with or without a Rink Amide linker. In all cases, the SNAC buffer led to the cleavage of the desired sequence from the tag-functionalised resin. Incomplete cleavage of the ubiquitin derivative still leave room for optimisation of the SNAC. The results suggest that the cleavage of bigger constructs, such as compound **5**, might need more SNAC iterations, or adjustment of the number of equivalents of NiCl₂. Furthermore, particular attention will be needed to improve the release of the protein of interest from the resin, in case of interaction with the solid support. Finally, tolerance of the SNAC towards C-terminal amino acid residues should be explored in constructs that range from small peptides to bigger proteins. Although I regard the addition of a C-terminal glycine to a protein sequence as a reasonable modification, a thorough scope will allow accessing constructs with different C-terminal residues. We envision that the described SNAC technology will be complementary to the existing mild cleavage techniques in enabling the preparation of peptides and proteins bearing base- and acid-labile modifications and provide a tool for solid-phase assisted folding of proteins and their release in a folded state.

2.6 Experimental Section

General Methods. Solid Phase Peptide Syntheses were performed on a CEM Liberty Blue™ Automated Microwave Peptide Synthesizer and in TELOS Filtration Columns equipped with 20 µm polyethylene frits. Reaction temperatures are stated as heating device temperature of the synthesiser, if not otherwise stated. Deionized water was obtained by an Elga PURELAB 8 Option system (15 MΩ·cm). Reagents obtained from commercial suppliers were used without further purification unless otherwise stated. Protected amino acids, Rink Amide MBHA resin, DIC, oxyma pure, piperazine, trifluoroacetic acid and triisopropylsilane (TIS) were purchased from Fluorochem. Fmoc-MeDbz-OH was purchased from Iris Biotech GmbH. DMF was purchased from Fisher Scientific. Fmoc-Asp(OtBu)-(Dmb)Gly-OH, Rink Amide ProTide (LL) and Cl-TCP(Cl) ProTide resins were purchased from CEM Corporation. For HPLC mobile phase, HPLC grade CH₃CN from Fisher Scientific and trifluoroacetic acid from Fluorochem were used. For LC/MS mobile phase, LC/MS grade water and CH₃CN from Fisher Scientific and formic acid from Fisher Scientific were used. Reagents were used without further purification unless otherwise noted. LC/MS was performed on an Agilent 1260 Infinity II HPLC system, equipped with an ACE 3 C18, 2.1 x 100 mm, particle size 3 µm, pore size 300 Å and connected to a 6120 Quadrupole MS. Preparative HPLC was performed on a LC20-AR Shimadzu HPLC system equipped with either a Vydac 208TP C8, 22 x 250 mm, particle size 10 µm, pore size 300 Å or a Shim-pack GIST C18, 20 x 150 mm, particle size 5 µm, pore size 100 Å and semi-preparative HPLC was performed on an Agilent 1206 Infinity HPLC system equipped with either a Zorbax-300SB C8, 4.6 x 150 mm, particle size 5 µm, pore size 300 Å or with an ACE C18, 10.0 x 250 mm, particle size 5 µm, pore size 100 Å. Determinations of PEGA, and ChemMatrix resins loading and ubiquitin derivative yield were conducted using a ThermoFisher NanoDrop ND-ONE-W spectrophotometer. Absorbance values were measured in 10 mm path-length cuvettes (Fisher Scientific, #11847832). For SPPS MW cycle and method descriptions of CEM Liberty Blue™ Automated Microwave Peptide Synthesizer, see Appendix.

2.6.1 SPPS procedure for peptide 1

Synthesis scale: 0.1 mmol. Resin: Cl-TCP(Cl) ProTide, loading 0.4 mmol/g – 250 mg. DIC concentration in DMF: 1 M. HOBt concentration in DMF: 1 M. Deprotection cocktail: 20% (v/v) piperidine in DMF + 1% (v/v) formic acid. Fmoc-amino acids in DMF: 0.33 M. Prior to the start of the automated synthesis, the resin was swollen in DMF for 5 min at rt and functionalised with hydrazine hydrate following the previously reported procedure.⁴²

Reagent	Method	Reagent concentration during coupling step (mM)
Fmoc-Ala-OH	5	167
Fmoc-Gly-OH	4	167
Fmoc-Trp(Boc)-OH	4	167
Fmoc-His(Trt)-OH	3	220
Fmoc-His(Trt)-OH	2	220
Fmoc-Ser(tBu)-OH	1	167
Fmoc-Gly-OH	1	167
Fmoc-Ala-OH	1	167
Fmoc-Gly-OH	1	167
Fmoc-Lys(Boc)-OH	1	167
Fmoc-Phe-OH	1	167
Fmoc-Leu-OH	1	167
Fmoc-Ala-OH	1	167

The last coupling is followed by a deprotection step, performed using 4 mL of deprotection cocktail with MW cycle 14. Cleavage was done with 10 mL of TFA/water/TIS (95:2.5:2.5) for 2 h. The resin was removed by filtration and the filtrate was concentrated by N₂ flow. The crude product was precipitated with cold diethyl ether, centrifuged (4,000 g for 10 min) and the supernatant was discarded. The precipitate was dissolved in water + 0.1% TFA and purified by HPLC. Product was characterised at the LC/MS (Figure 2.5).

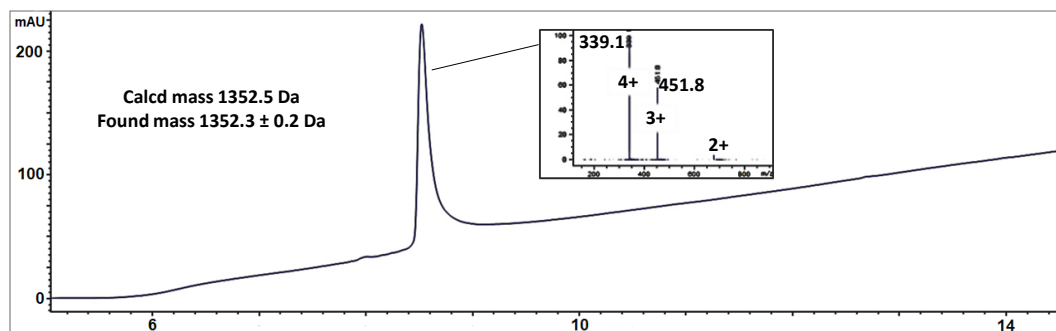


Figure 2.5. LC chromatogram recorded at 214 nm (+ mass spectrum of the indicated peak) of peptide **1**. Column: *ACE 3 C18*, 2.1 x 100 mm, 3 µm particle size, 300 Å pore size; Method: flow rate = 0.5 mL · min⁻¹, H₂O: CH₃CN, 0.1% HCOOH, 95:5 for 2 min → 95:5 to 43:57 over 13 min → 5:95 for 7 min.

2.6.2 SPPS procedure for polypeptide H-LFKAGCFKAGCFKGAG-NH₂ for calibration curve

Synthesis scale: 0.1 mmol. Resin: Rink Amide MBHA, loading 0.49 mmol/g – 204 mg. DIC concentration in DMF: 0.5 M. Oxyma pure concentration in DMF: 1 M. Deprotection cocktail: 20% (v/v) piperidine in DMF. Fmoc-amino acids in DMF: 0.2 M. Prior to the start of the synthesis, the resin was swollen in the reaction vessel of the automated synthesiser using 5 mL of DMF for 5 min at rt.

Reagent	Method	Reagent concentration during coupling step (mM)
Fmoc-Gly-OH	6	100
Fmoc-Ala-OH	6	100
Fmoc-Gly-OH	6	100
Fmoc-Lys(Boc)-OH	6	100
Fmoc-Phe-OH	6	100
Fmoc-Cys(Trt)-OH	7	100
Fmoc-Gly-OH	6	100
Fmoc-Ala-OH	6	100
Fmoc-Lys(Boc)-OH	6	100
Fmoc-Phe-OH	6	100
Fmoc-Cys(Trt)-OH	7	100
Fmoc-Gly-OH	6	100
Fmoc-Ala-OH	6	100

Fmoc-Lys(Boc)-OH	6	100
Fmoc-Phe-OH	6	100
Fmoc-Leu-OH	6	100

The last coupling was followed by a deprotection step, performed using 4 mL of deprotection cocktail with MW cycle 14. Cleavage was done with 10 mL of TFA/water/TIS/DODT (92.2:2.5:5:2.5:2.5) for 2 h. The resin was removed by filtration and the filtrate was concentrated by N₂ flow. The crude product was precipitated with cold diethyl ether, centrifuged (4,000 g for 10 min) and the supernatant was discarded. The precipitate was dissolved in water + 0.1% TFA and purified by HPLC. Product was characterised by LC/MS (Figure 2.6).

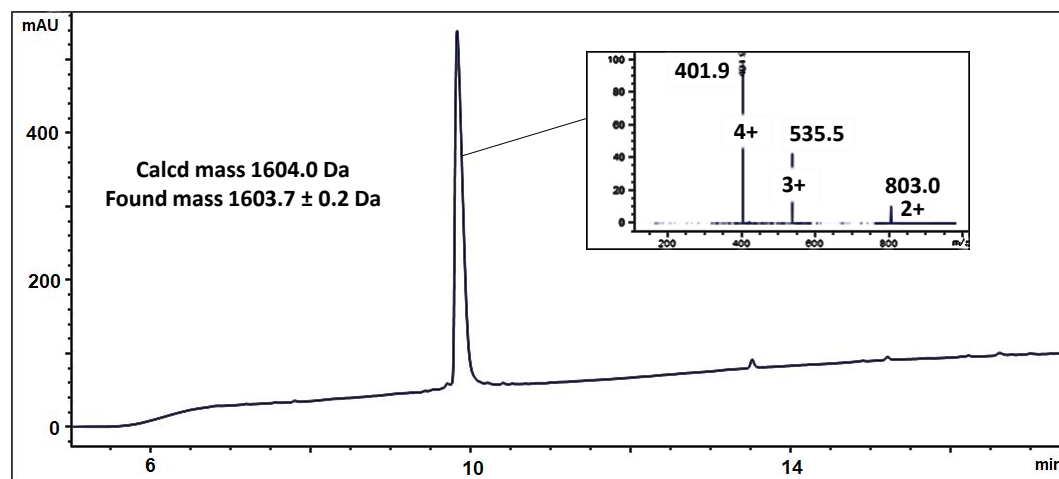


Figure 2.6. LC chromatogram recorded at 214 nm (+ mass spectrum of the indicated peak) of polypeptide **H-LFKAGCFKAGCFKGAG-NH₂**. Column: *ACE 3 C18*, 2.1 x 100 mm, 3 μ m particle size, 300 Å pore size; Method: flow rate = 0.5 mL · min⁻¹, H₂O: CH₃CN, 0.1% HCOOH, 95:5 for 2 min → 95:5 to 43:57 over 13 min → 5:95 for 7 min.

2.6.3 SPPS procedure for peptide 4a

Synthesis scale: 0.1 mmol. Resin: Cl-TCP(Cl) ProTide, loading 0.4 mmol/g – 250 mg. DIC concentration in DMF: 1 M. HOBt concentration in DMF: 1 M. Deprotection cocktail: 20% (v/v) piperidine in DMF + 1% (v/v) formic acid. Fmoc-amino acids in DMF: 0.33 M. Prior to the start of the automated synthesis, the resin was swollen in DMF for 5 min at rt and functionalised with hydrazine hydrate following the previously reported procedure.⁴²

Reagent	Method	Reagent concentration during coupling step (mM)
Fmoc-Ala-OH	5	167
Fmoc-Gly-OH	4	167
Fmoc-Trp(Boc)-OH	4	167
Fmoc-His(Trt)-OH	3	220
Fmoc-His(Trt)-OH	2	220
Fmoc-Ser(tBu)-OH	1	167
Fmoc-Gly-OH	1	167
Fmoc-Ala-OH	1	167
Fmoc-Gly-OH	1	167
Fmoc-Lys(Boc)-OH	1	167
Fmoc-Phe-OH	1	167
Fmoc-Leu-OH	1	167
Fmoc-Thz-OH	1	167

The last coupling was followed by a deprotection step, performed using 4 mL of deprotection cocktail with MW cycle 14. Cleavage was done with 10 mL of TFA/water/TIS (95:2.5:2.5) for 2 h. The resin was removed by filtration and the filtrate was concentrated by N₂ flow. The crude product was precipitated with cold diethyl ether, centrifuged (4,000 g for 10 min) and the supernatant was discarded. The precipitate was dissolved in 0.2 M phosphate buffer, containing 6 M GdmCl and the crude product was converted into the corresponding MPAA thioester as previously described.⁸⁷ The desired product was then isolated by HPLC. Product was characterised at the LC/MS (Figure 2.7).

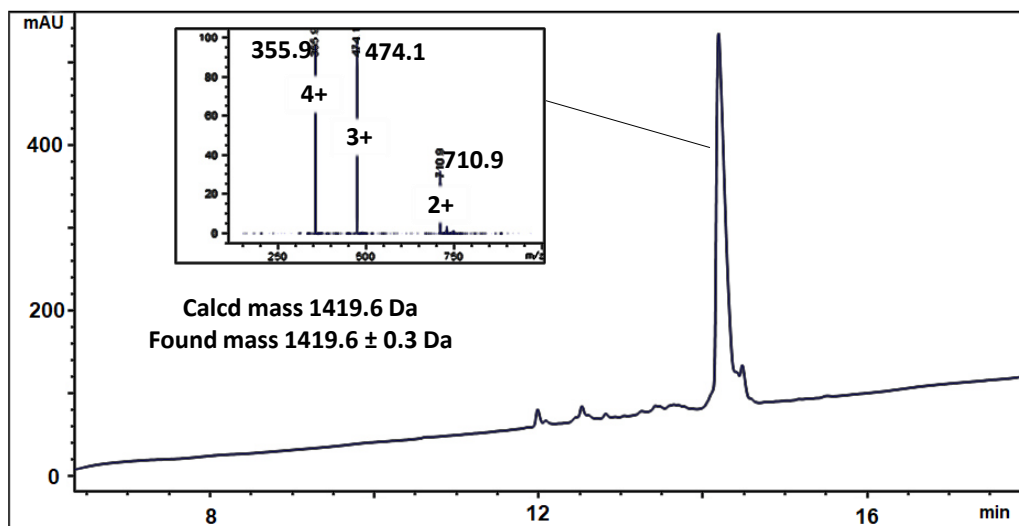


Figure 2.7. LC chromatogram recorded at 214 nm (+ mass spectrum of the indicated peak) of peptide **4a**. Column: *ACE 3 C18*, 2.1 x 100 mm, 3 μ m particle size, 300 Å pore size; Method: flow rate = 0.5 mL \cdot min⁻¹, H₂O: CH₃CN, 0.1% HCOOH, 95:5 for 2 min → 95:5 to 43:57 over 13 min → 5:95 for 7 min.

2.6.4 SPPS procedure for peptide **4b**

Synthesis scale: 0.1 mmol. Resin: Cl-TCP(Cl) ProTide, loading 0.4 mmol/g – 250 mg. DIC concentration in DMF: 1 M. HOBt concentration in DMF: 1 M. Deprotection cocktail: 20% (v/v) piperidine in DMF + 1% (v/v) formic acid. Fmoc-amino acids in DMF: 0.33 M. Prior to the start of the automated synthesis, the resin was swollen in DMF for 5 min at rt and functionalised with hydrazine hydrate following the previously reported procedure.⁴²

Reagent	Method	Reagent concentration during coupling step (mM)
Fmoc-Gly-OH	6	100
Fmoc-Ala-OH	6	100
Fmoc-Lys(Boc)-OH	6	100
Fmoc-Phe-OH	6	100
Fmoc-Thz-OH	7	100

The last coupling was followed by a deprotection step, performed using 4 mL of deprotection cocktail with MW cycle 14. Cleavage was done with 10 mL of

TFA/water/TIS (95:2.5:2.5) for 2 h. The resin was removed by filtration and the filtrate was concentrated by N₂ flow. The crude product was precipitated with cold diethyl ether, centrifuged (4,000 g for 10 min) and the supernatant was discarded. The precipitate was dissolved in 0.2 M phosphate buffer, containing 6 M GdmCl and the crude product was converted into the corresponding thiophenol thioester as previously described.⁸⁷ The desired product was then isolated by HPLC. Product was characterised by LC/MS (Figure 2.8).

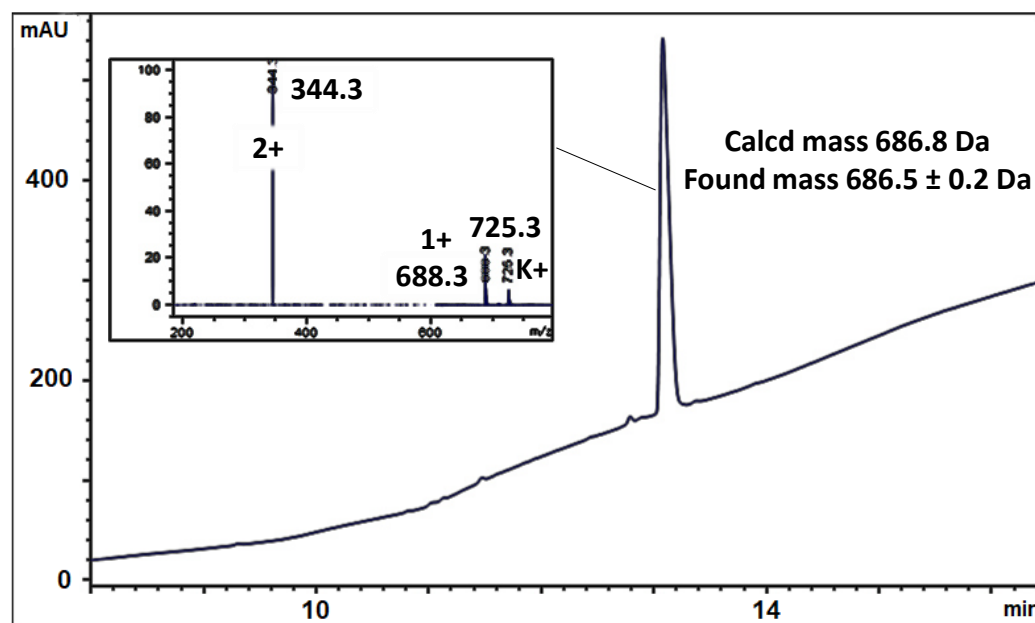


Figure 2.8. LC chromatogram recorded at 214 nm (+ mass spectrum of the indicated peak) of peptide **4b**. Column: ACE 3 C18, 2.1 x 100 mm, 3 µm particle size, 300 Å pore size; Method: flow rate = 0.5 mL · min⁻¹, H₂O: CH₃CN, 0.1% HCOOH, 95:5 for 2 min → 95:5 to 43:57 over 13 min → 5:95 for 7 min.

2.6.5 SPPS procedure for peptide **4c**

Synthesis scale: 0.1 mmol. Resin: Cl-TCP(Cl) ProTide, loading 0.4 mmol/g – 250 mg. DIC concentration in DMF: 1 M. HOBt concentration in DMF: 1 M. Deprotection cocktail: 20% (v/v) piperidine in DMF + 1% (v/v) formic acid. Fmoc-amino acids in DMF: 0.33 M. Prior to the start of the automated synthesis, the resin was swollen in DMF for 5 min at rt and functionalised with hydrazine hydrate following the previously reported procedure.⁴²

Reagent	Method	Reagent concentration during coupling step (mM)
Fmoc-Gly-OH	6	100
Fmoc-Ala-OH	6	100
Fmoc-Lys(Boc)-OH	6	100
Fmoc-Phe-OH	6	100
Fmoc-Leu-OH	6	100

The last coupling is followed by a deprotection step, performed using 4 mL of deprotection cocktail with MW cycle 14. Cleavage was done with 10 mL of TFA/water/TIS (95:2.5:2.5) for 2 h. The resin was removed by filtration and the filtrate was concentrated by N₂ flow. The crude product was precipitated with cold diethyl ether, centrifuged (4,000 g for 10 min) and the supernatant was discarded. The precipitate was dissolved in 0.2 M phosphate buffer, containing 6 M GdmCl and the crude product was converted into the corresponding thiophenol thioester as previously described.⁴² The desired product was then isolated by HPLC. Product was characterised by LC/MS (Figure 2.9).

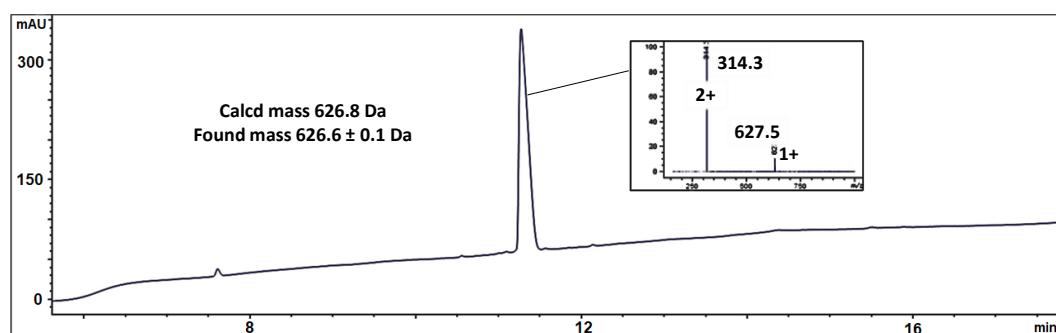


Figure 2.9. LC chromatogram recorded at 214 nm (+ mass spectrum of the indicated peak) of peptide **4c**. Column: *ACE 3 C18*, 2.1 x 100 mm, 3 µm particle size, 300 Å pore size; Method: flow rate = 0.5 mL · min⁻¹, H₂O: CH₃CN, 0.1% HCOOH, 95:5 for 2 min → 95:5 to 43:57 over 13 min → 5:95 for 7 min.

2.6.6 SPPS procedure for peptide 5a

Synthesis scale: 0.05 mmol. Resin: Rink Amide ProTide Resin (LL), loading 0.19 mmol/g – 263 mg. HATU concentration in DMF: 0.5 M. DIPEA concentration in NMP: 2 M. Deprotection cocktail: 20% (v/v) piperidine in DMF + 1% (v/v) formic

acid. Fmoc-MeDbz-OH in DMF: 0.05 M. Fmoc-Asp(OtBu)-(Dmb)Gly-OH in DMF: 0.15 M. Amino acids in DMF: 0.33 M. Prior to the start of the synthesis, the resin was swollen in the reaction vessel of the automated synthesiser using 5 mL of DMF for 5 min at rt.

Reagent	Method	Reagent concentration during coupling step (mM)
Fmoc-Gly-OH	20	167
Fmoc-MeDbz-OH	14	35
Fmoc-Ala-OH	20	167
Fmoc-Gly-OH	21	167
Fmoc-Trp(Boc)-OH	20	167
Fmoc-His(Trt)-OH	20	167
Fmoc-His(Trt)-OH	19	167
Fmoc-Ser(tBu)-OH	18	167
Fmoc-Gly-OH	17	167
Fmoc-Gly-OH	17	167
Fmoc-Arg(Pbf)-OH	16	167
Fmoc-Leu-OH	16	167
Fmoc-Arg(Pbf)-OH	16	167
Fmoc-Leu-OH	16	167
Fmoc-Val-OH	16	167
Fmoc-Leu-OH	16	167
Fmoc-His(Trt)-OH	16	167
Fmoc-Leu-OH	16	167
Fmoc-Thr(tBu)-OH	8	167
Fmoc-Ser(tBu)-OH	8	167
Fmoc-Glu(OtBu)-OH	8	167
Fmoc-Lys(Boc)-OH	8	167
Fmoc-Gln(Trt)-OH	8	167
Fmoc-Ile-OH	8	167
Fmoc-Asn(Trt)-OH	8	167
Fmoc-Tyr(tBu)-OH	8	167
Fmoc-Asp(OtBu)-OH	8	167

Fmoc-Ser(tBu)-OH	8	167
Fmoc-Leu-OH	8	167
Fmoc-Thr(tBu)-OH	8	167
Fmoc-Arg(Pbf)-OH	8	167
Fmoc-Asp(OtBu)-(Dmb)Gly-OH	15	107
Fmoc-Glu(OtBu)-OH	8	167
Fmoc-Leu-OH	8	167
Fmoc-Gln(Trt)-OH	8	167
Fmoc-Lys(Boc)-OH	8	167
Fmoc-Gly-OH	8	167
Boc-Thz-OH	8	167

After the last coupling, the MeDbz group was activated into MeNbz by incubating the resin with 5 equivalents of 4-nitrophenyl chloroformate in DCM (3 x 30 min), followed by 0.5 M DIPEA in DMF (3 x 10 min). Cleavage was done with 10 mL of TFA/water/TIS (95:2.5:2.5) for 2 h. The resin was removed by filtration and the filtrate was concentrated by N₂ flow. The crude product was precipitated with cold diethyl ether, centrifuged (4,000 g for 10 min) and the supernatant was discarded. The precipitate was dissolved in water/acetonitrile (1:1) + 0.1% TFA and purified by HPLC. Product was characterised by LC/MS (Figure 2.10).

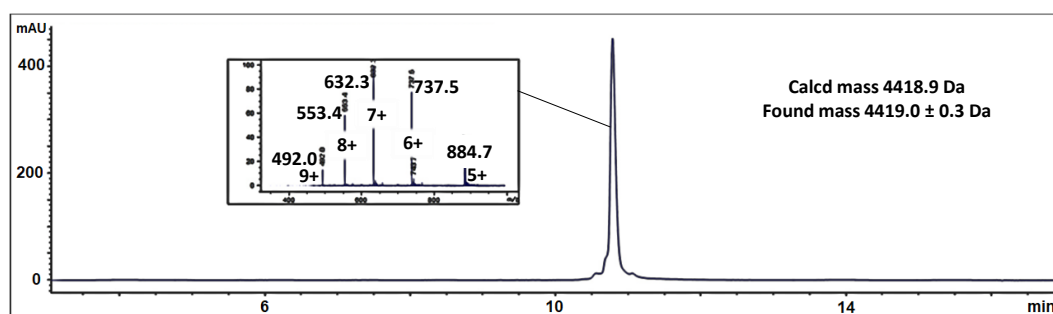


Figure 2.10. LC chromatogram recorded at 214 nm (+ mass spectrum of the indicated peak) of peptide **5a**. Column: ACE 3 C18, 2.1 x 100 mm, 3 µm particle size, 300 Å pore size; Method: flow rate = 0.5 mL · min⁻¹, H₂O: CH₃CN, 0.1% HCOOH, 95:5 for 2 min → 95:5 to 55:45 over 10 min → 5:95 for 5 min.

2.6.7 SPPS procedure for peptide 5b

Synthesis scale: 0.05 mmol. Resin: Rink Amide ProTide Resin (LL), loading 0.19 mmol/g – 263 mg. DIC concentration in DMF: 1 M. HOBT concentration in DMF: 1 M. Deprotection cocktail: 20% (v/v) piperidine in DMF + 1% (v/v) formic acid. Fmoc-MeDbz-OH in DMF: 0.05 M. Amino acids in DMF: 0.33 M. Prior to the start of the synthesis, the resin was swollen in the reaction vessel of the automated synthesiser using 5 mL of DMF for 5 min at rt.

Reagent	Method	Reagent concentration during coupling step (mM)
Fmoc-Gly-OH	22	167
Fmoc-MeDbz-OH	22	35
Fmoc-Phe-OH	22	167
Fmoc-Ile-OH	22	167
Fmoc-Leu-OH	22	167
Fmoc-Arg(Pbf)-OH	22	167
Fmoc-Gln(Trt)-OH	22	167
Fmoc-Gln(Trt)-OH	22	167
Fmoc-Asp(OtBu)-OH	22	167
Fmoc-Pro-OH	23	167
Fmoc-Pro-OH	23	167
Fmoc-Ile-OH	24	167
Fmoc-Gly-OH	24	167
Fmoc-Glu(OtBu)-OH	24	167
Fmoc-Lys(Boc)-OH	24	167
Fmoc-Asp(OtBu)-OH	24	167
Fmoc-Gln(Trt)-OH	24	167
Fmoc-Ile-OH	24	167
Fmoc-Lys(Boc)-OH	24	167
Boc-Thz-OH	24	167

After the last coupling, the MeDbz group was activated into MeNbz by incubating the resin with 5 equivalents of 4-nitrophenyl chloroformate in DCM (3 x 30 min),

followed by 0.5 M DIPEA in DMF (3 x 10 min). Cleavage was done with 10 mL of TFA/water/TIS (95:2.5:2.5) for 2 h. The resin was removed by filtration and the filtrate was concentrated by N₂ flow. The crude product was precipitated with cold diethyl ether, centrifuged (4,000 g for 10 min) and the supernatant was discarded. The precipitate was dissolved in water/acetonitrile (1:1) + 0.1% TFA and purified by HPLC. Product was characterised by LC/MS (Figure 2.11).

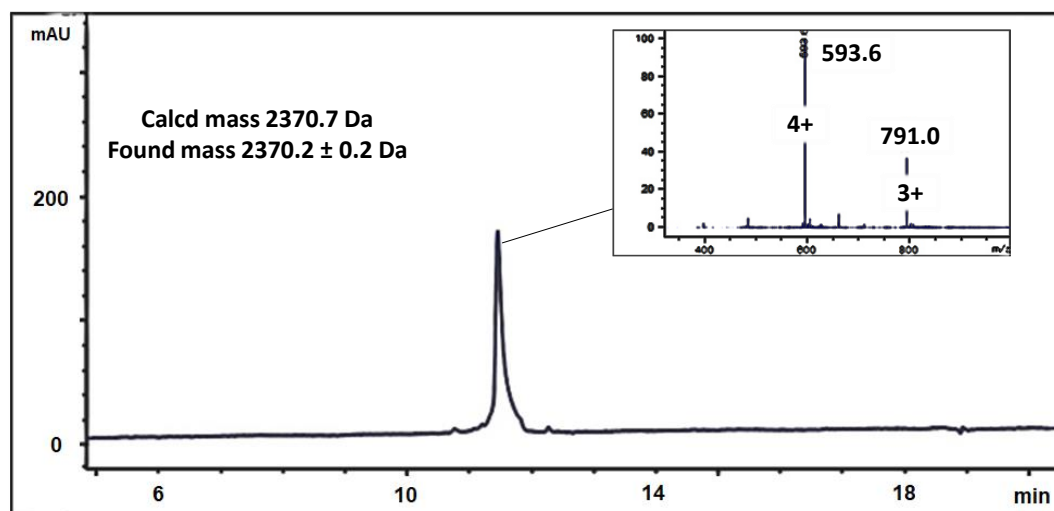


Figure 2.11. LC chromatogram recorded at 214 nm (+ mass spectrum of the indicated peak) of peptide **5b**. Column: ACE 3 C18, 2.1 x 100 mm, 3 μ m particle size, 300 Å pore size; Method: flow rate = 0.5 mL \cdot min⁻¹, H₂O: CH₃CN, 0.1% HCOOH, 95:5 for 2 min \rightarrow 95:5 to 43:57 over 13 min \rightarrow 5:95 for 7 min.

2.6.8 SPPS procedure for peptide **5c**

Synthesis scale: 0.05 mmol. Resin: Rink Amide ProTide Resin (LL), loading 0.19 mmol/g – 263 mg. HATU concentration in DMF: 0.5 M. DIPEA concentration in NMP: 2 M. Deprotection cocktail: 20% (v/v) piperidine in DMF + 1% (v/v) formic acid. Fmoc-MeDbz-OH in DMF: 0.05 M. Fmoc-amino acids in DMF: 0.33 M. Prior to the start of the synthesis, the resin was swollen in the reaction vessel of the automated synthesiser using 5 mL of DMF for 5 min at rt.

Reagent	Method	Reagent concentration during coupling step (mM)
Fmoc-Gly-OH	12	167
Fmoc-MeDbz-OH	14	35

Fmoc-Lys(Boc)-OH	12	167
Fmoc-Val-OH	12	167
Fmoc-Asn(Trt)-OH	12	167
Fmoc-Glu(OtBu)-OH	12	167
Fmoc-Ile-OH	12	167
Fmoc-Thr(tBu)-OH	13	167
Fmoc-Asp(OtBu)-OH	12	167
Fmoc-Ser(tBu)-OH	8	167
Fmoc-Pro-OH	11	167
Fmoc-Glu(OtBu)-OH	8	167
Fmoc-Val-OH	8	167
Fmoc-Glu(OtBu)-OH	8	167
Fmoc-Leu-OH	8	167
Fmoc-Thr(tBu)-OH	10	167
Fmoc-Ile-OH	9	167
Fmoc-Thr(tBu)-OH	10	167
Fmoc-Lys(Boc)-OH	8	167
Fmoc-Gly-OH	8	167
Fmoc-Thr(tBu)-OH	10	167
Fmoc-Leu-OH	8	167
Fmoc-Thr(tBu)-OH	10	167
Fmoc-Lys(Boc)-OH	8	167
Fmoc-Val-OH	9	167
Fmoc-Phe-OH	8	167
Fmoc-Ile-OH	9	167
Fmoc-Gln(Trt)-OH	8	167
Boc-NLe-OH	8	167

After the last coupling, the MeDbz group was activated into MeNbz by incubating the resin with 5 equivalents of 4-nitrophenyl chloroformate in DCM (3 x 30 min), followed by 0.5 M DIPEA in DMF (3 x 10 min). Cleavage was done with 10 mL of TFA/water/TIS (95:2.5:2.5) for 2 h. The resin was removed by filtration and the filtrate was concentrated by N₂ flow. The crude product was precipitated with cold

diethyl ether, centrifuged (4,000 g for 10 min) and the supernatant was discarded. The precipitate was dissolved in water/acetonitrile (1:1) + 0.1% TFA and purified by HPLC. Product was characterised by LC/MS (Figure 2.12).

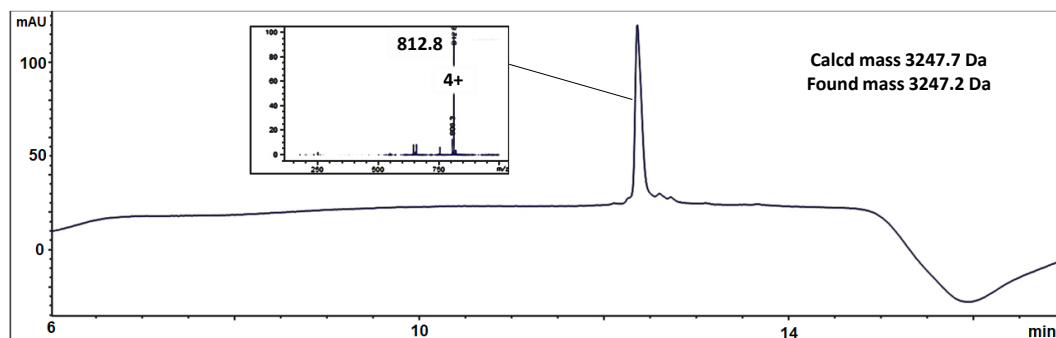
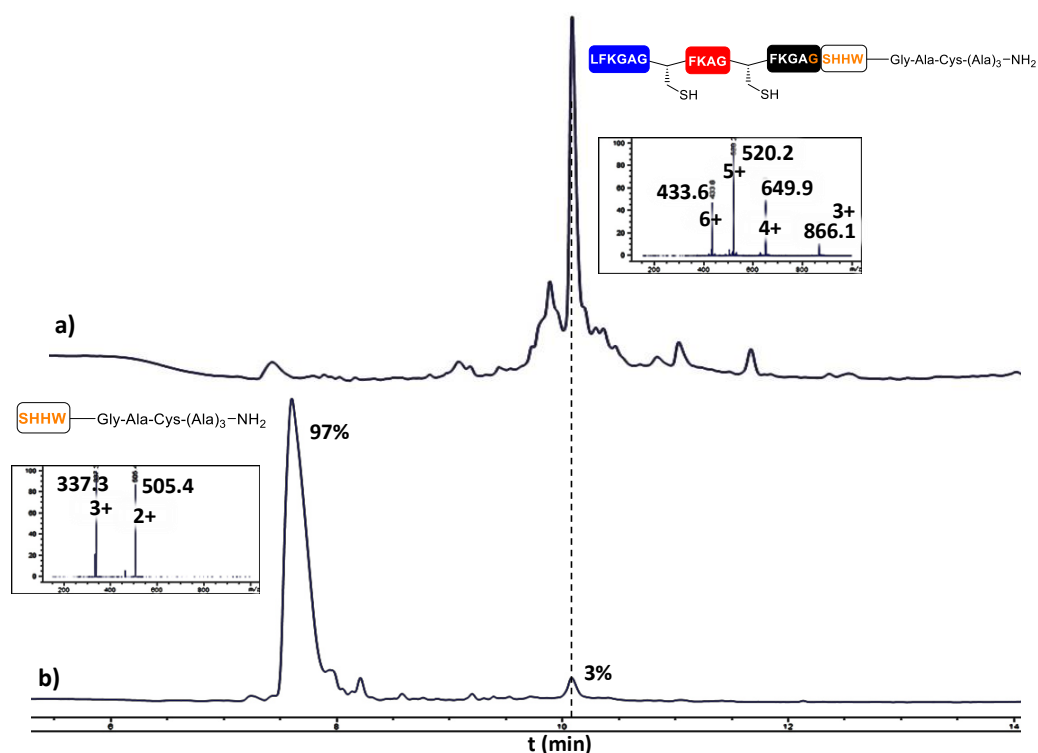


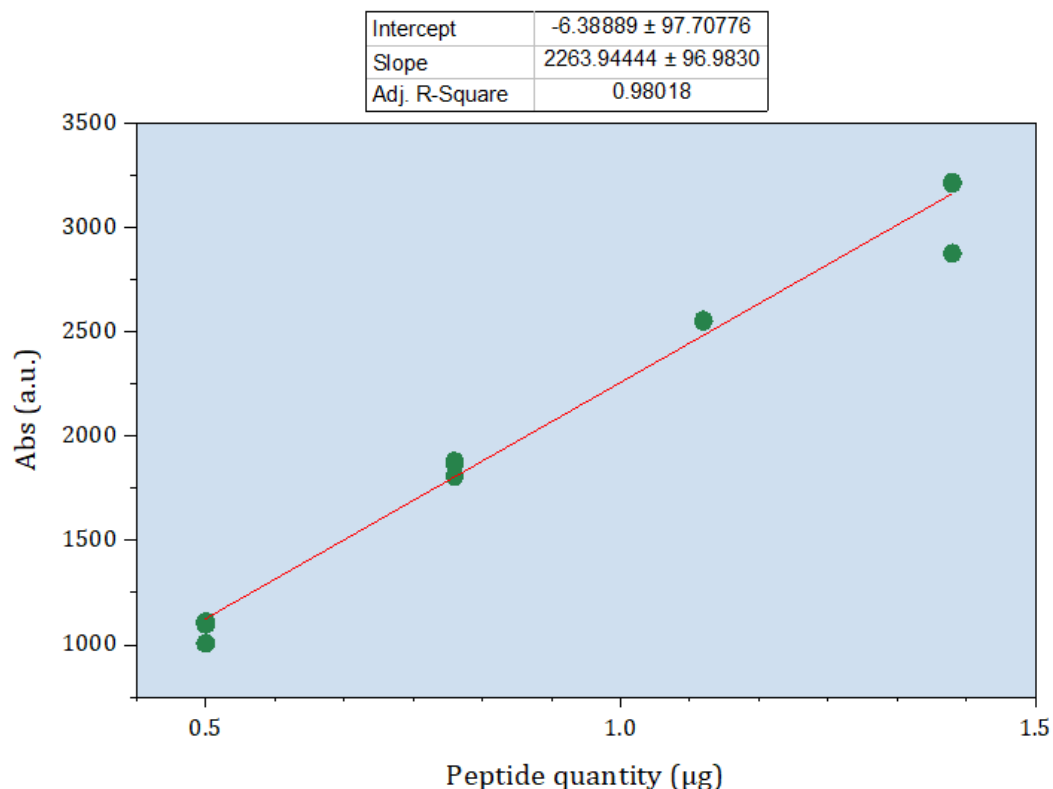
Figure 2.12. LC chromatogram recorded at 214 nm (+ mass spectrum of the indicated peak) of peptide **5c**. Column: *ACE 3 C18*, 2.1 x 100 mm, 3 μ m particle size, 300 Å pore size; Method: flow rate = 0.5 mL \cdot min⁻¹, H₂O: CH₃CN, 0.1% HCOOH, 95:5 for 2 min \rightarrow 95:5 to 55:45 over 10 min \rightarrow 5:95 for 5 min.

2.6.9 Supplementary figures

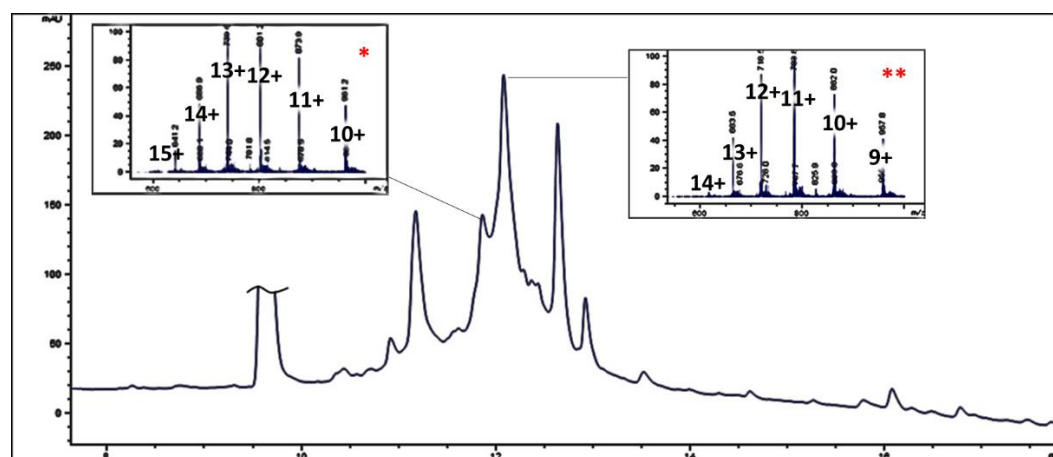


Supplementary figure 2.1. LC chromatogram recorded at 280 nm of TFA cleavages of polypeptide **4** before (a) and after (b) SNAC. Percentage of cleavage is worked out by integrating the areas of the peak corresponding to the cleaved linker and to the peptide remained on the resin. Column: *ACE 3 C18*, 2.1 x 100 mm, 3 μ m particle size, 300 Å pore

size; Method: flow rate = $0.5 \text{ mL} \cdot \text{min}^{-1}$, $\text{H}_2\text{O} : \text{CH}_3\text{CN}$, 0.1% HCOOH , 95:5 for 2 min \rightarrow 95:5 to 43:57 over 13 min \rightarrow 5:95 for 7 min.



Supplementary figure 2.2. Calibration curve for polypeptide H-LFKAGCFKAGCFKGAG-NH₂. The plot was obtained by plotting the absorbance obtained at the LC/MS of a stock solution of H-LFKAGCFKAGCFKGAG-NH₂. For each quantity point, LC/MS run was repeated three times. The calibration curve was obtained by fitting the data points using Origin, version 2019b, OriginLab Corporation, Northampton, MA, USA.



Supplementary figure 2.3. LC chromatogram recorded at 214 nm of TFA cleavages after SNAC for the synthesis of compound **5**. * denotes uncleaved intermediate **5c***, ** denotes cleaved product **5**.

CHAPTER 3

Synthesis and biological evaluation of trimethine cyanine dye- mitochondriolytic peptide conjugates

CHAPTER 3 - Synthesis and biological evaluation of trimethine cyanine dye-mitochondriolytic peptide conjugates

3.1 Abstract

With the view of increasing selectivity towards their biological target and enabling their visualisation inside the cell, a series of mitochondriolytic peptides were covalently linked to a trimethine cyanine dye. The cytotoxicity of the conjugates was assessed towards a collection of cancer and non-cancer cell lines. As envisioned, cyanine dye-containing constructs were all found to be more toxic than their native peptide sequences towards the tested cell lines.

3.2 Introduction

Mitochondriolytic peptides. Mitochondriolytic peptides, as discussed in the previous chapter, have been suggested to disrupt the mitochondrial membranes, leading to leakage of mitochondrial proteins (e.g. cytochrome c) into the cytosol.⁸⁸ Once in the cytosol, these mitochondrial proteins activate caspases and trigger the apoptosis.^{62, 63, 89} This pathway plays an important physiological role, as programmed cell death is often required to maintain homeostasis and to prevent pathological conditions.⁹⁰ Likewise, the apoptotic process is an important target for cancer therapy. In fact, the biological mechanisms controlling apoptosis are often malfunctioning in cancer cells which, consequently, become immortal.⁹¹ Thus, as apoptosis inducers, mitochondriolytic peptides are putative candidates as cancer therapeutics.

Peptide conjugates. However, mitochondriolytic peptides like **KLA** and **kla** only display low cytotoxicity towards mammalian cells, which is attributed to their low cell membrane permeability. To make them more cytotoxic and show their potential as chemotherapeutics, **KLA** and **kla** have been conjugated to different carriers, with the purpose of enhancing their cellular uptake.^{89, 92-96} For instance, cell-penetrating peptides (e.g. **r7**,⁸⁹ **TAT**,⁹⁶ **TCTP**⁹⁶), tumour-homing peptide **RGD-4C**,⁶² and the small organic mitochondrial-targeting moiety **TPP**⁹⁷ (Figure 3.1) have been fused to **kla**. For instance, **r7** conjugation to **kla** led to the remarkable increase in cytotoxicity of two order of magnitude compared to unconjugated peptide,⁸⁹ demonstrating the potential of these types of constructs for anti-cancer treatment.

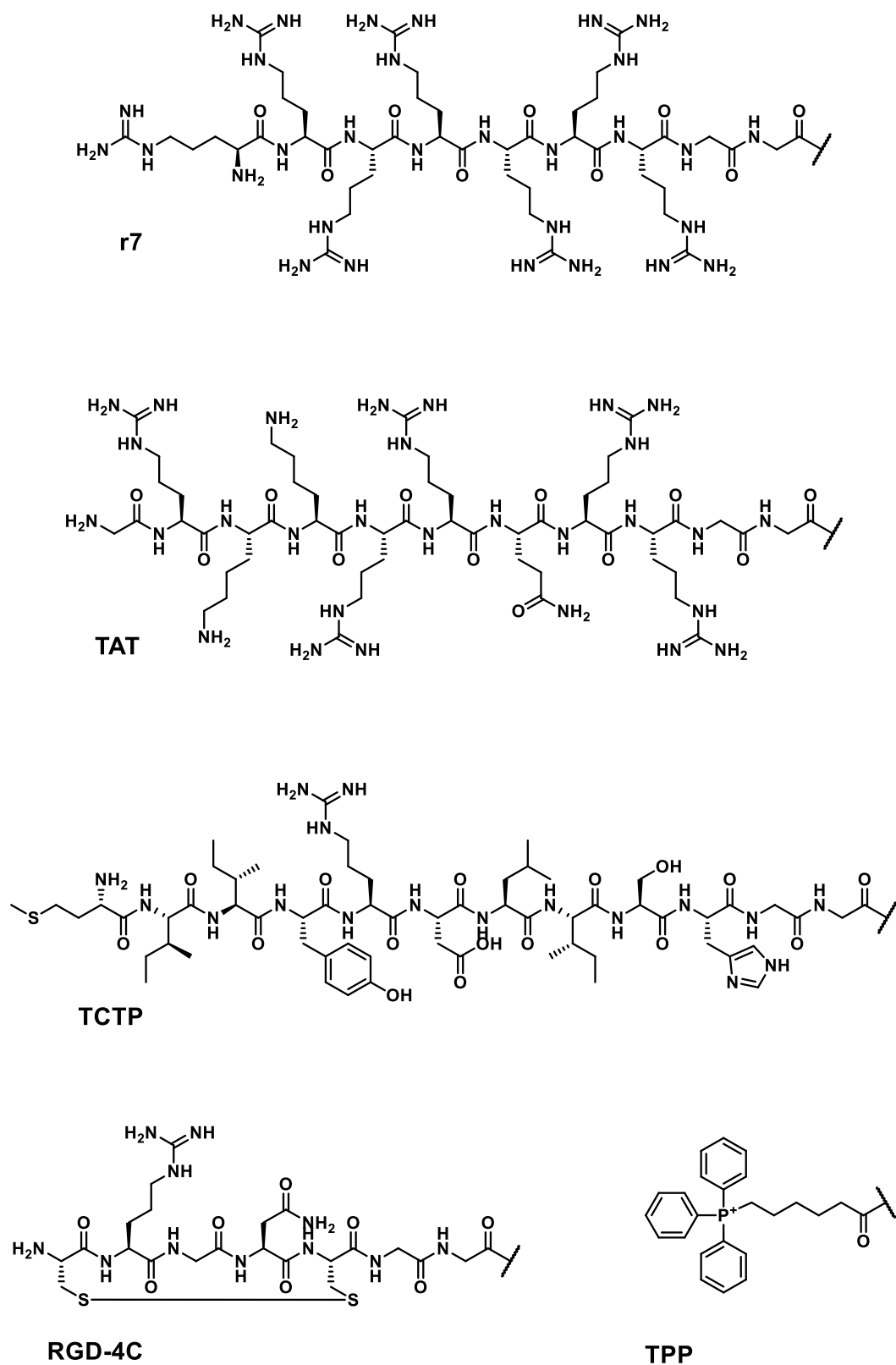


Figure 3.1. Molecular structures of some of the carriers that have been conjugated to **kla** thus far. R7, TAT, TCTP and RGD-4C have been covalently linked via an amide bond to the *N*-terminus of **kla** through a diglycyl spacer (**r7**, **TAT**, **TCTP**, **RDG-4C**) or a six-carbon chain (**TPP**).

Cyanine dyes as mitochondria-targeting carriers. While the cytotoxicity of mitochondriolytic peptides and their conjugates has been investigated,^{63, 89, 92-96} none of the investigated constructs features both selective mitochondria-targeting and the ability to report its subcellular localisation. A fluorescent conjugate with preferential mitochondrial localisation would be ideal for not only therapeutic but also diagnostic purposes. For instance, the “trackability” of such a conjugate can provide important information on the site of the pathology, by enabling imaging of the diseased tissue. In this way, the condition can be both treated and monitored at the same time.⁹⁸

3.3 Aim and Objectives

Cyanine dyes are delocalised-lipophilic cations. Heptamethine cyanine dyes were shown to localise within mitochondria and have found applications as theranostic agents bearing the ability to deliver cargoes to the organelle of cancer cells.^{67, 99-101} Despite the great potential as anticancer therapeutics, the mitochondria-delivery efficiency of other cyanine dyes has not been explored yet.

Here, I aimed to investigate the potential of a trimethine cyanine dye (**Cy3**) as a mitochondria-delivery system, to enhance the efficacy of mitochondriolytic peptides. The advantage of labelling a mitochondriolytic peptide with a cyanine dye is twofold. Firstly, it should bring the peptide to its subcellular target (Figure 3.2), consequently improving its biological activity and reducing off-target side effects. Secondly, it should enable direct visualisation of the conjugate by confocal microscopy, so the subcellular localisation of the conjugate can be easily determined and tracked.

Specific objectives are to:

- Synthesise the cyanine dye scaffold;
- Prepare conjugates containing a mitochondriolytic peptide and the cyanine dye;
- Assess the cytotoxic activity of the conjugates in comparison to the parent peptides.

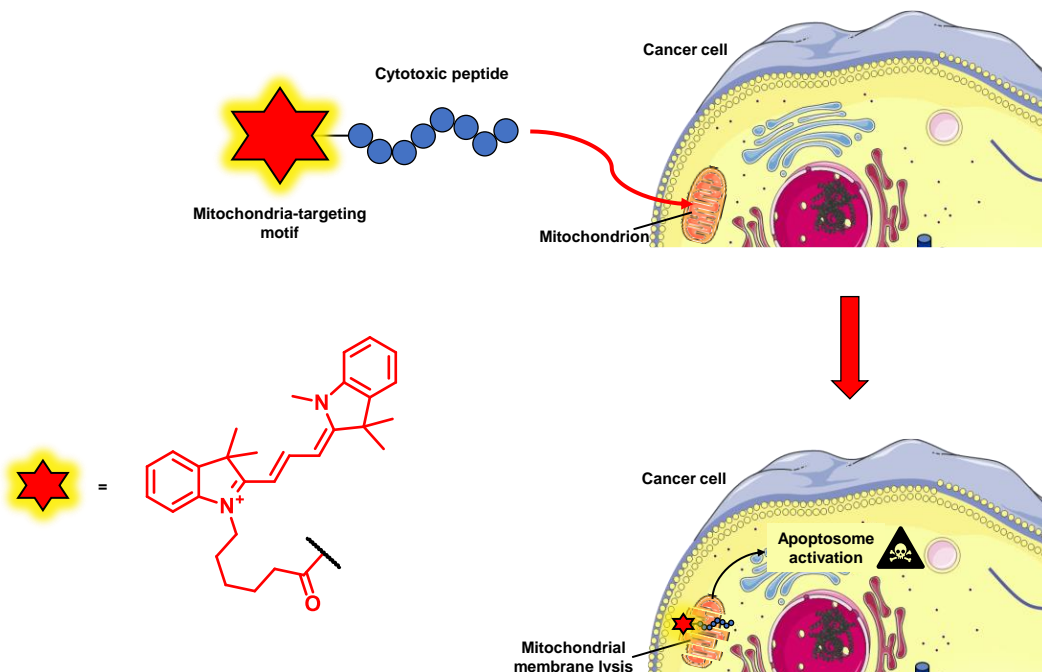


Figure 3.2. Mechanism of apoptosis induction of **Cy3**-conjugated peptides. Figure template provided by smart.servier.com.

3.4 Results and discussion

3.4.1 Synthesis of the cyanine dye scaffold

To explore the theranostic potential of a trimethine cyanine dye as mitochondria-delivery systems in anticancer therapy, **Cy3-COOH** (figure 3.3) was chemically synthesised.

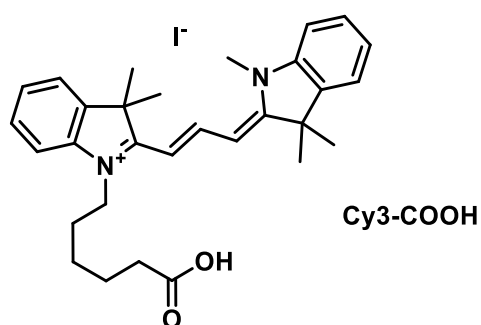
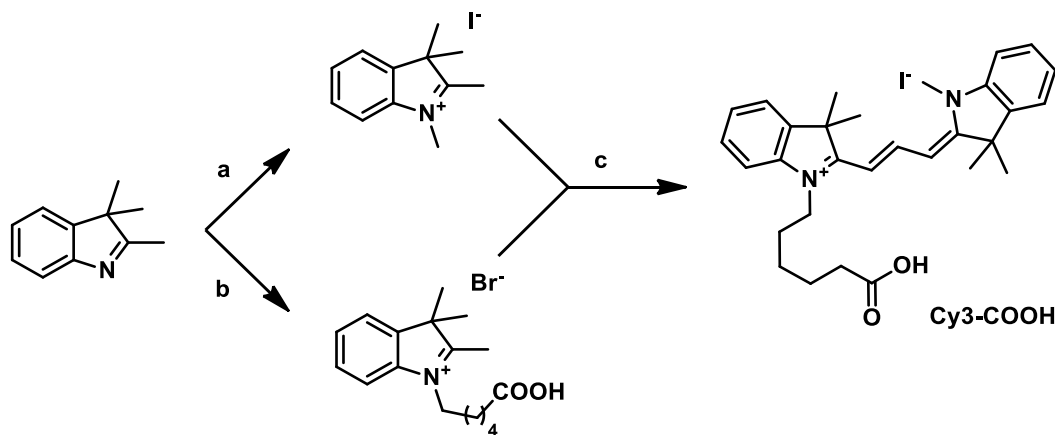


Figure 3.3. Molecular structures of compounds **Cy3-COOH**.

This compound bears a carboxylic moiety which can be used for the conjugation to a peptide sequence. For the synthesis of **Cy3-COOH**, a previously reported synthetic pathway was followed.¹⁰²



Scheme 3.1. Synthetic route for **Cy3-COOH**. *Reagents and conditions:* (a) iodomethane, MeNO₂, 60 h, rt, 92%; (b) 6-bromohexanoic acid, MeNO₂, 16 h, rt, 54%; (c) *N,N*-diphenylformamidinium, pyridine, Ac₂O, 16 h, 120 °C → rt, 40%.

The synthetic route of **Cy3-COOH** (scheme 3.1) starts with the commercially available 2,3,3-trimethylindolenine. This molecule was reacted via S_N2 mechanism with iodomethane. The reaction was conducted using one equivalent of iodomethane in nitromethane; these mild conditions were sufficient to obtain the desired **1,2,3,3-tetramethyl-3H-indol-1-ium iodide** in almost quantitative isolated yield.

Using the same conditions, the **2,3,3-trimethylindolenine** was reacted with 6-bromohexanoic acid to obtain the consequent alkylation product **1-(5-carboxypentyl)-2,3,3-trimethyl-3H-indol-1-ium bromide** in an independent reaction.

Cy3-COOH was obtained by a one-pot reaction between the two indolium salts and *N,N*-diphenylformamidinium. In the first instance, **1-(5-carboxypentyl)-2,3,3-trimethyl-3H-indol-1-ium bromide** reacted at 120 °C with *N,N*-diphenylformamidinium in acetic anhydride, to form an hemicyanine intermediate. At the aforementioned conditions, the intermediate is not very stable; it is indeed important to keep short the time of this first part of the reaction, as prolonged incubation of *N,N*-diphenylformamidinium and **1-(5-carboxypentyl)-2,3,3-trimethyl-3H-indol-1-ium bromide** produced side products and reduced the yield significantly. Therefore, the reaction progress is constantly monitored by thin-layer chromatography. As the spot corresponding to the **1-(5-carboxypentyl)-2,3,3-trimethyl-3H-indol-1-ium bromide** disappears, pyridine and **1,2,3,3-tetramethyl-3H-indol-1-ium iodide** are added to the mixture (previously allowed

to cool down to room temperature) to react with the hemicyanine and yield the desired compound. To minimise compound loss and shorten the purification time, the reprecipitation and washing steps reported in the literature procedure are skipped, and the crude mixture was concentrated *in vacuo* and directly purified by silica column chromatography.

3.4.2 Solid-Phase Peptide Synthesis of mitochondriolytic peptides

As discussed earlier, peptides **KLA** and **kla** were reported to trigger apoptosis once inside the cell. Due to their low cell permeability, they need to be conjugated to a carrier to exhibit significant cytotoxicity,^{89, 92-96} but none of the carriers employed thus far have any significance for theranostic applications. **kXa** (Figure 3.5), a derivative of **kla**, has better mitochondria-targeting ability.⁶³ The rationale behind the design of **kXa** was to obtain a peptide more potent by increasing its hydrophobicity but with no haemolytic activity. In fact, other attempts of engineering mitochondriolytic peptides by increasing their hydrophobicity but keeping their α -helical structure led to highly haemolytic compounds. Unlike **KLA** and **kla**, peptide **kXa** does not exist in a helical conformation and helical peptides are often haemolytic. **kXa** was found to be more toxic than the parent sequences towards HeLa cells, without showing significant haemolytic activity which was instead observed for other similarly engineered peptides, all displaying high degree of helicity.⁶³ Such a feature makes **kXa** an ideal candidate for theranostic applications. Therefore, **KLA**, **kla** and **kXa** were chosen to be labelled with **Cy3-COOH**, affording conjugates **Cy3-KLA**, **Cy3-kla** and **Cy3-kXa** (Figure 3.4).

H-KLAKLAKKLAKLAK-NH ₂	(KLA)
H-klaklakklaklak-NH ₂	(kla)
H-kxakXakkXakxak-NH ₂	(kXa)
Cy3-KLAKLAKKLAKLAK-NH ₂	(Cy3-KLA)
Cy3-klaklakklaklak-NH ₂	(Cy3-kla)
Cy3-kxakXakkXakxak-NH ₂	(Cy3-kXa)
Cy5-KLAKLAKKLAKLAK-NH ₂	(Cy5-KLA)

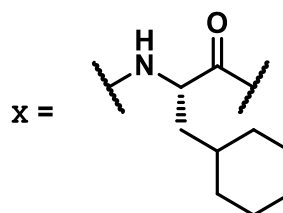


Figure 3.4. Peptide sequences synthesised and tested in this chapter. Lower-case letters denote D-configuration.

Peptides and their conjugates were obtained by automated microwave-assisted SPPS.¹⁰³ As a solid support for the synthesis, a Rink Amide MBHA resin was used. The loading of the employed resin was around 0.49 mmol/g, as determined spectrophotometrically (see experimental procedure). The peptide chains were built by using two equivalents (relative to the resin loading) of Fmoc-protected (and side chain protected, in case of residues with reactive side chains) amino acids. The couplings were performed with four equivalents of *N*, *N'*-diisopropylcarbodiimide (DIC) as a reagent activating the carboxylic functionality of the amino acid residue to be connected to the elongating peptide chain, and two equivalents of oxyma pure as an additive (see section 1.3.1.1 for a brief discussion about coupling strategies in SPPS). For **Cy3**-labelled sequences, three equivalents of **Cy3-COOH** were used in the final coupling to link the cyanine dye scaffold to the α -amine of the *N*-terminal lysine residue by the same coupling method. Finally, molecules were cleaved from the resin by treatment with TFA and purified by reverse phase HPLC. Their purity was assessed by LC/MS analysis.

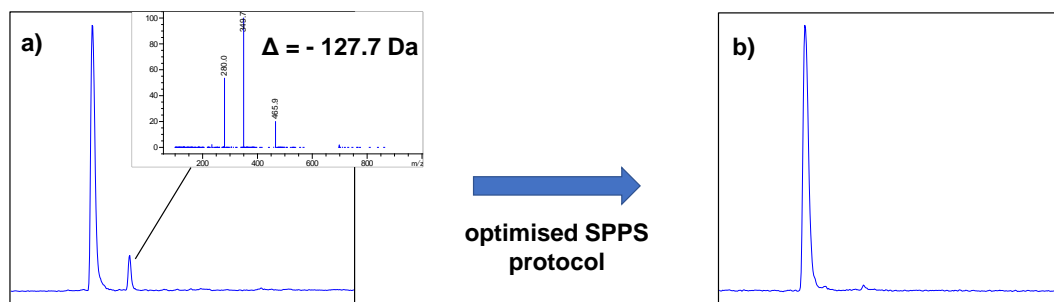


Figure 3.5. TIC chromatograms of the crude of **KLA** synthesis a) before and b) after optimising the SPPS protocol.

In the crude mixture of all syntheses, along with the major peak attributed to the desired compound, a small peak was detected in the TIC chromatograms from LC/MS analysis (figure 3.5a). As having a found mass of 127.7 Da difference to the desired product, this peak was attributed to the truncated peptide sequence which lacks a lysine residue. Moreover, it was difficult to separate this truncated peptide from the desired product by HPLC. Therefore, the more convenient way to obtain the pure product appeared to be the optimisation of the SPPS protocol, aiming to bring the coupling reaction of the deleted lysine to completion. In the first instance, the deleted lysine had to be identified amongst the six lysine residues within the sequences. For this purpose, the synthesis of **KLA** was taken as a case study. Therefore, after every lysine coupling (but the C-terminal one), a microcleavage was carried out thus to look for any potential deletions by LC/MS. Finally, the deleted lysine residue was found to be the *N*-terminal one. Fortunately, after screening different conditions, the deletion issue was overcome by prolonging the coupling time of the *N*-terminal lysine residue without increasing the amount of reagents (figure 3.5b).

It is noteworthy that literature procedures for preparing **KLA** and **kla** used four or more equivalents of amino acids,^{89, 97} whereas I found two equivalents of amino acids was sufficient to achieve the desired peptides in high yield and high purity. This is of great relevance when D-amino acids or unnatural amino acids (i.e. cyclohexylalanine) are employed, given their higher cost compared to naturally occurring L-amino acids.

3.4.3 Cell viability assay

It was envisioned that, once inside the cell, the cyanine dye-labelled peptides would go to mitochondria, disrupt mitochondrial membranes, and trigger apoptosis (figure 3.2). As discussed in chapter 1, the mitochondrial membrane permeabilisation has been identified as a “point of no return” for the cell. Therefore, initiating apoptosis by mitochondrial membrane disruption should lead to cell death in cancer cells, in which apoptosis mechanisms are usually deregulated.

To investigate the cytotoxicity of the new constructs, peptides **KLA**, **kla** and **kXa**, their cyanine dye conjugates **Cy3-KLA**, **Cy3-kla**, **Cy3-kXa**, along with the cyanine dye **Cy3-COOH**, will be tested towards an array of cell lines via Cell-Titer Blue assay. For this purpose, KB, MCF-7, SK-OV-3 and HEK cells were chosen. KB and MCF-7 cells are both human tumour cell lines. KB cells are derived from human cervical cancer,¹⁰⁴ while SK-OV-3 cells are derived from human ovarian cancer. Both KB and SK-OV-3 cell lines exhibit high levels of folate receptor α on the cell surface.^{72, 105, 106} This feature is of particular relevance in anticancer applications, as it can be exploited for selective targeting and delivery. MCF-7 is a cell line derived from human breast cancer with low-level of folate receptor α ;¹⁰⁷ therefore, these cells can serve as negative control for folate receptor α mediated tumour-targeted drug delivery systems. HEK cells are non-cancer cells and were chosen to evaluate the specificity of the tested compounds towards cancer cells.

For the Cell-Titer Blue assay, cells were seeded in a 96-multiwell plate and then treated with a range of different concentrations of the examined compounds. At least five different concentrations were tested for each compound. Cell viability after 24 h of treatment was assessed for KB, MCF-7, SK-OV-3 and HEK cells by fitting the data points via a dose-response curve to compute the EC₅₀ values (table 3.1). Each data point represents mean value from three biological replicates (*i.e.* cells split from three different passages), and each biological replicate is composed of three technical replicates (*i.e.* cells split from the same passage).

Table 3.1. The EC₅₀ values (expressed in μM) on different cell lines of different molecules and their cyanine dye conjugates were quantified using cell viability assays. The values in brackets represent the standard error of the curve fitting using Origin, version 2019b, OriginLab Corporation, Northampton, MA, USA.

	EC ₅₀ (μM)			
Compound	KB	SK-OV-3	MCF7	HEK
Cy3-COOH	36.5 (3.6)	8.6 (6.70)	110 (13.2)	221 (53.8)
KLA	> 400	> 400	> 400	> 400
kla	331 (152)	> 400	> 400	> 400
kXa	6.5 (0.5)	11.6 (2.37)	50.9 (3.0)	15.6 (2.6)
Cy3-KLA	6.7 (0.2)	11.0 (2.56)	7.37 (0.2)	44.3 (7.0)
Cy3-kla	3.5 (0.1)	6.39 (0.79)	5.7 (0.7)	5.3 (0.2)
Cy3-kXa	5.5 (0.5)	23.0 (1.64)	11.6 (1.5)	8.2 (0.5)

The cytotoxicity of **Cy3-COOH** was found to be SK-OV-3 (EC₅₀ = 8.6 μM) > KB (EC₅₀ = 36.5 μM) > MCF-7 (EC₅₀ = 109.7 μM) > HEK cells (EC₅₀ = 217.9 \pm 23.4 μM). Although not very pronounced, this selectivity might be due to the higher expression of some organic anion transporting polypeptides on the surface of cancer cells;¹⁰⁸ these transporters are observed to be involved in the cellular uptake of cyanine dyes and cyanine dye conjugates.^{99, 109-114} **KLA** and **kla** only displayed low cytotoxicity towards the tested cell lines, which can be attributed to their low cell permeability, as already discussed in section 3.2. Amongst the unlabelled peptides, **kXa** presented the lowest EC₅₀. This peptide is an engineered version of **KLA** and **kla**, designed to be more hydrophobic; it was in fact postulated that increased hydrophobicity can lead to enhanced mitochondria-targeting properties.⁶³ This result, comparable with the cytotoxic data reported in the literature,⁶³ reinforces the concept that the hydrophobicity of amphipathic peptides might have a positive influence in terms of mitochondriolytic ability, without the need of an helical structure.

In all the investigated cases, **Cy3** conjugation further improved the cytotoxicity ($p < 0.01$). This result can be due to the better cell permeability and the enhanced targeting of the organelle, given the delocalised cationic nature of the cyanine moiety along with its positive contribution to the hydrophobicity of the constructs. In fact, these two features may concur in improving the capability of the compounds of targeting the mitochondrial membrane, in virtue of its structural composition and negative potential.¹¹⁵

Remarkably, when conjugated with **TPP**, **kla** was reported not to show significant toxicity towards KB cells after 48 h of incubation in a literature study.⁹⁷ In fact, the assumption of the organic anion transporting polypeptides mediated uptake is consistent with the better cytotoxicity of the **Cy3** conjugation over **TPP**. Therefore, **Cy3** might be a better intracellular delivery platform than **TPP** in terms of cell permeability properties.

3.4.4 Subcellular localisation and cellular uptake of folate conjugates

To gain further insights on the mechanism of action on the newly synthesised compounds, subcellular localization of the constructs was evaluated by Wenjing Deng, who is a researcher working in the Shenzhen Bay Laboratory of the Gaoke Innovation Center in Shenzhen, China.

Subcellular localisation was studied via confocal microscopy: SK-OV-3 and MCF7 cells were stained with MitoTracker Green and Hoechst 33258 (fluorescent molecules known to localise within cell mitochondria and nucleus respectively)^{116, 117} and then incubated with **Cy3-COOH**, **Cy3-KLA**, **Cy3-kla** and **Cy3-kXa**. Next, the fluorescent patterns of the tested molecules and stains were analysed to determine colocalization within the cell.

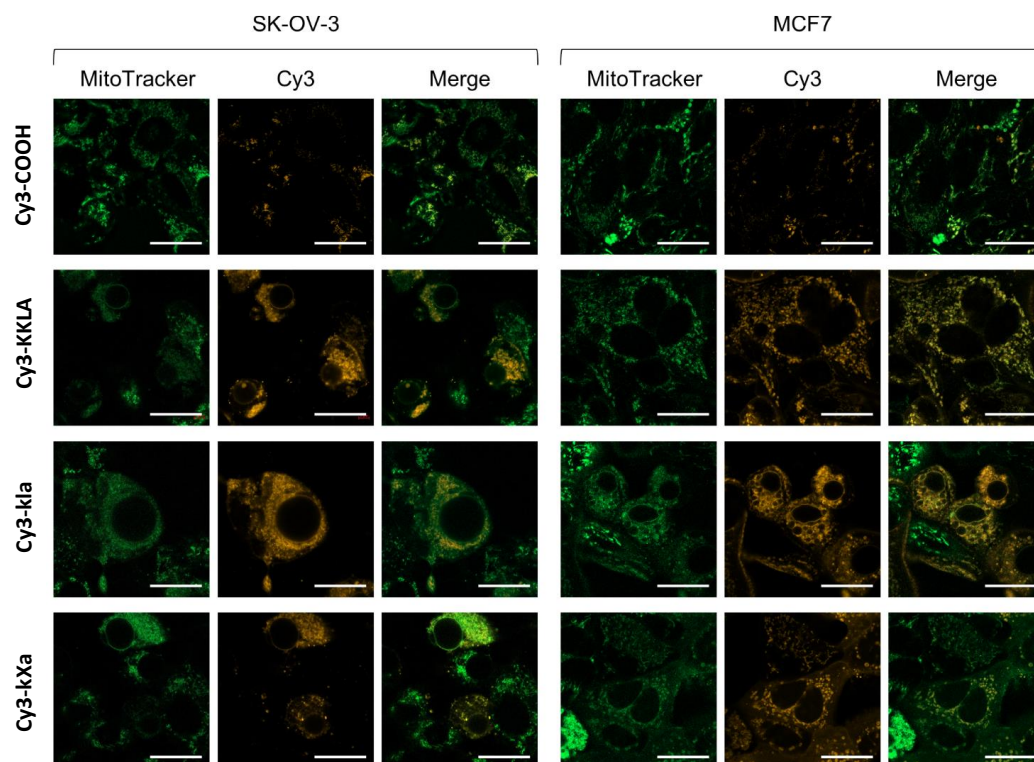


Figure 3.6. Confocal microscopy images of SK-OV-3 and MCF7 cells treated with **Cy3-COOH**, **Cy3-KLA**, **Cy3-kla** and **Cy3-kXa**. Cells were treated with 10 μ M of the indicated conjugate for 10 min at 37 $^{\circ}$ C, washed, stained with 50 nM MitoTracker Green and 10 μ g/ml Hoechst33258 for 10 min at 37 $^{\circ}$ C, washed and imaged at 63X. Excitation wavelengths for Hoechst 33258, MitoTracker Green and Cy3 were set as 405, 488 and 561 nm, respectively. Pearson's correlation coefficients of MitoTracker Green FM and Cy3 fluorescence for compounds **Cy3-COOH**, **Cy3-KLA**, **Cy3-kla** and **Cy3-kXa** in SK-OV-3 and MCF cells are 0.75/0.64, 0.73/0.81, 0.91/0.61, and 0.78/0.63, respectively. Scale bars denote 25 μ m.

As indicated in Figure 3.6, cyanine dye-labelled compounds colocalise with MitoTracker Green, therefore confirming their mitochondrial localisation.

3.5 Conclusions and perspectives

As proposed, **Cy3** enhanced the cytotoxicity of all the tested peptides. Moreover, this screening indicated a positive correlation between hydrophobicity and cytotoxicity, already suggested in previous studies.^{63, 115} Its conjugation with the tested peptide sequences led to a clear increase in cytotoxicity and to the expected mitochondrial localisation. Unlike the compounds previously reported in literature, this is the first case of pro-apoptotic peptide conjugation with fluorescent and mitochondria-targeting carriers, thus laying the foundations for a new platform of mitochondria-targeting cancer theranostics. Following this work,

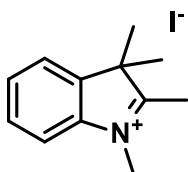
the possibility to enhance the selectivity of the cyanine dye labelled peptides towards a specific cancer cell line was investigated.

3.6 Experimental section

3.6.1 Organic chemical synthesis of the cyanine scaffold

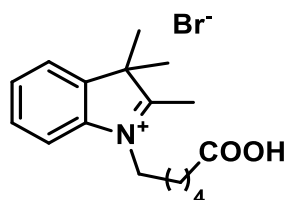
General Methods. Reactions were performed in oven dried glassware. Reaction temperatures are stated as heating device temperature (e.g. oil bath, shaker, etc.), if not otherwise stated. Concentrations under reduced pressure were performed by rotary evaporation at 40 °C at the appropriated pressure, unless otherwise noted. Deionized water was obtained by an Elga PURELAB 8 Option system (15 MΩ·cm). Reagents obtained from commercial suppliers were used without further purification; 2,3,3-trimethyl-3H-indole, *N,N'*-diphenylformamidine, acetic anhydride and pyridine dry were from Acros Organics; methyl iodide were from Sigma–Aldrich; 6-bromohexanoic acid was from Lancaster Synthesis; solvents were from Fisher Scientific, except nitromethane which was from Acros Organics. They were all laboratory reagent grade and were used without further purification unless otherwise noted. For HPLC mobile phase, deionised water, acetonitrile HPLC grade from Fisher Scientific and trifluoroacetic acid from Fluorochem were used. Analytical thin layer chromatography was carried out with silica gel 60 F254 aluminium sheets from Merck. Detection was carried out using UV light ($\lambda = 254$ nm and 366 nm), followed by immersion in permanganate staining solution with subsequent development via careful heating with a heat gun. Flash column chromatography was performed using silica gel (pore size 60 Å, 0.040-0.063 mm, 230-400 mesh) from Sigma Aldrich. ^1H - and ^{13}C -NMR spectra were recorded in CDCl_3 , DMSO-d_6 on Bruker Ultrashield 400, or Ascend 500 instruments.

3.6.1.1 Synthesis of 1,2,3,3-tetramethyl-3H-indolium iodide



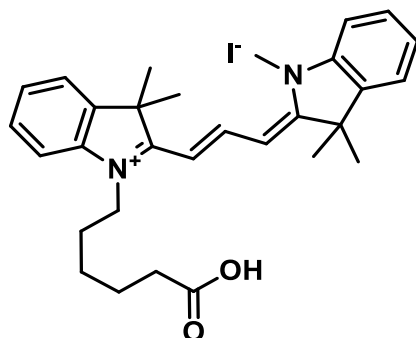
Methyl iodide (496 μL , 8.0 mmol, 1.0 eq) was added to a solution of 2,3,3-trimethyl-3H-indole (1280 μL , 8.0 mmol, 1.0 eq) in nitromethane (4.8 mL) and the reaction mixture was stirred for 60 h at room temperature. The reaction was cooled down to room temperature and triturated with diethyl ether (15 mL). The precipitated was filtered off, washed with diethyl ether (50 mL) and dried under vacuo. The title compound (2.23 g, 7.4 mmol, 92% yield) was obtained as pale-pink solid. $^1\text{H-NMR}$ (500 MHz, DMSO-d_6): δ = 7.92 (d, J = 7.3 Hz, 1 H, ArH), 7.84 (d, J = 6.8 Hz, 1 H, ArH), 7.64 (m, 2H, ArH), 3.97 (s, 3 H), 2.76 (s, 3 H), 1.53 (s, 6 H, CH_3) ppm. HRMS (ES $^+$): calcd. for $\text{C}_{12}\text{H}_{16}\text{IN}$ $[\text{M} - \text{I}]^+$ 174.1283; found 174.1286. The analytical data were in accordance with the literature.¹⁰²

3.6.1.2 Synthesis of 1-(5-carboxypentyl)-2,3,3-trimethyl-3H-indolium bromide

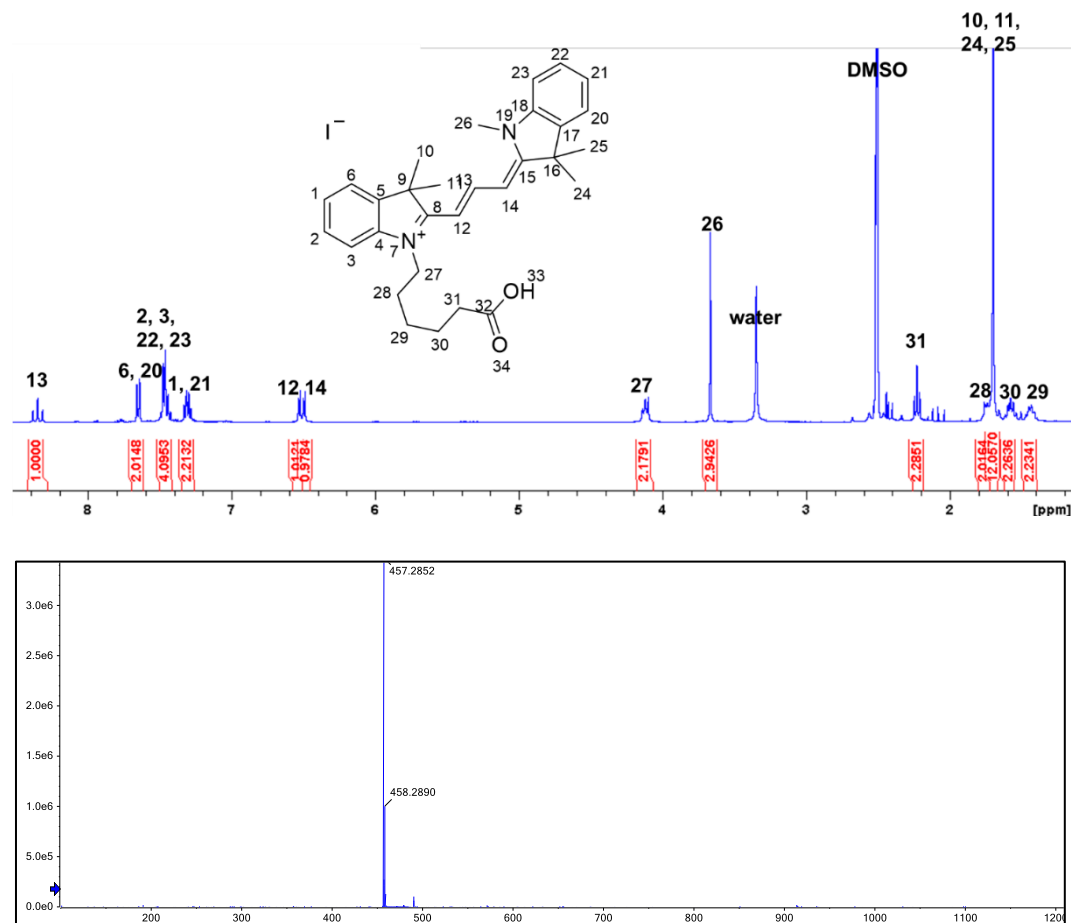


6-bromohexanoic acid (787 mg, 3.0 mmol, 1.0 eq) was added to a solution of 2,3,3-trimethyl-3H-indole (481 μL , 3.0 mmol, 1.0 eq) in nitromethane (2 mL) and the reaction mixture was stirred for 16 h at room temperature. The reaction is cooled down to room temperature and triturated with diethyl ether (25 mL). The precipitated was filtered off, washed with diethyl ether three times, and dried under vacuo. The title compound (574 mg, 1.6 mmol, 54% yield) was obtained as pink solid. $^1\text{H-NMR}$ (400 MHz, DMSO-d_6): δ = 7.97 (m, 1 H, 7-H), 7.84 (m, 1 H, 4-H), 7.64 (m, 2 H, 5-H, 6-H), 4.45 (t, 2 H, NCH_2), 2.84 (s, 3 H, 2- CH_3), 2.23 (t, 2 H, COCH_2), 1.85 (m, 2 H, NCH_2CH_2), 1.55 (m, 8 H, COCH_2CH_2 , 3- CH_3), 1.43 (m, 2 H, $\text{NCH}_2\text{CH}_2\text{CH}_2$) ppm. HRMS (ES $^+$): calcd. for $\text{C}_{17}\text{H}_{24}\text{NO}_2\text{Br}$ $[\text{M} - \text{Br}]^+$ 274.1807; found 274.1815. The analytical data were in accordance with the literature.¹⁰²

3.6.1.3 Synthesis of Cy3-COOH (1-(5-carboxypentyl)-3,3-dimethyl-2-[(1E,3Z)-3-(1,3,3-trimethyl-1,3-dihydro-2H-indol-2-ylidene)-1-propen-1-yl]-3H-indolium iodide)



N,N'-diphenylformamidine (512 mg, 2.6 mmol, 1.2 eq) was added to a solution of **1-(5-carboxypentyl)-2,3,3-trimethyl-3H-indolium bromide** (750 mg, 2.2 mmol, 1.0 eq) in acetic anhydride (6.3 mL, 61.7 mmol, 31 eq), the reaction mixture was heated in an oil bath at 120 °C and stirred for 30 min. The reaction mixture was allowed to cool down to room temperature and a solution of **1,2,3,3-tetramethyl-3H-indolium iodide** (915 mg, 3.0 mmol, 1.4 eq) in dry pyridine (6.3 mL, 78.1 mmol, 36.4 eq) is added. The mixture was stirred for 16 h at room temperature, then it was concentrated in vacuo and purified by chromatography on silica (97:3→9:1 CH₂Cl₂/CH₃OH). The title compound (514 mg, 0.9 mmol, yield 40%) was obtained as red film. ¹H-NMR (CDCl₃): δ= 12.05 (br. s, 1H, CO₂H), 8.35 (t, J_{a,b}=J_{b,c}= 13.4 Hz, 1 H, b-H), 7.64 (m, 2 H, 4-H, 4-H), 7.45 (m, 4 H, 6-H, 7-H, 6-H, 7-H), 7.30 (m, 2 H, 5-H, 5-H), 6.53 (d, J_{a,b}= 13.4 Hz, 1 H, a-H), 6.51 (d, J_{b,c}= 13.4 Hz, 1 H, c-H), 4.12 (t, J= 7.5 Hz, 2 H, NCH₂), 3.66 (s, 3 H, NCH₃), 2.22 (t, J= 7.2 Hz, 2 H, COCH₂), 1.75 (m, 2 H, NCH₂CH₂), 1.69 (s, 12 H, 3-CH₃, 3-CH₃), 1.57 (m, 2 H, COCH₂CH₂), 1.43 (m, 2H, NCH₂CH₂CH₂) ppm. HRMS (ES⁺): calcd. for C₃₀H₃₇N₂O₂I [M - I]⁺ 457.2855; found 457.2852. The analytical data were in accordance with the literature.¹⁰²



3.6.2 Solid Phase Peptide Synthesis

General Methods. Solid Phase Peptide Syntheses (SPPSs) were performed on a CEM Liberty Blue™ Automated Microwave Peptide Synthesizer and in TELOS Filtration Columns equipped with 20 μm polyethylene frits. Reaction temperatures are stated as heating device temperature of the synthesiser, if not otherwise stated. Deionized water was obtained by an Elga PURELAB 8 Option system (15 MΩ·cm). Reagents obtained from commercial suppliers were used without further purification unless otherwise stated. Protected amino acids and triisopropylsilane (TIS) were purchased from Cambridge Reagents. DIC, oxyma pure, piperazine and trifluoroacetic acid were purchased from Fluorochem. DMF was purchased from Fisher Scientific. For HPLC mobile phase, HPLC grade CH₃CN from Fisher Scientific and trifluoroacetic acid from Fluorochem were used. They were all laboratory reagent grade and were used without further purification unless otherwise noted. LC/MS was performed on a 1260 Infinity II from Agilent Technologies. Semi-preparative HPLC was performed on a 1206 Infinity from

Agilent Technologies equipped with a Phenomenex Gemini C18, 10.0 x 250 mm, particle size 10 μm , pore size 110 Å or with an ACE C18, 10.0 x 250 mm, particle size 5 μm , pore size 100 Å. Determination of Rink Amide resin loading was conducted using a ThermoFisher NanoDrop ND-ONE-W spectrophotometer. Absorbance values were measured in 10 mm path-length cuvettes (Fisher Scientific, #11847832).

3.6.2.1 Determination of Rink Amide resin loading

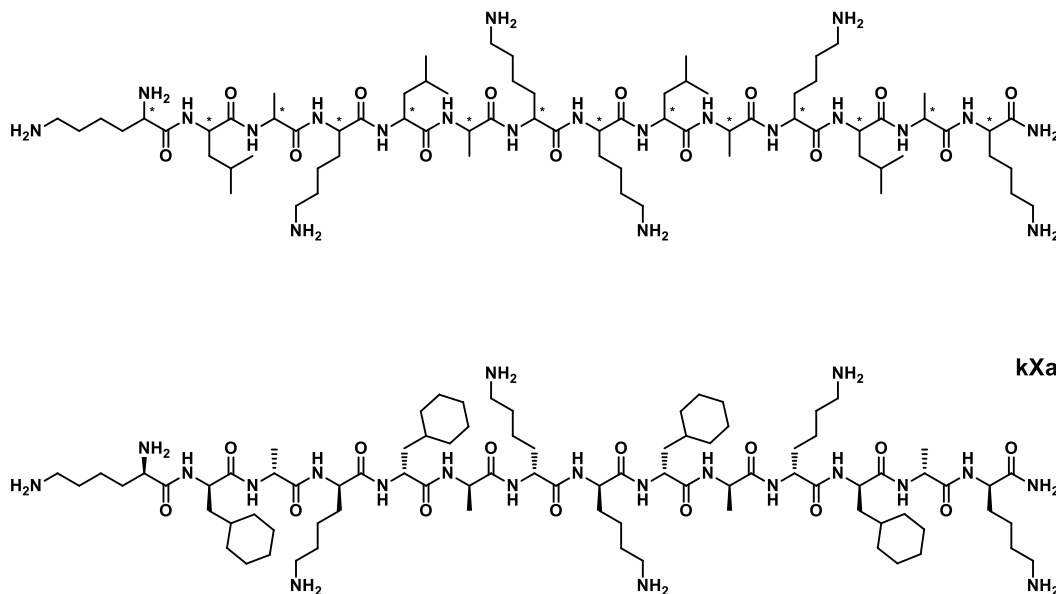
10 mg of resin were weighed into an eppendorf tube to which 800 μL of DMF were added. After allowing the resin to swell for 15 min, 200 μL of piperidine were added to the suspension; at this point the tube was vortexed and allowed to stand for 15 min at room temperature. Afterwards, the tube was centrifuged and 100 μL of the supernatant were transferred to a 1 cm path-length cuvette and diluted with 900 μL of DMF. The absorbance at 301 nm was measured versus a blank, which was prepared with the same procedure but without the use of the resin. The concentration c of dibenzofulvene-piperidine adduct released from the resin was determined by applying the Lambert-Beer law ($Abs = \epsilon c l$), where Abs is the absorbance value, l is the path length (1 cm) and ϵ is the extinction coefficient of the dibenzofulvene-piperidine adduct (7800 $\text{mL}/\text{mmol}\cdot\text{cm}$, $\lambda = 301 \text{ nm}$)¹¹⁸, averaging the values resulted from three independent experiments. Finally, the loading was worked out using the formula

$$\text{Loading} = c \times V \times d / m$$

Where V is the volume of solution in the cuvette, d is the dilution coefficient, and m is the mass of the weighted resin. In the described procedure, $V = 1 \text{ mL}$, $d = 10$ and $m = 10 \text{ mg}$.

3.6.2.2 General procedure for the synthesis of KLA, kla and kXa

KLA, * = (S)

$$\mathbf{kla},^* = (R)$$


The peptide chain was synthesised by SPPS on Rink Amide MBHA resin. Each amino acid coupling step was carried out with Fmoc-protected amino acid (2 eq), DIC (4 eq), ethyl cyanohydroxyiminoacetate (2 eq) in DMF at 75 °C (155 W) for 0.25 min and at 90 °C (30 W) for further 2 min. For the last lysine, the coupling was carried out at 75 °C (155 W) for 0.5 min seconds and at 90 °C (30 W) for further 4 min. After each coupling step, the respective Fmoc protecting group was removed by 10% Piperazine (w/v) in ethanol:NMP (1:9). After the final Fmoc deprotection, cleavage was performed in TFA/Water/TIS 95:2.5:2.5 solution for 2 h. The resin was removed by filtration and the filtrate was concentrated by N₂ flow. The crude product was precipitated with cold diethyl ether, centrifuged (4,000 g for 10 min) and the supernatant was discarded. The precipitate was dissolved in water and purified by HPLC. Lyophilisation of the pure product fractions afforded the desired compound as white powder. Desired product was characterised by LC/MS (Figure 3.7-9).

Table 3.2 Calculated and expected molecular weight for the synthesised compounds

Compound	Calculated mw	Found mw*
KLA	1523.0	1523.1 ± 0.3
kla	1523.0	1523.0 ± 0.2
kXa	1683.3	1683.2 ± 0.2
Cy3-KLA	1962.6	1962.6 ± 0.3
Cy3-kla	1962.6	1962.6 ± 0.2
Cy3-kXa	2122.9	2123.0 ± 0.3

* as per manufacturer's specifications, the mass accuracy of the Agilent 6120B Single Quadrupole instrument is ± 0.1 Da.

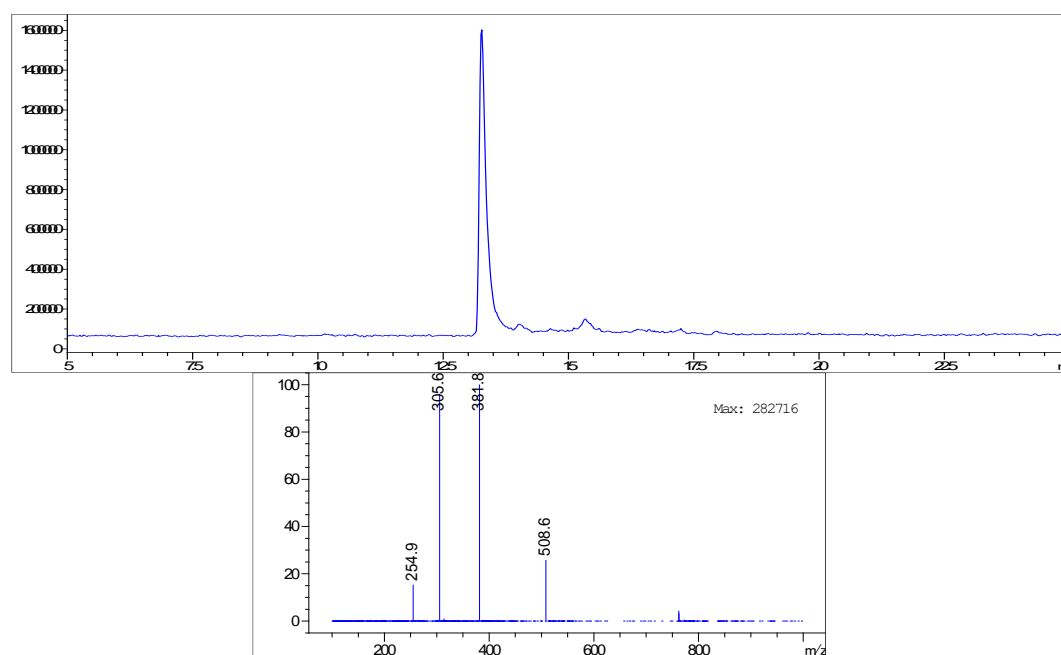


Figure 3.7. TIC chromatogram (+ mass spectrum at 13.181:13.509 min) of **KLA**. Column: *Poroshell 120 EC-C18*, 2.1 x 100 mm, 4 µm particle size, 120 Å pore size; Method: flow rate = 0.5 mL · min⁻¹, H₂O: CH₃CN, 0.1% HCOOH, 95:5 for 2 min → 95:5 to 70:30 over 25 min → 5:95 for 5 min.

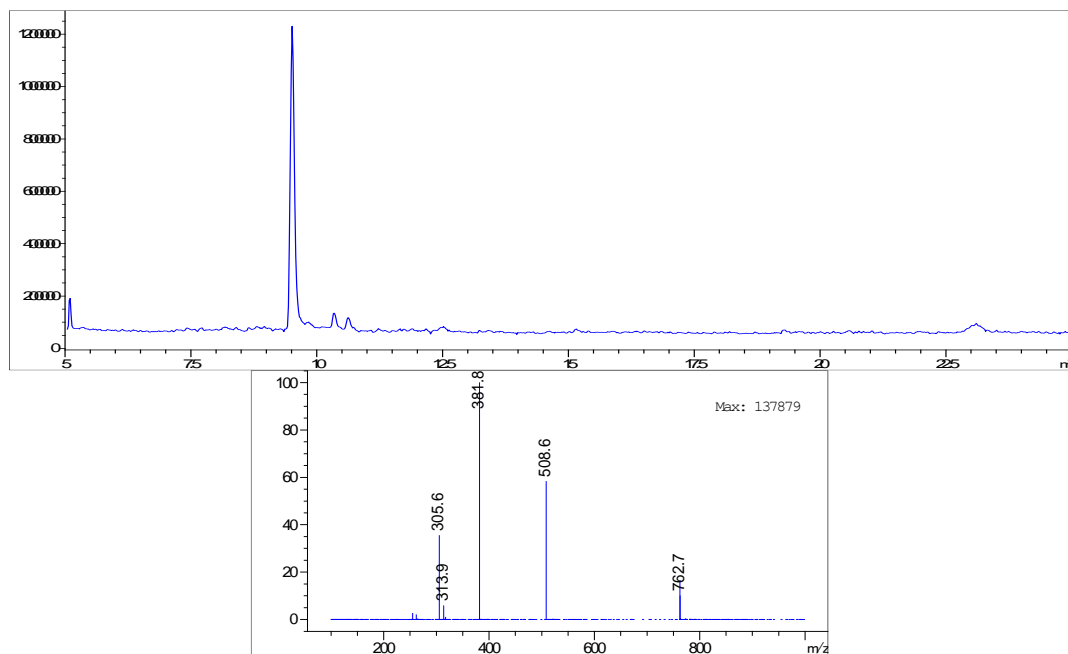


Figure 3.8. TIC chromatogram (+ mass spectrum at 9.439:9.639 min) of **kla**. Column: *Poroshell 120 EC-C18*, 2.1 x 100 mm, 4 μ m particle size, 120 Å pore size; Method: flow rate = 0.5 mL \cdot min⁻¹, H₂O: CH₃CN, 0.1% HCOOH, 95:5 for 2 min \rightarrow 95:5 to 40:60 over 23 min \rightarrow 5:95 for 5 min.

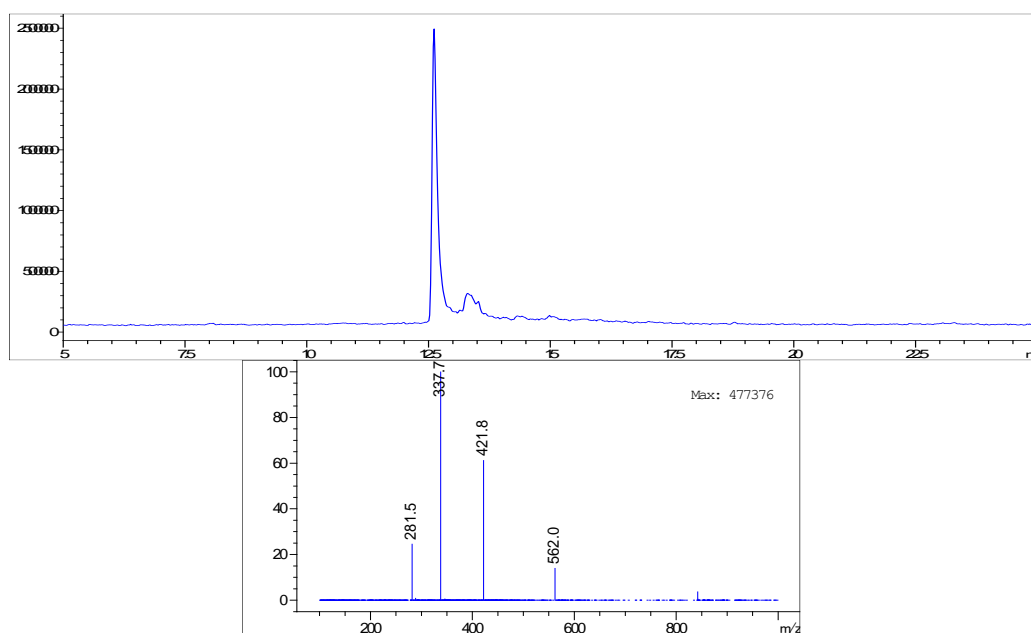
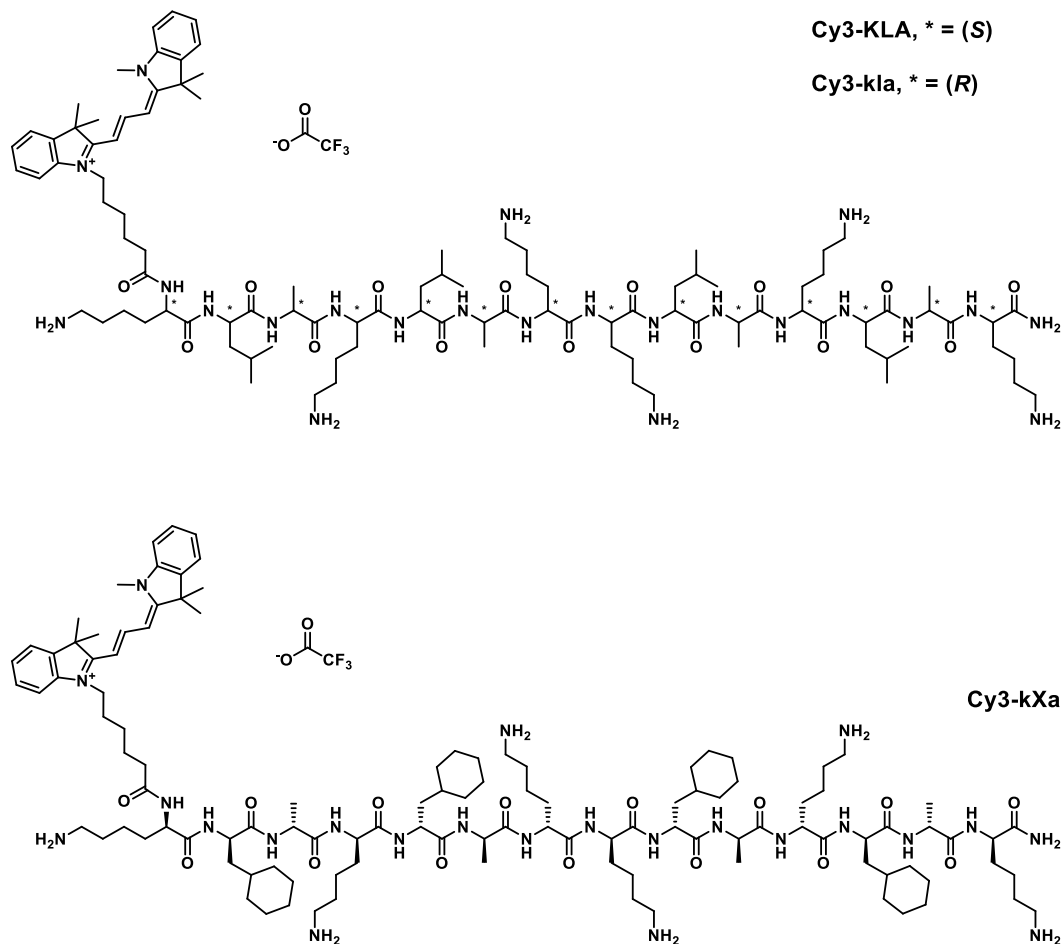


Figure 3.9. TIC chromatogram (+ mass spectrum at 12.562:12.853 min) of **kxa**. Column: *Poroshell 120 EC-C18*, 2.1 x 100 mm, 4 μ m particle size, 120 Å pore size; Method: flow rate = 0.5 mL \cdot min⁻¹, H₂O: CH₃CN, 0.1% HCOOH, 95:5 for 2 min \rightarrow 95:5 to 40:60 over 23 min \rightarrow 5:95 for 5 min.

3.6.2.3 General procedure for the synthesis of cyanine dye-labelled peptides



The peptide chain was synthesised by SPPS on Rink Amide MBHA resin. Each amino acid coupling step was carried out with Fmoc-protected amino acid (2 eq), DIC (4 eq), ethyl cyanohydroxyiminoacetate (2 eq) in DMF at 75 °C (155 W) for 0.25 min and at 90 °C (30 W) for further 2 min. For the last lysine, the coupling was carried out at 75 °C (155 W) for 0.5 min seconds and at 90 °C (30 W) for further 4 min. After each coupling step, the respective Fmoc protecting group was removed by 10% Piperazine (w/v) in ethanol:NMP (1:9). After the final Fmoc deprotection, the cyanine dye scaffold was manually coupled using 3 eq of **Cy3-COOH**, 6 eq of DIC, 3 eq of ethyl cyanohydroxyiminoacetate for 16 h at room temperature. Cleavage was performed in TFA/Water/TIS 95:2.5:2.5 solution for 2 h. The resin was removed by filtration and the filtrate was concentrated by N₂ flow. The crude product was precipitated with cold diethyl ether, centrifuged (4,000 g for 10 min) and the supernatant was discarded. The precipitate was dissolved in water and purified by HPLC. Lyophilisation of the pure product fractions afforded the desired

compounds as red powders. Desired product was characterised by LC/MS (Figure 3.10-12).

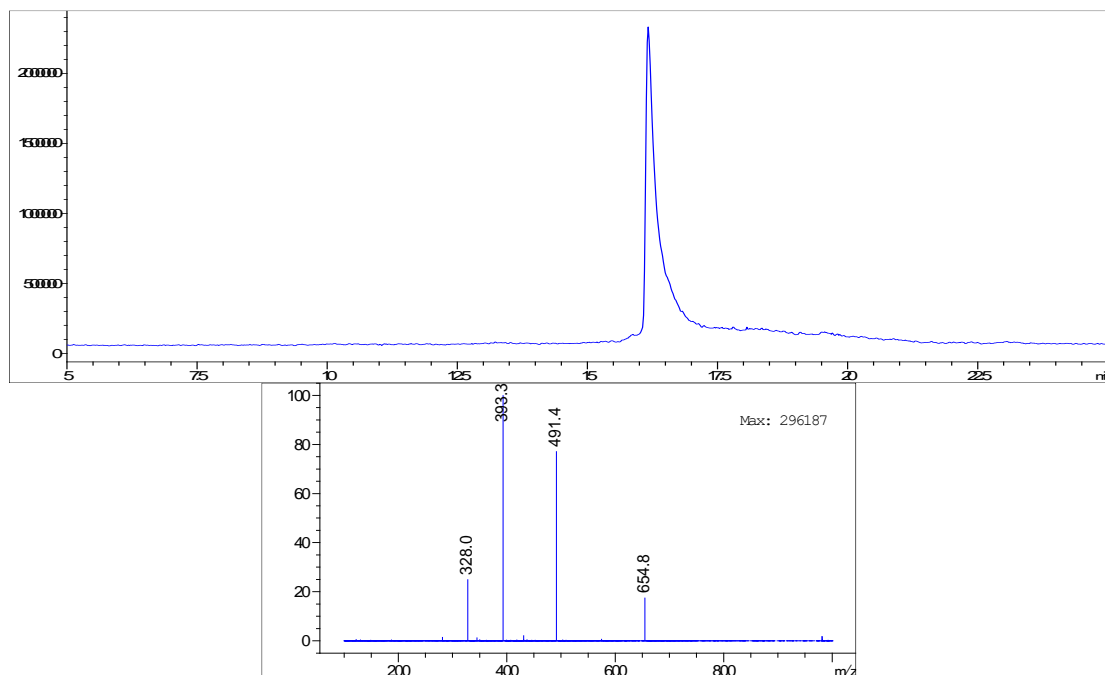


Figure 3.10. TIC chromatogram (+ mass spectrum at 16.042:16.771 min) of **Cy3-KLA**. Column: *Poroshell 120 EC-C18*, 2.1 x 100 mm, 4 μ m particle size, 120 Å pore size; Method: flow rate = 0.5 mL \cdot min⁻¹, H₂O: CH₃CN, 0.1% HCOOH, 95:5 for 2 min \rightarrow 95:5 to 40:60 over 23 min \rightarrow 5:95 for 5 min.

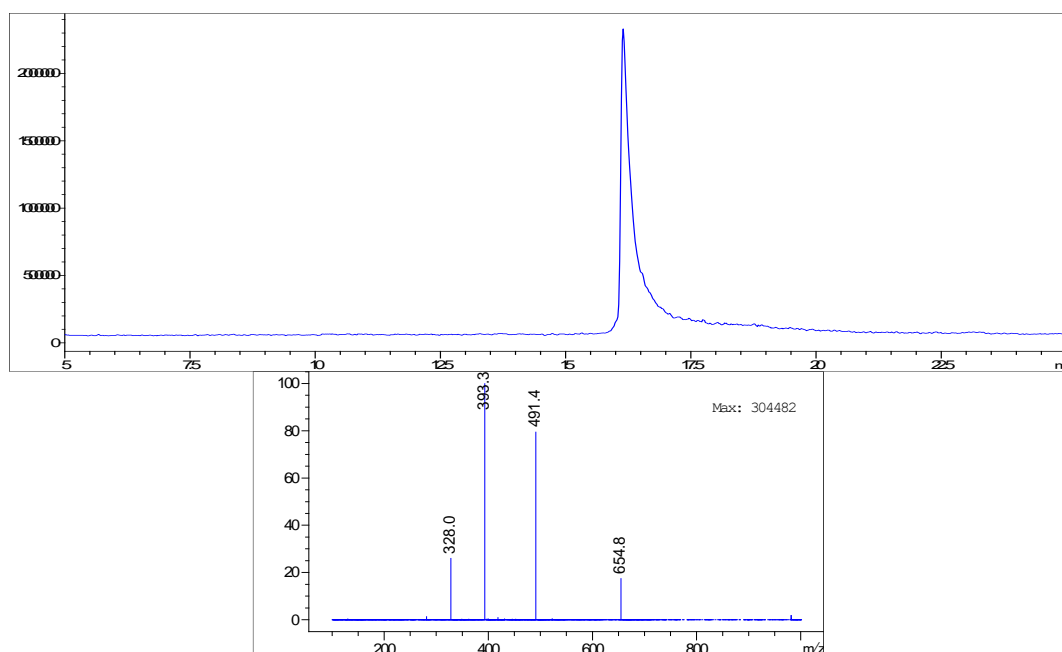


Figure 3.11. TIC chromatogram (+ mass spectrum at 16.188:16.680 min) of **Cy3-*kla***. Column: *Poroshell 120 EC-C18*, 2.1 x 100 mm, 4 μm particle size, 120 Å pore size; Method: flow rate = 0.5 mL \cdot min⁻¹, H₂O: CH₃CN, 0.1% HCOOH, 95:5 for 2 min → 95:5 to 40:60 over 23 min → 5:95 for 5 min.

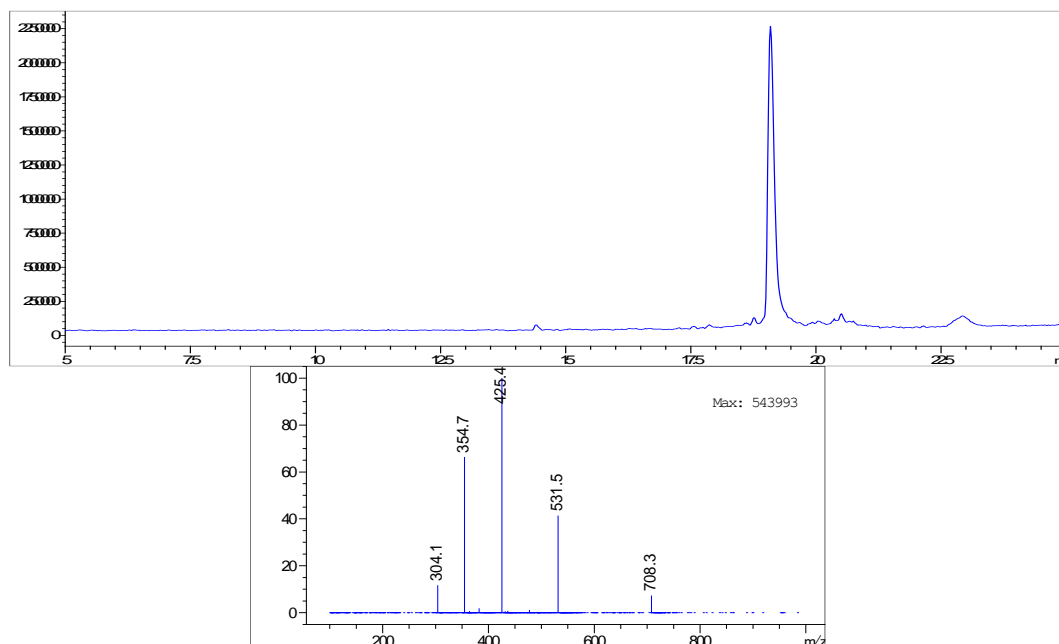


Figure 3.12. TIC chromatogram (+ mass spectrum at 19.056:19.256 min) of **Cy3-*kXa***. Column: *ACE 3 C18*, 2.1 x 100 mm, 3 μm particle size, 100 Å pore size; Method: flow rate = 0.3 mL \cdot min⁻¹, H₂O: CH₃CN, 0.1% HCOOH, 85:15 to 5:95 over 35 min → 5:95 for 2 min.

3.6.3 Biological evaluation

3.6.3.1 Cell culture

MCF-7 and HEK cells were maintained in T75 flasks at 37 °C in a 5% CO₂ atmosphere in Dulbecco's modified eagle medium (DMEM) supplemented with 10% (v/v) fetal bovine serum (FBS). KB and SK-OV-3 cells were maintained in T75 flasks at 37 °C in a 5% CO₂ atmosphere in RPMI 1640 medium supplemented with 10% (v/v) FBS. Cells were maintained at a sub-confluent monolayer and split at 80-85% confluency. For splitting, cells were washed with phosphate-buffered saline (PBS), trypsinised in 1 mL of trypsin and 200 μL of the 1000 μL trypsin cell suspension was re-suspended in a new T75 flask in 12 mL fresh medium containing 10% (v/v) FBS.

3.6.3.2 Cell viability assay

MCF-7 and HEK cells were seeded at a density of 2×10^4 cells per well in a Corning 96-well plate and grown at 37 °C in a 5% CO₂ atmosphere DMEM supplemented with 10% (v/v) FBS for 24 h. KB and SK-OV-3 cells were seeded at a density of 7×10^3 cells per well in a Corning 96-well plate and grown at 37 °C in a 5% CO₂ atmosphere Roswell Park memorial institute 1640 (RPMI-1640) medium supplemented with 10% (v/v) FBS for 24 h. Stock solutions of **KLA**, **kla**, **kXa**, **Cy3-KLA** and **Cy3-kla** were obtained by dissolving the compounds in sterile deionised water. **Cy3-kXa** and **Cy3-COOH** were dissolved in pure DMSO. The stock solutions were diluted into the proper medium (according to the tested cell line) supplemented with 10% FBS to the appropriate concentration, and cells in each well were incubated with 100 µL of the solution. The solutions in each well were then adjusted to a concentration of 1% (v/v) DMSO. After 24 h at 37 °C, 20 µL of CellTiter-Blue® was added to each well. The plate was incubated for another 4 h at 37 °C before analysis on a Perkin Elmer Victor X plate reader (excitation 531 nm; emission 595 nm). Each data point is calculated from three biological replicates (*i.e.* cells split from three different passages), and each biological replicate is calculated from three technical replicates (*i.e.* cells split from the same passage). Value from media-only with CellTiter-Blue was set as 0% viability. This value was then subtracted from the values from cell-only (*i.e.* non-treated) wells with CellTiter-Blue in each biological replicate and set as 100% viability. For treatments containing **Cy3-COOH** and cyanine dye-labelled constructs, blanks were generated with cell-free wells containing the compounds and adding CellTiter-Blue. The fluorescent reading for these wells was deducted from the treatment readings.

EC₅₀ values were derived by generating dose-response curves (Figure 3.13-16) using Origin, version 2019b, OriginLab Corporation, Northampton, MA, USA.

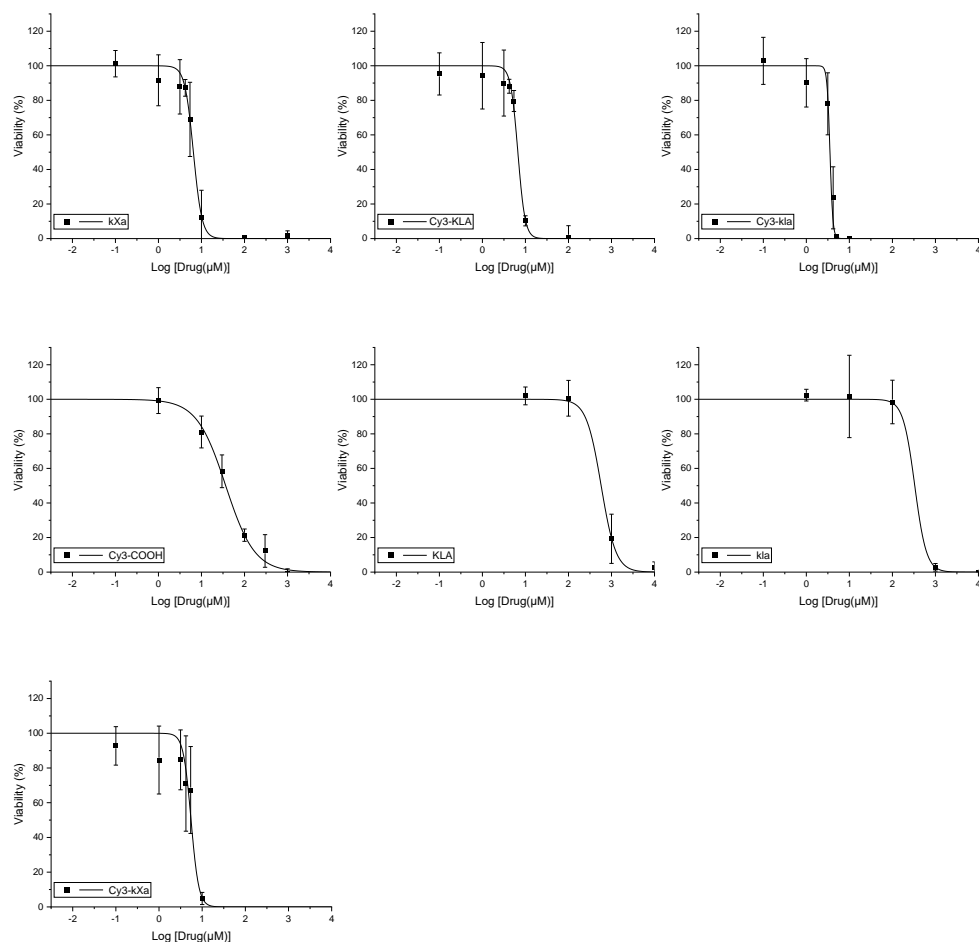


Figure 3.13. Cytotoxicity of tested compounds towards KB cell lines. Fitting curves are shown as solid black lines. Dots and error bars represent the mean and the standard deviation from a minimum of nine values resulted from three biological replicates (i.e. cells split from three different passages); each biological replicate is calculated from three technical replicates (i.e. cells split from the same passage).

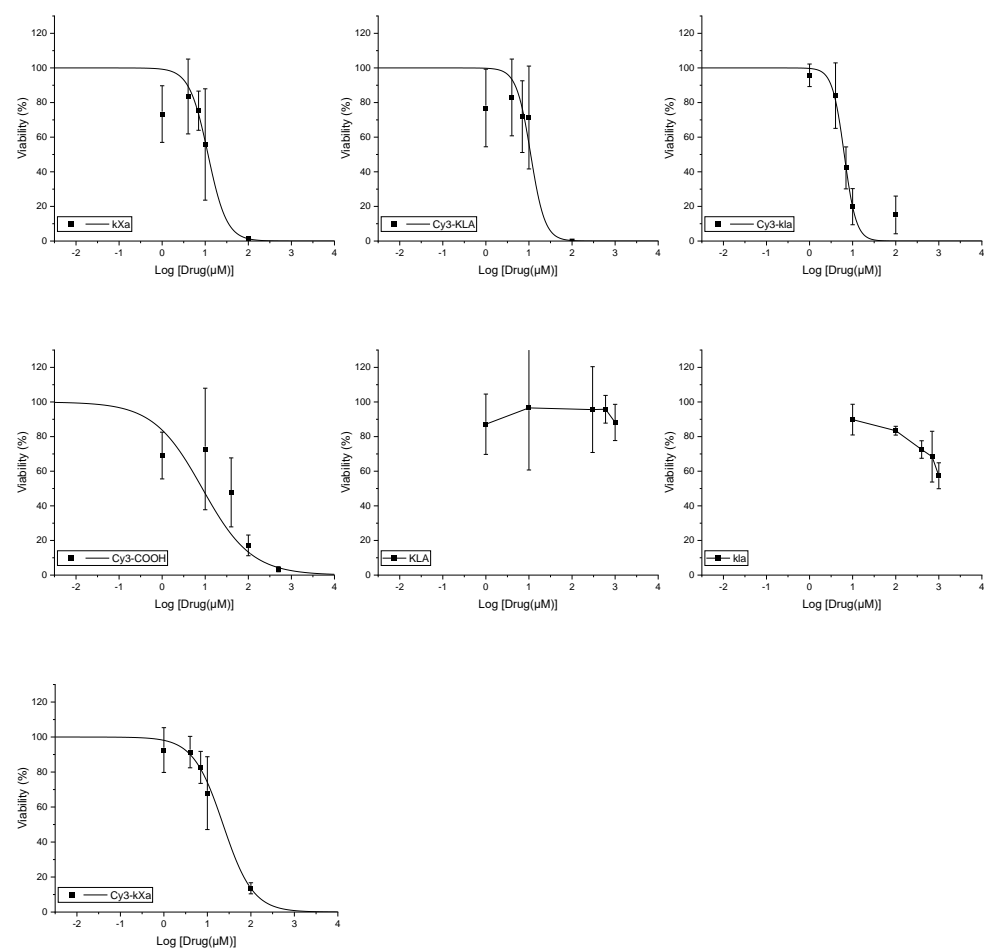


Figure 3.14. Cytotoxicity of tested compounds towards SK-OV-3 cell lines. Fitting curves are shown as solid black lines. Data for compounds **KLA** and **kla** were not fitted. Dots and error bars represent the mean and the standard deviation from a minimum of nine values resulted from three biological replicates (i.e. cells split from three different passages); each biological replicate is calculated from three technical replicates (i.e. cells split from the same passage).

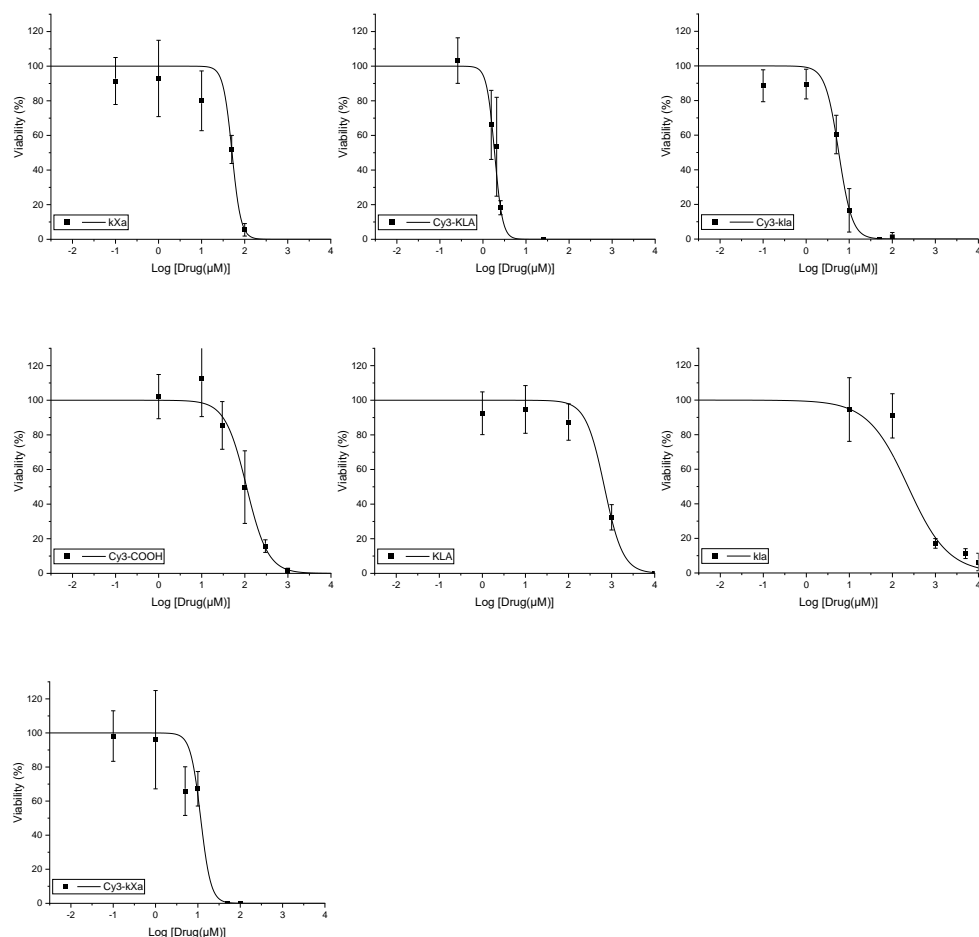


Figure 3.15. Cytotoxicity of tested compounds towards MCF7 cell lines. Fitting curves are shown as solid black lines. Dots and error bars represent the mean and the standard deviation from a minimum of nine values resulted from three biological replicates (i.e. cells split from three different passages); each biological replicate is calculated from three technical replicates (i.e. cells split from the same passage).

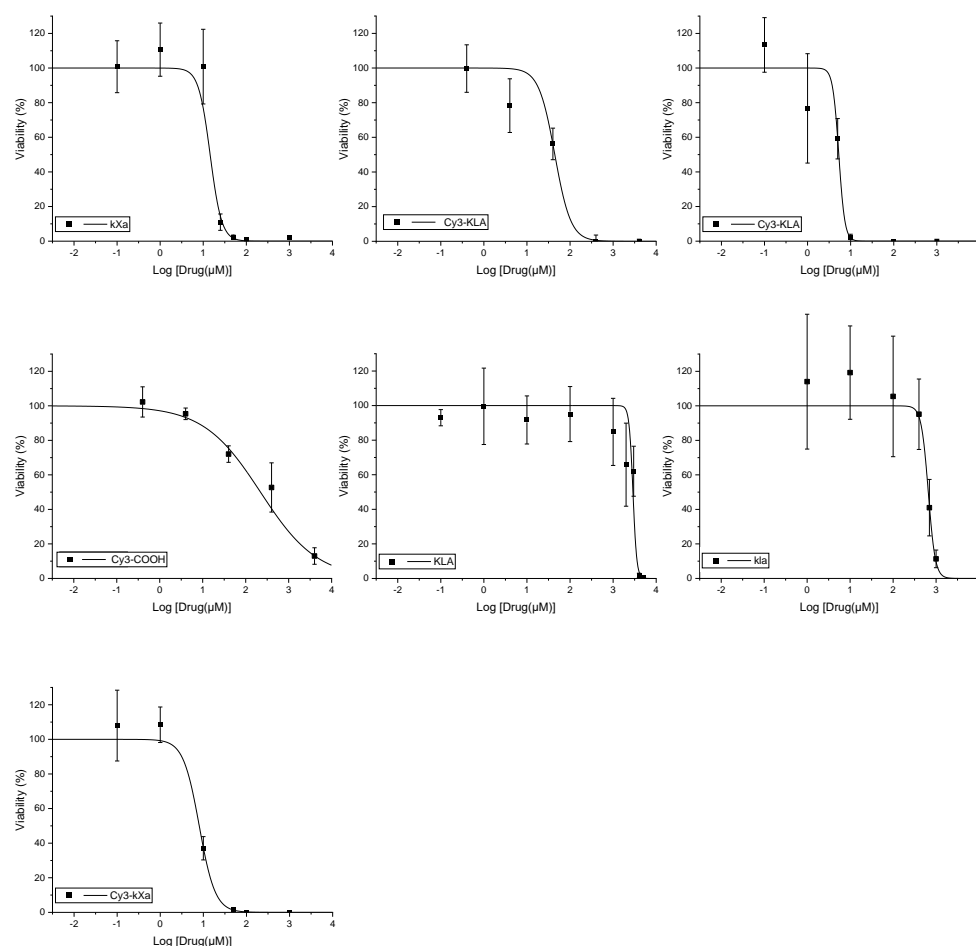


Figure 3.16. Cytotoxicity of tested compounds towards HEK293 cell lines. Fitting curves are shown as solid black lines. Dots and error bars represent the mean and the standard deviation from a minimum of nine values resulted from three biological replicates (i.e. cells split from three different passages); each biological replicate is calculated from three technical replicates (i.e. cells split from the same passage).

3.6.3.3 Confocal microscopy

SK-OV-3 and MCF7 were seeded at a density of 1×10^6 cells per well in glass bottom culture dishes and grown at 37 °C in a 5% CO₂ atmosphere in medium supplemented with 10% (v/v) FBS for 24 h. Cells were washed once with the RPMI-1640 medium supplemented with 10% (v/v) FBS before staining. **Cy3-COOH**, **Cy3-KLA**, **Cy3-kla** and **Cy3-kXa** were diluted into the RPMI-1640 medium supplemented with 10% (v/v) FBS to 10 μM and then add to the culture dishes respectively. After 10-min incubation at 37 °C, cells were washed with RPMI-1640 medium supplemented with 10% (v/v) FBS. Cells were then treated with 50 nM MitoTracker Green FM and 10 μg/ml Hoechst 33258 pre-formulated with RPMI-

1640 medium supplemented with 10% (v/v) FBS, and then incubated for another 10 min at 37 °C before analysis on ZEISS LSM 900 with Airyscan 2. The results were analysed using Image J software.

3.6.3.4 Flow cytometry

SK-OV-3 and MCF7 were seeded at a density of 2×10^5 cells per well in 24-well plate and grown at 37 °C in a 5% CO₂ atmosphere in DMEM medium supplemented with 10% (v/v) FBS for 24 h. Cells were washed once with the RPMI-1640 medium supplemented with 10% FBS before staining. **Cy3-COOH**, **Cy3-KLA**, **Cy3-kla** and **Cy3-kXa** were diluted into the RPMI-1640 medium supplemented with 10% FBS to 10 µM and then add to the culture dishes. After 10-min incubation at 37 °C, cells were washed with RPMI-1640 medium supplemented with 10% FBS. Cells were then treated with 50 nM Mitotracker Green FM and 10 µg/ml Hoechst 33258 pre-formulated with RPMI-1640 medium supplemented with 10% FBS for another 10 min at 37 °C. Cells were washed once with PBS before trypsinization for flow cytometry analysis on Invitrogen Attune NxT. The results were analysed using FlowJo™ v10 Software (BD Life Sciences).

3.6.3.5 Statistical analysis

Comparison of cytotoxicity fitting curves was achieved by applying the extra sum-of-squares F test, performed using GraphPad Prism version 9 for Windows, GraphPad Software, La Jolla California USA, www.graphpad.com. Statistical difference between cytotoxicity values was assumed when *p*-value, as output of the extra sum-of-squares F test, was found to be below 0.05.

CHAPTER 4

Enhancing the selectivity of Cy3-labelled mitochondriolytic peptides towards cancer cells

CHAPTER 4 - Enhancing the selectivity of Cy3-labelled mitochondriolytic peptides towards cancer cells

4.1 Abstract

After achieving improved cytotoxicity by Cy3-conjugation, we sought to enhance the selectivity of the cyanine dye-labelled peptides towards cancer cells. Therefore, the peptide constructs synthesised in chapter 3 are covalently labelled with folate by SPPS. These new constructs were not found to be more toxic towards cells known to overexpress the folate receptor- α (KB and SK-OV-3 cells), compared to low level folate receptor- α expressing cells (MCF-7 and HEK cells).

4.2 Introduction

Receptor mediated tumour-targeted drug delivery systems are an established and very promising tool in the field of cancer treatment.⁶⁸ They are intended to selectively target cancer tissues by exploiting the unique expression of specific receptors on the surface of cancer cells. In this way, chemotherapeutics are preferentially delivered to cancer cells.⁶⁹

Since its discovery as a tumour-selective ligand,⁷¹ folate has been extensively used as a cancer cell targeting moiety in drug delivery systems.⁷²⁻⁷⁴ This strategy takes advantage of the paucity or absence of the folate receptor α from normal tissues to deliver chemotherapeutics to cancer cells via endocytosis.⁷⁵

Folate (or vitamin B₉) is a key component of the one-carbon metabolism, which provides – amongst others – the building blocks for DNA replication;¹¹⁹ therefore, folate is mostly taken up by rapidly proliferating cells. In physiological conditions, the uptake is mediated in large part by the reduced folate carrier, which is a membrane transporter ubiquitously expressed on the cell membrane.⁷³ An alternative, and less exploited route for folate internalisation is the one mediated by folate receptor α . This receptor is poorly expressed, or absent on the basolateral membrane of the majority of healthy cells.⁷² On the other hand, folate receptor α is overexpressed in many malignant cells.⁷² Additionally, the binding constant of folate receptor α for folate ($K_d = 0.1 - 1$ nM)⁷² is significantly smaller than the one of the reduced folate carrier (K_d in the micro- and millimolar range).¹²⁰

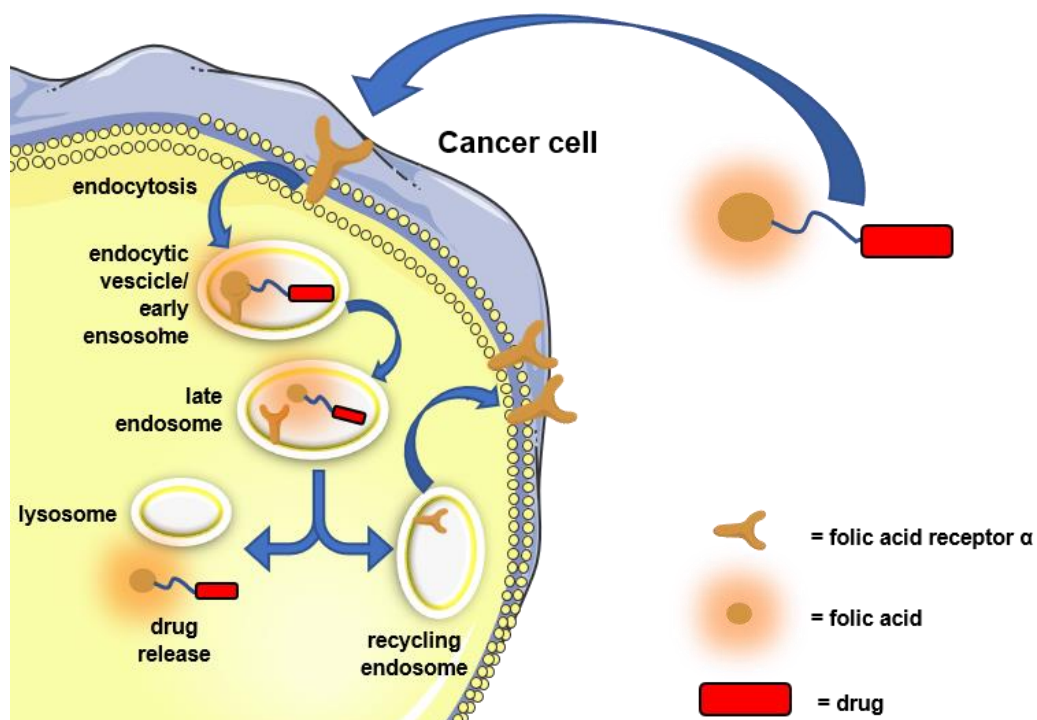


Figure 4.1. Folate receptor α -mediated endocytosis of a folic acid-conjugated drug. Figure template provided by smart.servier.com.

By delivering chemotherapeutics to cancer cells via folate receptor α -mediated endocytosis, the drug is covalently attached to folate by one of its two carboxylic groups. Once approaching the cell expressing the folate receptor α on its membrane, the conjugate interacts with the receptor, triggering the invagination of the cell membrane.⁷² This event leads to the formation inside the cell of an early endosome, within which the receptor is still anchored to the membrane and tightly interacts with the drug conjugate. When the early endosome evolves into a late endosome, the pH inside the organelle reaches slightly lower values, causing conformational changes in the protein structure that lead to the detachment of the drug conjugate from the receptor. Finally, the late endosome merges with the lysosome, where the drug can be released, and the recycling endosome brings the receptor back onto the cell surface (figure 4.1).⁷²

4.3 Aim and Objectives

Although **Cy3-KLA**, along with the other cyanine dye labelled compounds, shows a certain degree of selectivity towards some cancer cell lines,¹²¹ it was still

exhibiting a low EC_{50} ($43.6 \pm 9.1 \mu M$) when incubated with the non-cancer cell line HEK. Therefore, these constructs need to be engineered to be more selective towards cancer cells, so to have less non-specific toxicity. Given the ease of conjugating small molecules to a peptide directly on a solid support (as already proven for conjugation of various sequences to **Cy3**), we decided to attach a tumour-targeting moiety, such as folate, to increase the drug uptake by cancer cells (figure 4.2).

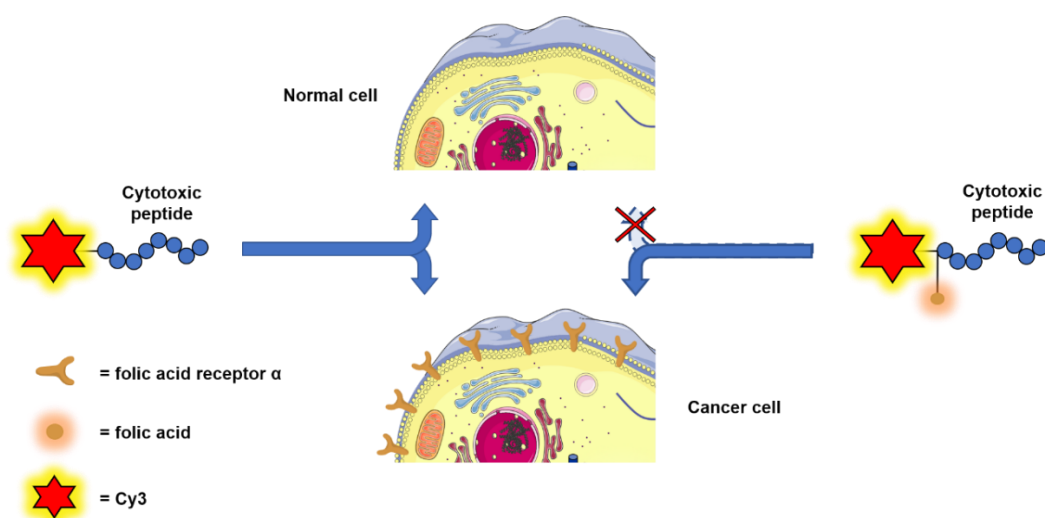


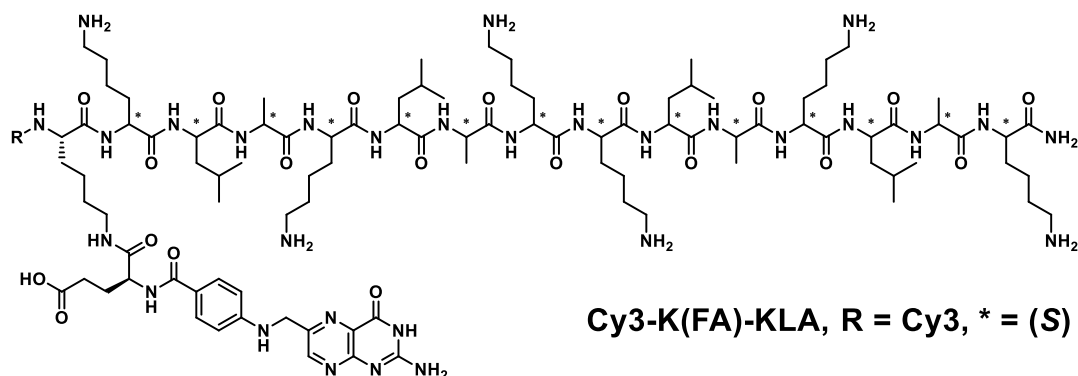
Figure 4.2. Increasing selectivity towards cancer cells via folate labelling. Figure template provided by smart.servier.com.

With the aim of generating selective anticancer theranostics, we set to conjugate folate (referred to in the compound name as FA), through its α -carboxylic moiety, to the ϵ -amino group of an extra lysine added to the *N*-terminus of the peptide sequence, yielding **Cy3-K(FA)-KLA**, **Cy3-K(FA)-kla** and **Cy3-K(FA)-kXa** (figure 4.3). To evaluate the contribution of the **Cy3**-labelling on the cytotoxic activity, compounds not bearing the cyanine scaffold were also synthesised, where **Cy3** was replaced by an acetyl group (figure 4.3). The biological activity of these new constructs was then assessed via Cell-Titer blue assay.

Specific objectives are:

- Synthesis of folate-conjugated peptides;

- Evaluation of their cytotoxicity and selectivity towards cancer cells compared to the unconjugated peptides.

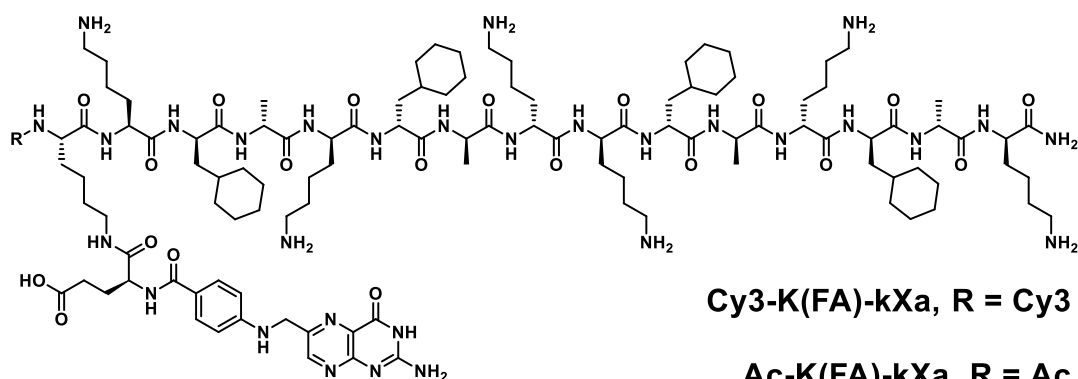


Cy3-K(FA)-KLA, R = Cy3, * = (S)

Cy3-K(FA)-kla, R = Cy3, * = (R)

Ac-K(FA)-KLA, R = Ac, * = (S)

Ac-K(FA)-kla, R = Ac, * = (R)



Cy3-K(FA)-kXa, R = Cy3

Ac-K(FA)-kXa, R = Ac

Figure 4.3. Molecular structures of the compounds synthesised and tested in this chapter.

4.4 Results and discussion

4.4.1 Solid-Phase Peptide Synthesis of folate-conjugated peptides

To generate the folate conjugates depicted in Figure 4.3, an extra lysine was added to the *N*-terminus sequence of compounds **KLA**, **kla**, and **kXa** via the same SPPS strategy. **Cy3** or an acetyl group would be coupled to the α -amino group of the extra lysine and the folate moiety attached on the ϵ -amino group.

The strategy employed for this purpose requires the usage of a protecting group for the extra lysine side chain which can be cleaved under conditions that are orthogonal to the other protecting groups and with the linker of the resin. Here, the side chain of the *N*-terminal lysine was protected with the 4-methyltrityl (Mtt) group. This protective group is cleaved in 1% TFA (v/v) in DCM,¹²² a condition in which the other commonly used protective groups (e.g., -tBu, -Boc, -Trt) and linkers for SPPS are preserved. Once Mtt is cleaved, the ϵ -amino group of the lysine can be used for the coupling while still attached to the solid support.

The literature procedure for the conjugation of folate to **KLA** reports the direct use of folic acid in the coupling reaction.⁹⁷ When applied to the SPPS of **Cy3-K(FA)-KLA**, this strategy led to the folate moiety to be coupled via either its α - or γ -carboxylic moiety, giving rise to a mixture of the α - and γ -labelled isomers which cannot be easily purified (Figure 4.4).

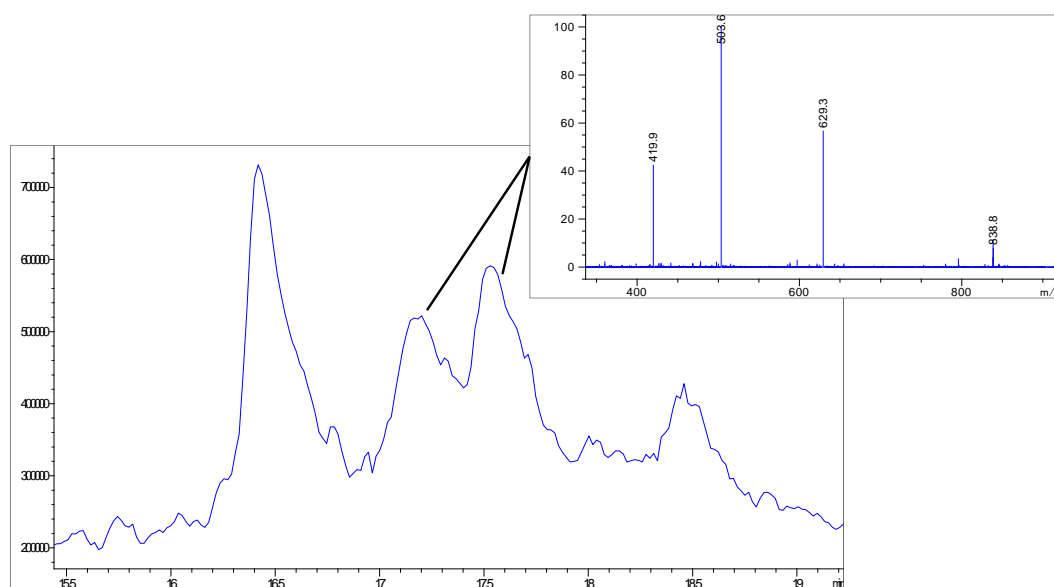


Figure 4.4. TIC chromatogram of the crude of **Cy3-K(FA)-KLA** synthesis after coupling folic acid to the ϵ -amino group of the *N*-terminal lysine. Mass spectrum shows the same m/z peaks for two different chromatogram peaks, indicating the formation of two folate-labelled isomers.

To overcome this issue, Fmoc-protected glutamic acid (where the carboxylic group in the side chain is protected as *tert*-butyl ester) was first coupled to the lysine side chain. In this way, only the α -carboxylic group of the glutamic acid would react. Fmoc deprotection of the glutamic acid residue followed by

coupling with the pteric acid, would yield a construct in which the folate is conjugated with the lysine side chain with only its α -carboxylic group.

For the peptidyl backbone of the folate-labelled compounds, the synthesis was carried out the same way as for compounds **KLA**, **kla** and **kxa**. For the preparation of **Cy3-K(FA)-KLA**, **Cy3-K(FA)-kla**, **Ac-K(FA)-KLA**, **Ac-K(FA)-kla** and **Ac-K(FA)-kXa**, the *N*-terminal lysine was then introduced as Fmoc-Lys(Mtt)-OH. For this last residue, three equivalents of the amino acid were employed which needed to be double coupled to the elongating peptide chain to bring the coupling to completion. Following Fmoc cleavage, the peptidyl resin was either coupled to **Cy3-COOH** (applying the same conditions used for **Cy3**-labelled compounds in chapter 3) or was capped by treatment with a large excess of acetic anhydride/pyridine. For the folate labelling, the Mtt group was cleaved via treatment with 1% TFA. The resulted free amine was coupled with Fmoc-Glu(OtBu)-OH. Fmoc cleavage and final coupling of the pteric acid were followed by a TFA cleavage and HPLC purification, thus yielding the desired compounds.

The preparation of **Cy3-K(FA)-kXa** proved to be more challenging. In fact, upon Mtt deprotection and Fmoc-Glu(OtBu)-OH coupling and Fmoc deprotection, the Mtt strategy led to the presence of a peak in the LC/MS chromatogram with a difference of +129 *m/z* compared to the desired intermediate, attributable to an extra glutamic acid residue (Figure 4.5). This is likely due to Boc deprotection during the Mtt cleavage conditions (1% TFA in DCM). Finally, conjugate 10 was obtained using 1-(4,4-dimethyl-2,6-dioxocyclohex-1-ylidene)-3-methylbutyl (ivDde) as a protecting group, which could be cleaved in 4% (v/v) hydrazine hydrate in DMF, leading to selective labelling of one folate molecule to the peptide.

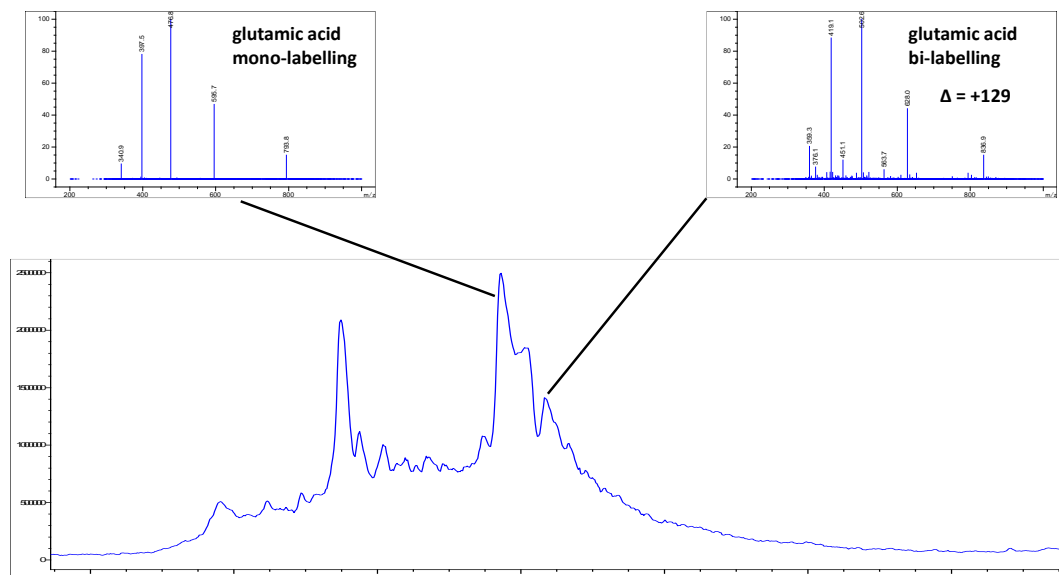


Figure 4.5. TIC chromatogram of the crude of synthesis for **Cy3-K(FA)-kXa** after coupling and deprotection of glutamic acid to the ϵ -amino group of the *N*-terminal lysine. Mass spectrum shows the desired m/z for the mono-labelled glutamic acid intermediate (on the left) along with the bi-labelled glutamic acid intermediate (on the right). This led to an inseparable mixture of the desired product and bi-labelled folate side product.

4.4.2 Cell viability assay

To explore whether the conjugation of folate to the previously tested cyanine dye-labelled peptides enhanced the cytotoxicity towards cancer over non-cancer cells, a Cell-Titer Blue assay was performed towards KB, SK-OV-3, MCF7 and HEK293 cells.

Table 4.1. The EC_{50} values (expressed in μM) on different cell lines of different molecules and their cyanine dye conjugates were quantified using cell viability assays. The values in brackets represent the standard error of the curve fitting using Origin, version 2019b, OriginLab Corporation, Northampton, MA, USA.

Compound	EC_{50}			
	KB	SK-OV-3	MCF7	HEK
Cy3-K(FA)-KLA	38.8 (6.6)	8.8 (3.7)	49.4 (4.3)	35.6 (3.4)
Cy3-K(FA)-kla	22.4 (1.4)	8.0 (2.2)	13.2 (5.6)	6.9 (1.8)
Cy3-K(FA)-kXa	3.4 (0.7)	6.0 (1.1)	6.9 (0.9)	6.8 (1.4)
Ac-K(FA)-KLA	242 (33.2)	> 400	> 400	> 400

Ac-K(FA)-kla	151 (38.7)	388.4 (21.3)	> 400	> 400
Ac-K(FA)-kXa	9.8 (0.6)	41.5 (4.0)	26.9 (7.2)	20.4 (5.7)

As shown in Table 4.1, **Cy3-K(FA)-kXa**, **Ac-K(FA)-KLA** and **Ac-K(FA)-kla**, **Ac-K(FA)-kXa** showed enhanced toxicity in KB, but not in SK-OV-3 cells, when compared to MCF7 and HEK293 cells. Nonetheless, potency of **Ac-K(FA)-KLA** and **Ac-K(FA)-kla** in cells not overexpressing folate receptor α is comparable to that of their native peptides. Lastly, dual labelled constructs **Cy3-K(FA)-KLA**, **Cy3-K(FA)-kla** and **Cy3-K(FA)-kXa** showed enhanced potency compared to the parent sequences and folate conjugates without **Cy3** ($p < 0.05$), although no selectivity was observed toward KB and SK-OV-3 cells.

4.4.3 Subcellular localisation and cellular uptake of folate conjugates

To gain further insights on the mechanism of action on the newly synthesised compounds and on the reasons why the expected selectivity could not be achieved, subcellular localization and cellular uptake if the constructs were evaluated by Wenjing Deng who is a researcher working in the Shenzhen Bay Laboratory of the Gaoke Innovation Center in Shenzhen, China.

Subcellular localisation was studied via confocal microscopy: SK-OV-3 and MCF7 cells were stained with MitoTracker Green and Hoechst33258 and then incubated with dual-labelled compounds. Next, the fluorescent patterns of the tested molecules and stains were analysed to determine colocalization within the cell.

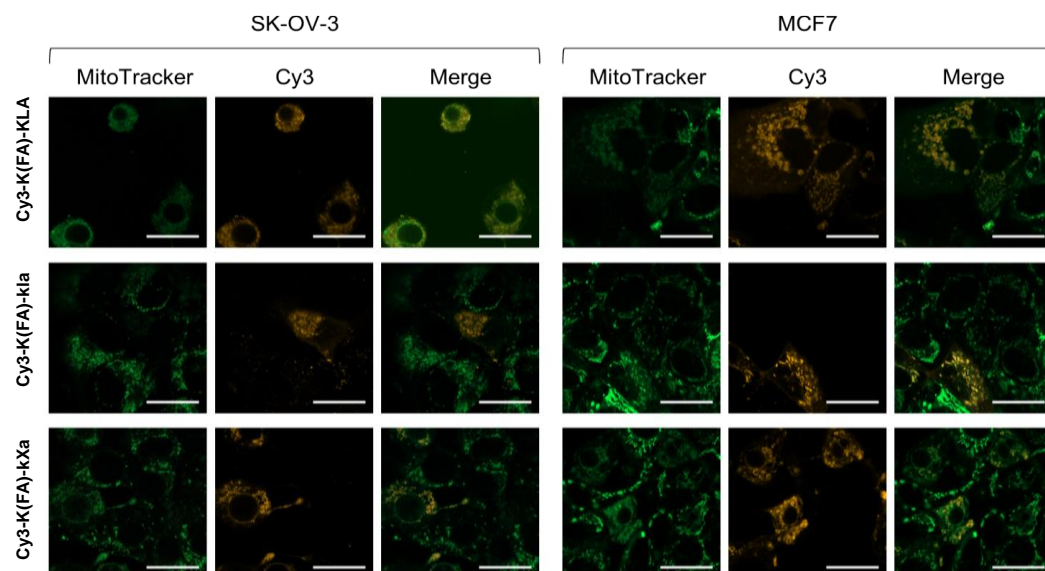


Figure 4.6. Confocal microscopy images of SK-OV-3 and MCF7 cells treated with dual-labelled conjugates. Cells were treated with 10 μ M of the indicated conjugate for 10 min at 37 $^{\circ}$ C, washed, stained with 50 nM MitoTracker Green and 10 μ g/ml Hoechst33258 for 10 min at 37 $^{\circ}$ C, washed and imaged at 63X. Excitation wavelengths for Hoechst 33258, MitoTracker Green and Cy3 were set as 405, 488 and 561 nm, respectively. Pearson's correlation coefficients of MitoTracker Green FM and Cy3 fluorescence for **Cy3-K(FA)-KLA**, **Cy3-K(FA)-kla** and **Cy3-K(FA)-kXa** in SK-OV-3 and MCF cells are 0.85/0.69, 0.43/0.82, and 0.78/0.60, respectively. Scale bars denote 25 μ m.

Cellular uptake of **Cy3-K(FA)-KLA**, **Cy3-K(FA)-kla** and **Cy3-K(FA)-kXa** was assessed via flow cytometry: SK-OV-3 and MCF7 cells were incubated with the tested compounds and with MitoTracker Green (used as a reference), and then analysed by the flow cytometer to output a fluorescence value generated by the uptake of the constructs.

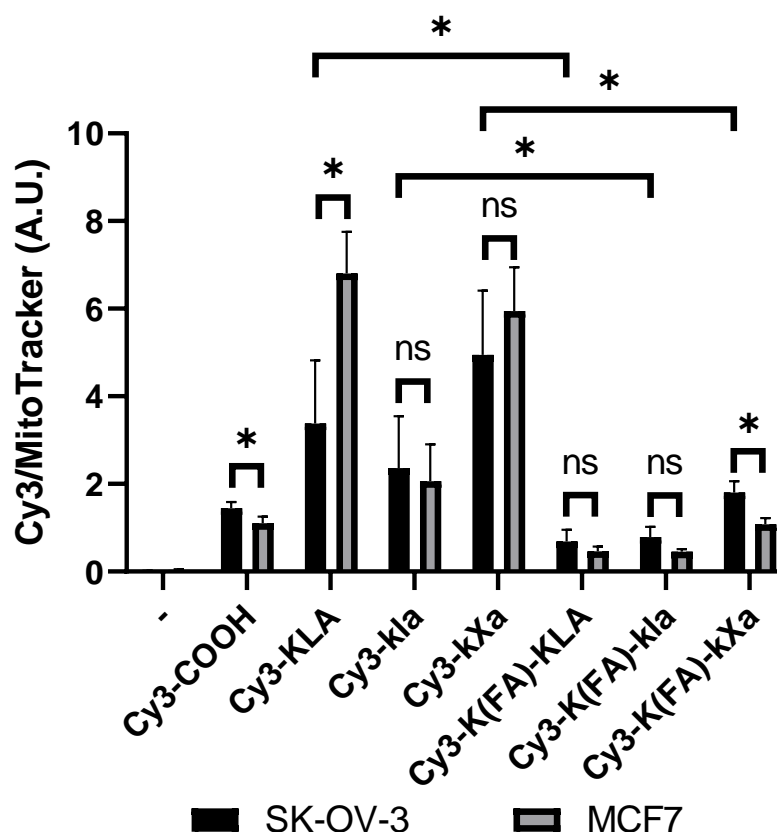


Figure 4.7. Flow cytometry analysis of cyanine dye- and dual-labelled conjugates uptakes by SK-OV-3 and MCF7 cells. Cells were treated with 10 μ M of the indicated conjugate for 10 min at 37 $^{\circ}$ C, washed, stained with 50 nM MitoTracker Green for 10 min at 37 $^{\circ}$ C, washed, trypsinized and subjected to flow cytometry analysis. Cellular uptakes are shown as the ratios of Cy3 and MitoTracker fluorescence. Mean ratios \pm standard deviations are calculated from three biological replicates and plotted in arbitrary unit (A.U.) The negative control (-) refers to cells only stained with MitoTracker Green. Statistical analysis was performed by applying the extra sum-of-squares F test, performed using GraphPad Prism version 6 for Windows, GraphPad Software, La Jolla California USA, www.graphpad.com. ns = non statistically significant, * = $p < 0.05$.

As indicated in Figure 4.6, dual-labelled compounds colocalise with MitoTracker Green, therefore confirming their mitochondrial localisation. Yet, folate conjugation led to a decrease in cellular uptake, when compared to the cyanine dye-labelled constructs discussed in chapter 3 (Figure 4.7).

4.5 Conclusions and perspectives

Folate-labelled constructs, with and without the cyanine dye scaffold, were successfully synthesised by SPPS. Generally, folate conjugation did not result in

the expected selectivity; moreover, it led in some cases to diminished potency compared to the peptides labelled with **Cy3-COOH** only. Additionally, notwithstanding the predicted mitochondrial localisation, **Cy3-K(FA)-KLA**, **Cy3-K(FA)-kla** and **Cy3-K(FA)-kXa** performed worse in the cellular uptake experiment compared to their analogues without the folate component.

Previously, attachment of a folate motif to the *N*-terminus,^{97, 123, 124} C-terminus¹²⁵ or in the middle of peptides¹²⁶ has led to either enhanced selectivity of the construct towards cells overexpressing the folate receptor α or enhanced binding affinity to recombinant folate receptor α . It has been reported that linking the folate via α - or γ -carboxylic group does not affect the uptake efficiency.¹²⁷ However, a different study had claimed otherwise¹²⁸ and, in most of the successful examples, the folate is connected through its γ -carboxylic group.⁷² Many of these constructs also bear a spacer between the folate and the cargo.⁷² Although the effects of the linker length and type has not been systematically evaluated, the steric environment around the folate fragment is known to be an important factor for the interaction of the conjugate with the receptor.¹²⁷ Besides, some proteins have shown improved uptake by folate receptor α positive cells when labelled with multiple folate molecules.¹²⁹ For future work, the attachment site, linkage, linker and valency of the folate within the constructs will be evaluated.

4.6 Experimental procedure

4.6.1 Solid Phase Peptide Synthesis

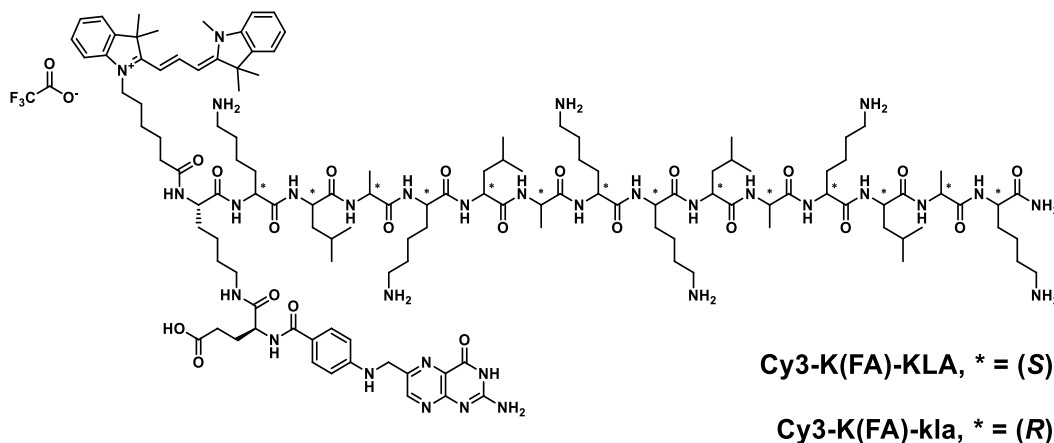
For General Methods and determination of Rink Amide resin loading, see 3.4.2 and 3.4.2.1.

Table 4.2. Calculated and expected molecular weight for the folate conjugates synthesised in this chapter

Compound	Calculated mw	Found mw*
Cy3-K(FA)-KLA	2514.2	2514.1 \pm 0.3
Cy3-K(FA)-kla	2514.2	2513.9 \pm 0.3
Cy3-K(FA)-Kxa	2674.5	2674.2 \pm 0.5
Ac-K(FA)-KLA	2116.6	2116.6 \pm 0.3
Ac-K(FA)-kla	2116.6	2116.6 \pm 0.3

* as per manufacturer's specifications, the mass accuracy of the Agilent 6120B Single Quadrupole instrument is ± 0.1 Da.

4.6.1.1 Synthesis of Cy3-K(FA)-KLA and Cy3-K(FA)-kla



The peptide chain was synthesised by SPPS on Rink Amide MBHA resin. Each amino acid coupling step was carried out with Fmoc-protected amino acid (2 eq), DIC (4 eq), ethyl cyanohydroxyiminoacetate (2 eq) in DMF at 75 °C (155 W) for 0.25 min and at 90 °C (30 W) for further 2 min. For the penultimate lysine, the coupling was carried out using Fmoc-Lys(Boc)-OH (2 eq), DIC (4 eq), ethyl cyanohydroxyiminoacetate (2 eq) at 75 °C (155 W) for 0.5 min and at 90 °C (30 W) for further 4 min. For the last lysine, the coupling was carried out using Fmoc-Lys(Mtt)-OH (3 eq), DIC (6 eq), ethyl cyanohydroxyiminoacetate (3 eq) at 75 °C (155 W) for 1 min and at 90 °C (30 W) for further 7 min. After each coupling step, the respective Fmoc protecting group was removed by 10% piperazine (w/v) in ethanol:NMP (1:9). After the final Fmoc deprotection, the peptidyl resin was removed from the automated synthesiser and **Cy3-COOH** was manually coupled using 3 eq of **Cy3-COOH**, 6 eq of DIC, 3 eq of ethyl cyanohydroxyiminoacetate, 16 h. For the Mtt group cleavage, the resin is treated with 1% TFA (v/v) in DCM for 2 min and then the solution is filtrated off. The procedure is repeated for 12 times. Then, glutamic acid was coupled using 4 eq of Fmoc-Glu(OtBu)-OH, 4 eq of HBTU, 4 eq of HOBt and 8 eq of DIPEA. Deprotection of the Fmoc protecting group was achieved by treatment with 5 mL of 20% (v/v) piperidine in DMF, for 10 min for 2

times. For the pterioic acid coupling, 2 eq of pterioic acid were suspended in 10 mL of DMSO and were heated up at 50 °C for 1 h. 8 eq of DIPEA and 2 eq of benzotriazol-1-yl-oxytripyrrolidinophosphonium hexafluorophosphate (PyBOB) were added to the suspension which was then reacted with the peptidyl-resin for 16 h at 40 °C. The pterioic acid coupling was then repeated for further 16 h at 40 °C. Cleavage from the resin was performed in TFA/H₂O/TIS 95:2.5:2.5 solution for 2 h. The resin was removed by filtration and the filtrate was concentrated by N₂ flow. The crude product was precipitated with cold diethyl ether, centrifuged (4,000 g for 10 min) and the supernatant was discarded. The precipitate was dissolved in 2 mL of CH₃CN + 0.1% TFA, diluted with 13 mL of H₂O + 0.1% TFA, filtrated through a 0.22 µm syringe filter and purified by HPLC. Lyophilisation of the pure product fractions afforded the desired compound as a red powder.

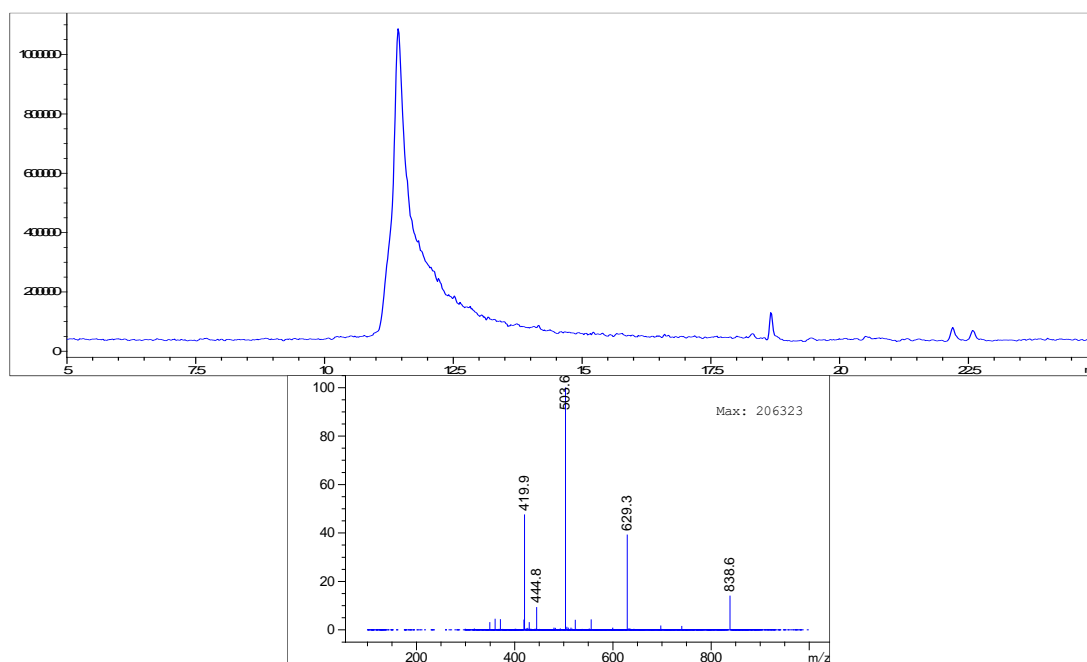


Figure 4.8. TIC chromatogram (+ mass spectrum at 11.300:11.719 min) of **Cy3-K(FA)-KLA**. Column: *ACE 3 C18*, 2.1 x 100 mm, 3 µm particle size, 100 Å pore size; Method: flow rate = 0.3 mL · min⁻¹, H₂O: CH₃CN, 0.1% HCOOH, 85:15 for 2 min → 85:15 to 40:60 over 13 min → 5:95 for 7 min → 5:95 to 85:15 over 0.5 min → 85:15 for 7 min.

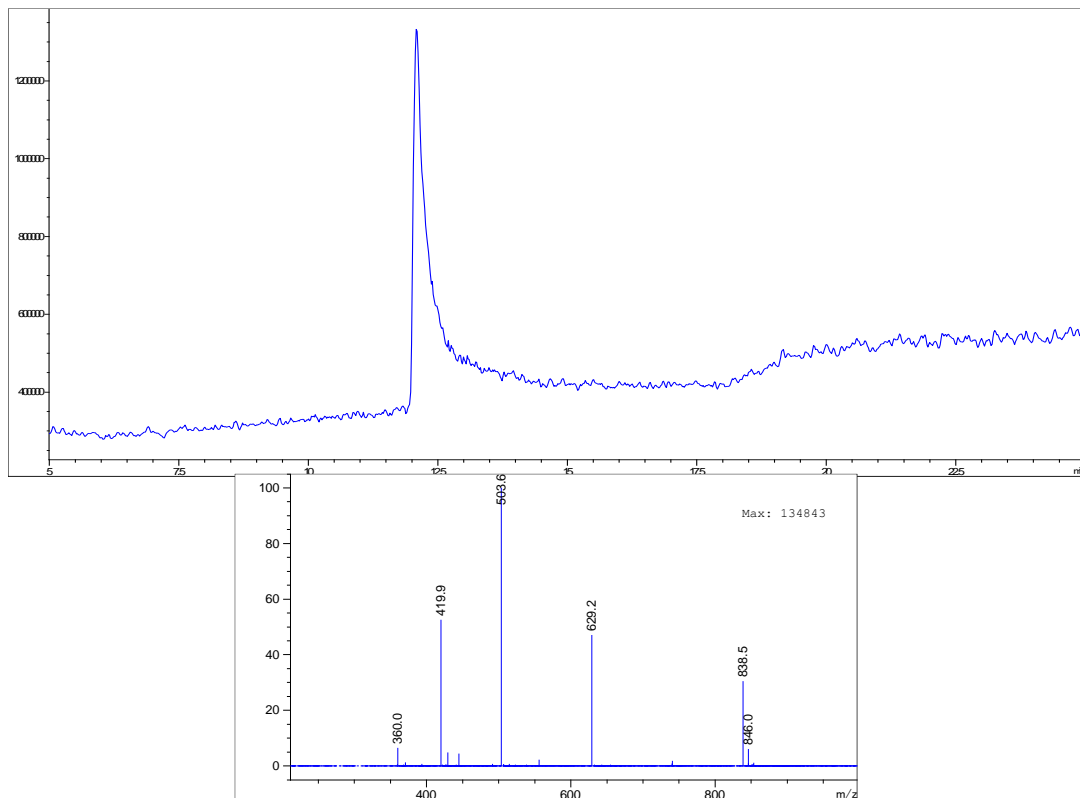
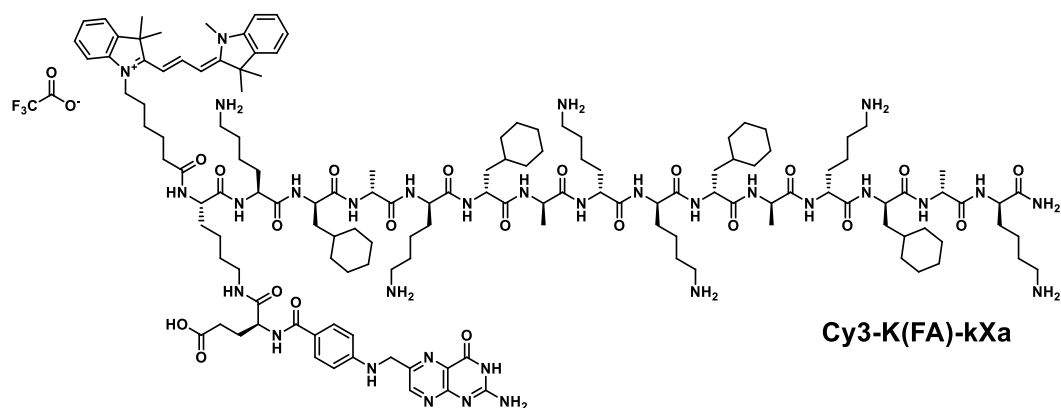


Figure 4.9. TIC chromatogram (+ mass spectrum at 11.956:12.667 min) of **Cy3-K(FA)-kIa**. Column: ACE 3 C18, 2.1 x 100 mm, 3 μ m particle size, 100 Å pore size; Method: flow rate = 0.3 mL \cdot min⁻¹, H₂O: CH₃CN, 0.1% HCOOH, 85:15 for 2 min \rightarrow 85:15 to 40:60 over 13 min \rightarrow 5:95 for 7 min \rightarrow 5:95 to 85:15 over 0.5 min \rightarrow 85:15 for 7 min.

4.6.1.2 Synthesis of Cy3-K(FA)-kXa



The peptide chain was synthesized by SPPS on Rink Amide MBHA resin. Each amino acid coupling step was carried out with Fmoc-protected amino acid (2 eq), DIC (4 eq), ethyl cyanohydroxyiminoacetate (2 eq) in DMF at 75 °C (155 W) for 0.25 min and at 90 °C (30 W) for further 2 min. For the penultimate lysine, the coupling was carried out using Fmoc-Lys(Boc)-OH (2 eq), DIC (4 eq), ethyl

cyanohydroxyiminoacetate (2 eq) at 75 °C (155 W) for 0.5 min and at 90 °C (30 W) for further 4 min. For the last lysine, the coupling was carried out using Fmoc-Lys(ivDde)-OH (3 eq), DIC (6 eq), ethyl cyanohydroxyiminoacetate (3 eq) at 75 °C (155 W) for 1 min and at 90 °C (30 W) for further 7 min. After each coupling step, the respective Fmoc protecting group was removed by 10% piperazine (w/v) in ethanol:NMP (1:9). After the final Fmoc deprotection, the peptidyl resin was removed from the automated synthesizer and the trimethine cyanine dye was manually coupled using 3 eq of compound **Cy3-COOH**, 6 eq of DIC, 3 eq of ethyl cyanohydroxyiminoacetate, 16 h. For the ivDde group cleavage, the resin was treated with 4% hydrazine hydrate (v/v) in DMF for 45 min and then the solution filtrated off. The procedure was repeated twice. Then, glutamic acid was coupled using 4 eq of Fmoc-Glu(OtBu)-OH, 4 eq of HBTU, 4 eq of HOBt and 8 eq of DIPEA. Deprotection of the Fmoc protecting group was achieved by treatment with 5 mL of 20% (v/v) piperidine in DMF, for 10 min for 2 times. For the pterioic acid coupling, 2 eq of pterioic acid were suspended in 10 mL of DMSO and heated at 50 °C for 1 h. 8 eq of DIPEA and 2 eq of PyBOP were added to the suspension, which was then reacted with the peptidyl-resin for 16 h at 40 °C. The pterioic acid coupling was then repeated for further 16 h at 40 °C. Cleavage from the resin was performed in TFA/H₂O/TIS 95:2.5:2.5 solution for 2 h. The resin was removed by filtration and the filtrate concentrated by N₂ flow. The crude product was precipitated with cold diethyl ether, centrifuged (4,000 g for 10 min) and the supernatant was discarded. The precipitate was dissolved in 2 mL of CH₃CN + 0.1% TFA, diluted with 13 mL of H₂O + 0.1% TFA, filtrated through a 0.22 µm syringe filter and purified by HPLC. Lyophilization of the pure product fractions afforded the desired compound as a red powder.

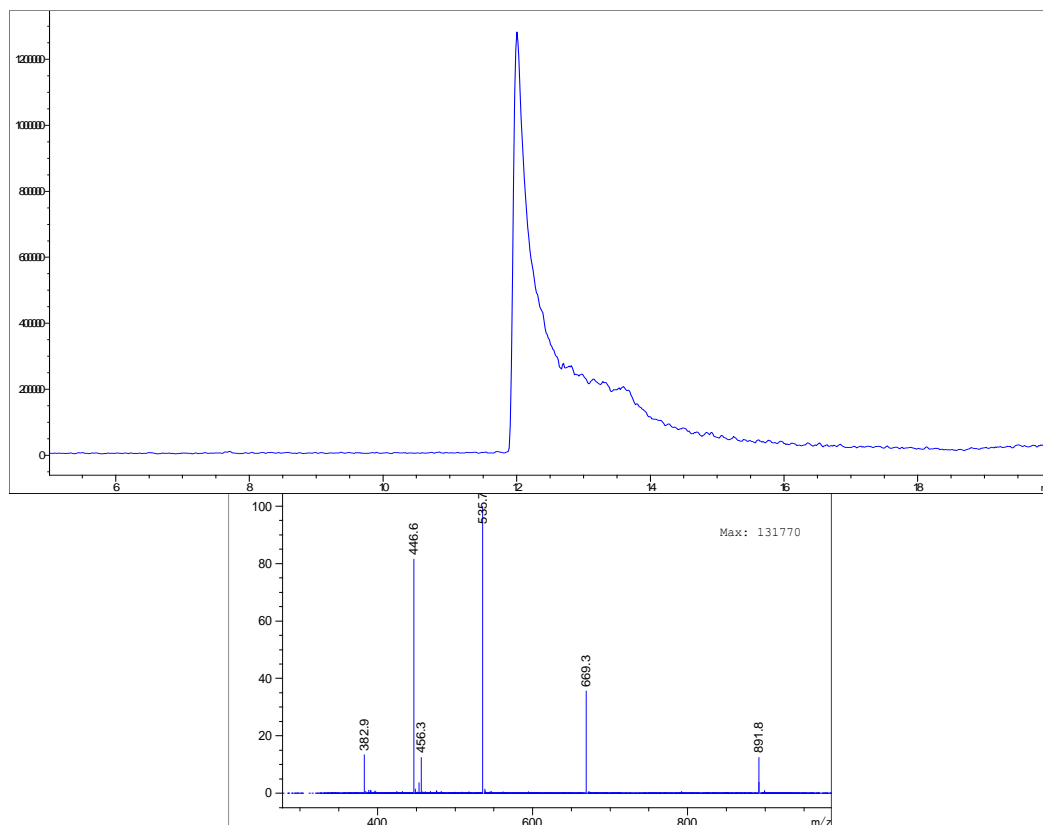
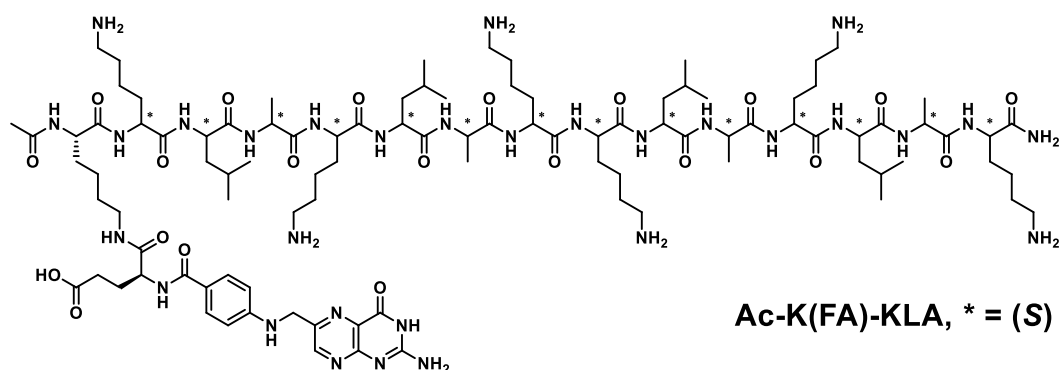
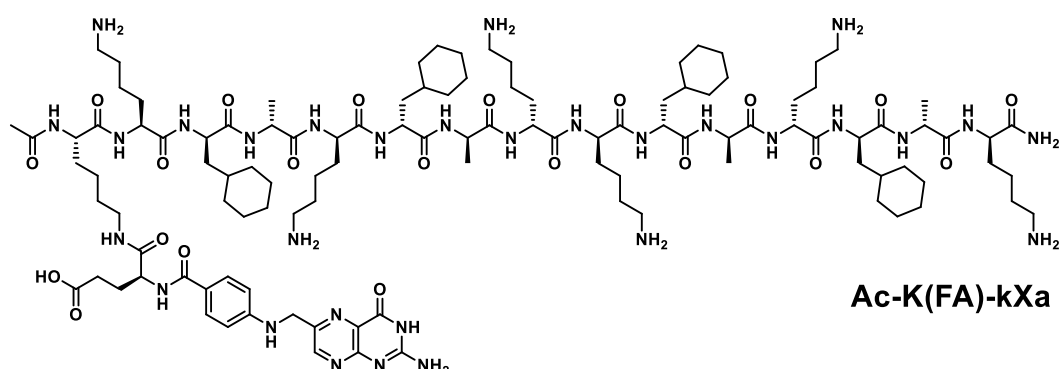


Figure 4.10. TIC chromatogram (+ mass spectrum at 11.985:12.654 min) of Cy3-K(FA)-kXa. Column: *ACE 3 C18*, 2.1 x 100 mm, 3 μm particle size, 100 \AA pore size; Method: flow rate = $0.3 \text{ mL} \cdot \text{min}^{-1}$, H_2O : CH_3CN , 0.1% HCOOH , 85:15 for 2 min \rightarrow 85:15 to 40:60 over 13 min \rightarrow 5:95 for 7 min \rightarrow 5:95 to 85:15 over 0.5 min \rightarrow 85:15 for 7 min.

4.6.1.3 General procedure for the synthesis of Ac-K(FA)-KLA, Ac-K(FA)-kla and Ac-K(FA)-kXa



Ac-K(FA)-kla, * = (R)



The peptide chain was synthesised by SPPS on Rink Amide MBHA resin. Each amino acid coupling step was carried out with Fmoc-protected amino acid (2 eq), DIC (4 eq), ethyl cyanohydroxyiminoacetate (2 eq) in DMF at 75 °C (155 W) for 0.25 min and at 90 °C (30 W) for further 2 min. For the penultimate lysine, the coupling was carried out using Fmoc-Lys(Boc)-OH (2 eq), DIC (4 eq), ethyl cyanohydroxyiminoacetate (2 eq) at 75 °C (155 W) for 0.5 min and at 90 °C (30 W) for further 4 min. For the last lysine, the coupling was carried out using Fmoc-Lys(Mtt)-OH (3 eq), DIC (6 eq), ethyl cyanohydroxyiminoacetate (3 eq) at 75 °C (155 W) for 1 min and at 90 °C (30 W) for further 7 min. After each coupling step, the respective Fmoc protecting group was removed by 10% Piperazine (w/v) in ethanol:NMP (1:9). After the final Fmoc deprotection, the peptidyl-resin is

removed from the automated synthesiser and the *N*-terminal amine is capped by using acetic anhydride (50 eq) and pyridine (50 eq) in 8 mL of DMF, for 30 min for 2 times. For the Mtt group cleavage, the resin is treated with 1% TFA (v/v) in DCM for 2 min and then the solution is filtrated off; this procedure is repeated for 12 times. Then, glutamic acid was coupled using 4 eq of Fmoc-Glu(OtBu)-OH, 4 eq of HBTU, 4 eq of HOBt and 8 eq of DIPEA. Deprotection of the Fmoc protecting group was achieved by treatment with 5 mL of 20% (v/v) piperidine in DMF, for 10 min for 2 times. For the pterioic acid coupling, 2 eq of pterioic acid were suspended in 10 mL of DMSO and were heated up at 50 °C for 1 h. 8 eq of DIPEA and 2 eq of PyBOP were added to the suspension which is then reacted with the peptidyl-resin for 16 h, at 40 °C. The pterioic acid coupling was then repeated for further 16 h, at 40 °C. Cleavage from the resin was then performed in TFA/ H₂O/TIS 95:2.5:2.5 solution for 2 h. The resin was removed by filtration and the filtrate was concentrated by N₂ flow. The crude product was precipitated with cold diethyl ether, centrifuged (4,000 g for 10 min) and the supernatant was discarded. The precipitate was dissolved in 2 mL of CH₃CN + 0.1% TFA, diluted with 13 mL of H₂O + 0.1% TFA, filtrated through a 0.22 µm syringe filter and purified by HPLC. Lyophilisation of the pure product fractions afforded the desired compound as a pale-yellow powder.

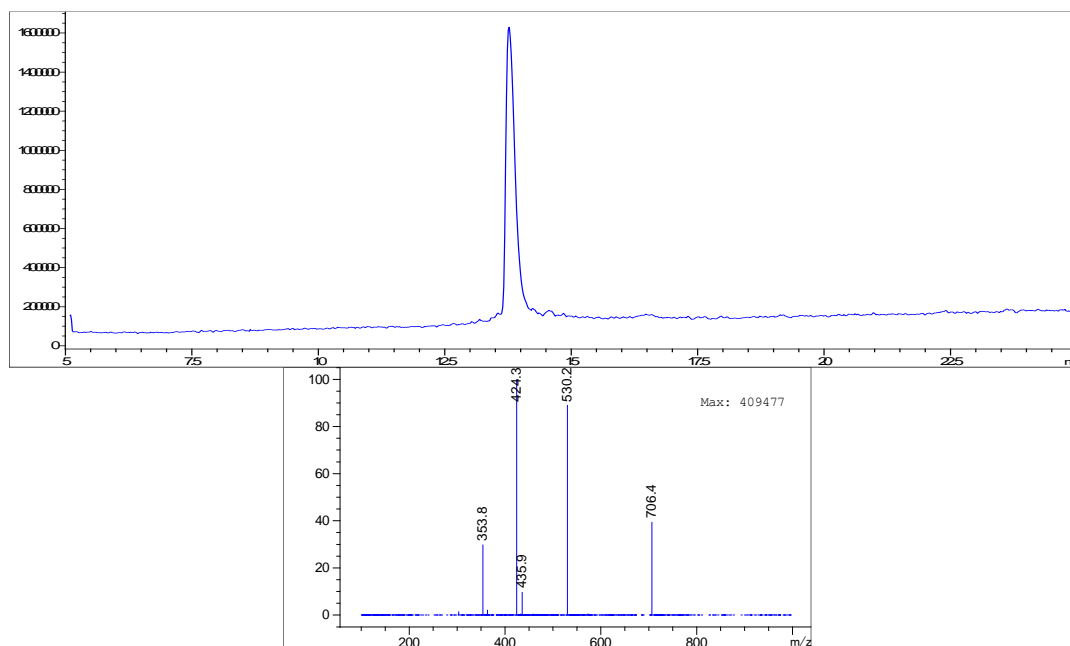


Figure 4.11. TIC chromatogram (+ mass spectrum at 13.721:13.940 min) of **Ac-K(FA)-KLA**. Column: *Poroshell 120 EC-C18*, 2.1 x 100 mm, 4 µm particle size, 120 Å pore size; Method:

flow rate = $0.5 \text{ mL} \cdot \text{min}^{-1}$, H_2O : CH_3CN , 0.1% HCOOH , 95:5 for 2 min \rightarrow 95:5 to 40:60 over 23 min \rightarrow 5:95 for 5 min.

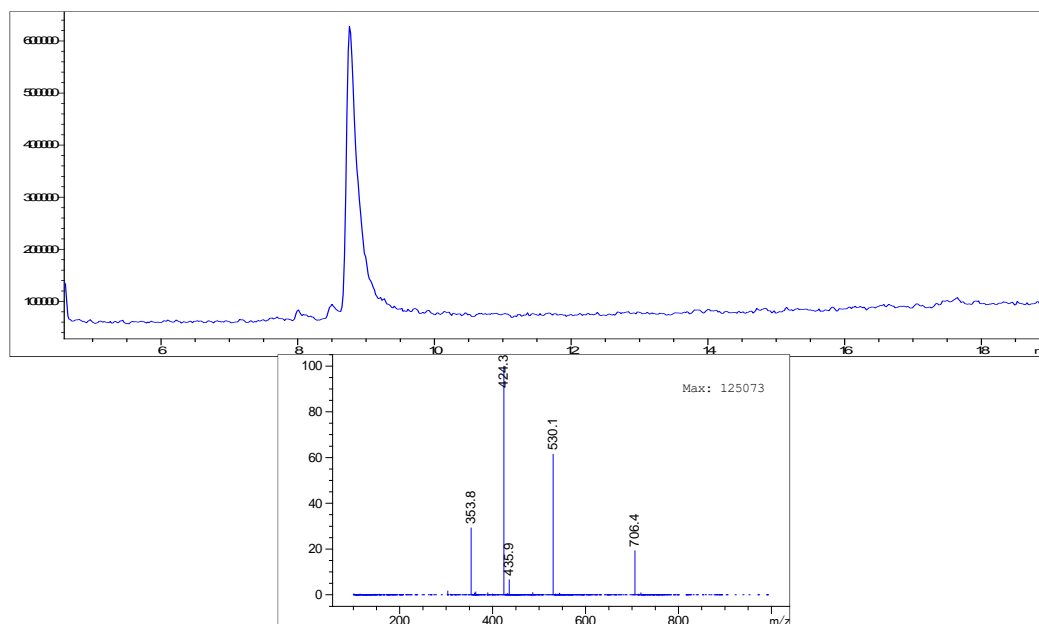


Figure 4.12. TIC chromatogram (+ mass spectrum at 8.684:9.012 min) of **Ac-K(FA)-kIa**. Column: *Poroshell 120 EC-C18*, 2.1 x 100 mm, 4 μm particle size, 120 \AA pore size; Method: flow rate = $0.5 \text{ mL} \cdot \text{min}^{-1}$, H_2O : CH_3CN , 0.1% HCOOH , 95:5 for 1 min \rightarrow 95:5 to 45:65 over 15 min \rightarrow 5:95 for 5 min.

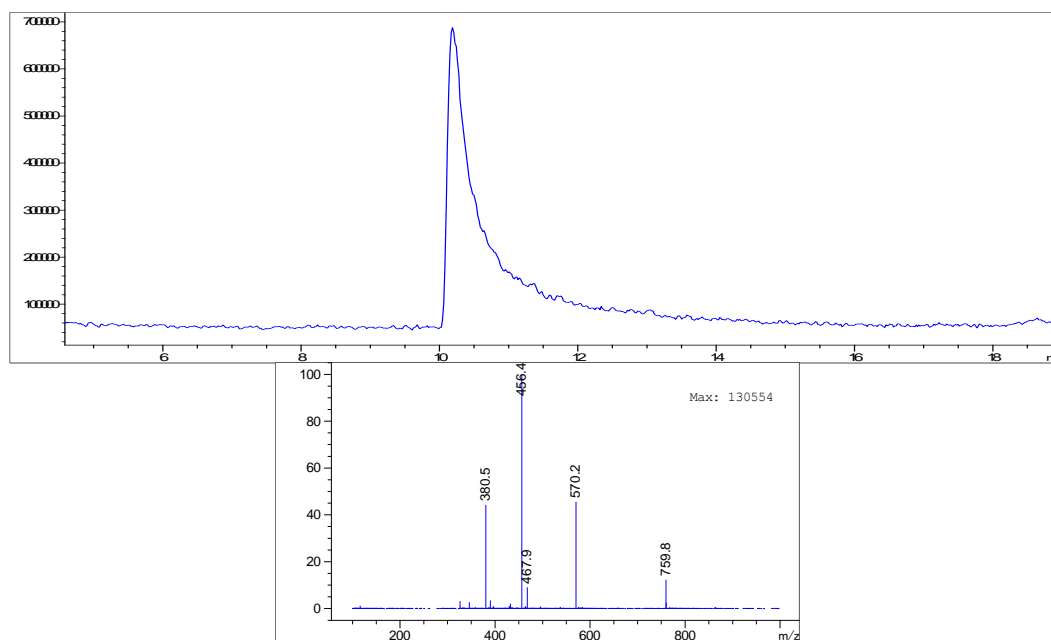


Figure 4.13. TIC chromatogram (+ mass spectrum at 10.097:10.735 min) of **Ac-K(FA)-kXa**. Column: *ACE 3 C18*, 2.1 x 100 mm, 3 μm particle size, 100 \AA pore size; Method: flow rate = $0.3 \text{ mL} \cdot \text{min}^{-1}$, H_2O : CH_3CN , 0.1% HCOOH , 85:15 for 2 min \rightarrow 85:15 to 40:60 over 13 min \rightarrow 5:95 for 7 min \rightarrow 5:95 to 85:15 over 0.5 min \rightarrow 85:15 for 7 min.

4.6.2 Biological Evaluation

4.6.2.1 Cell Culture

See 3.4.3.1

4.6.2.2 Cell viability assay

MCF-7 and HEK cells were seeded at a density of 2×10^4 cells per well in a Corning 96-well plate and grown at 37 °C in a 5% CO₂ atmosphere DMEM supplemented with 10% (v/v) FBS for 24 h. KB and SK-OV-3 cells were seeded at a density of 7×10^3 cells per well in a Corning 96-well plate and grown at 37 °C in a 5% CO₂ atmosphere RPMI 1640 medium supplemented with 10% (v/v) FBS for 24 h. Stock solutions of folate conjugates were obtained by dissolving the compounds in pure DMSO. The stock solutions were diluted into the proper medium (according to the tested cell line) supplemented with 10% FBS to the appropriate concentration, and cells in each well were incubated with 100 µL of the solution. The solutions in each well were then adjusted to a concentration of 1% (v/v) DMSO. After 24 h at 37 °C, 20 µL of CellTiter-Blue® was added to each well. The plate was incubated for another 4 h at 37 °C before analysis on a Perkin Elmer Victor X plate reader (excitation 531 nm; emission 595 nm). Each data point is calculated from three biological replicates (*i.e.* cells split from three different passages), and each biological replicate is calculated from three technical replicates (*i.e.* cells split from the same passage). Value from media-only with CellTiter-Blue was set as 0% viability. This value was then subtracted from the values from cell-only (*i.e.* non-treated) wells with CellTiter-Blue in each biological replicate and set as 100% viability. For treatments containing cyanine dye-labelled constructs, blanks were generated with cell-free wells containing the compounds and adding CellTiter-Blue. The fluorescent reading for these wells was deducted from the treatment readings.

EC₅₀ values were derived by generating dose-response curves (Figures 4.14-17) using Origin, version 2019b, OriginLab Corporation, Northampton, MA, USA.

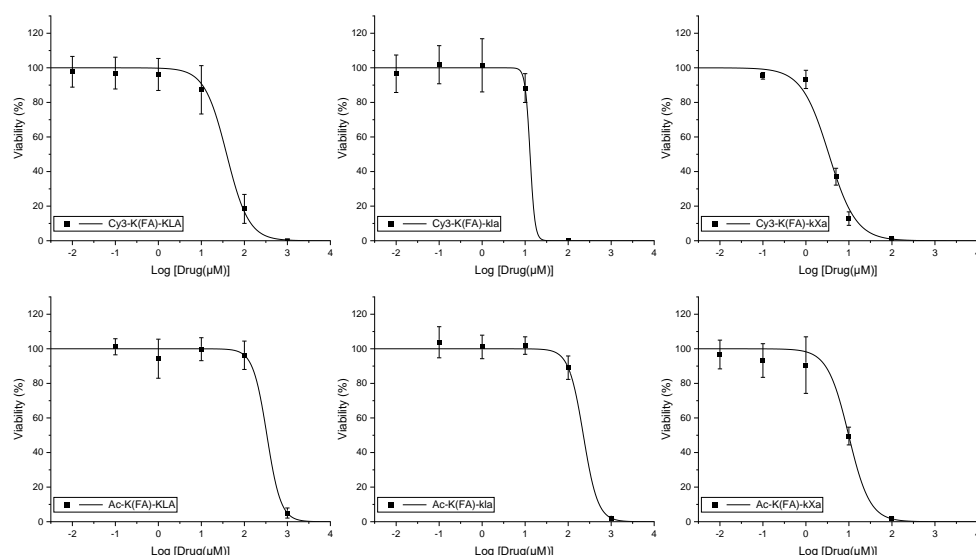


Figure 4.14. Cytotoxicity of tested compounds towards KB cell lines. Fitting curves are shown as solid black lines. Dots and error bars represent the mean and the standard deviation from a minimum of nine values resulted from three biological replicates (i.e. cells split from three different passages); each biological replicate is calculated from three technical replicates (i.e. cells split from the same passage).

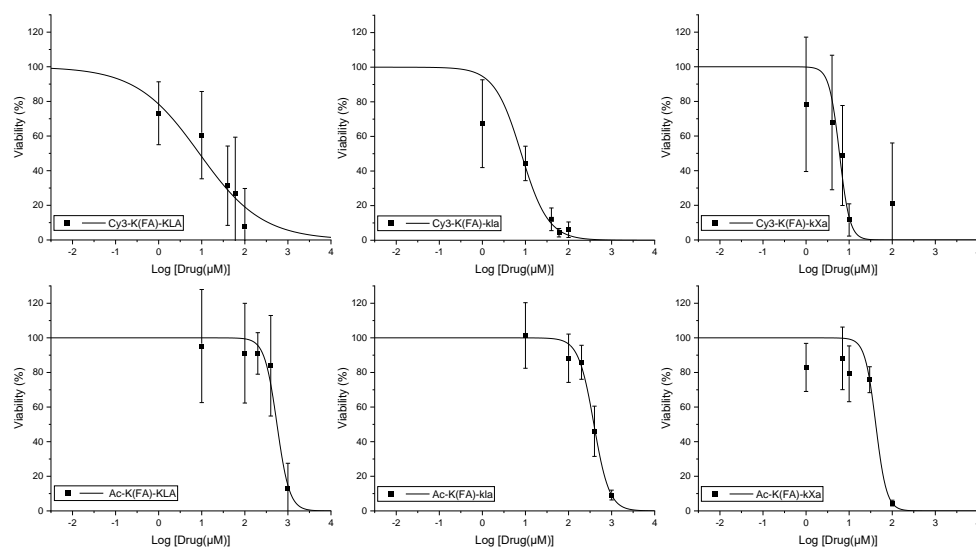


Figure 4.15. Cytotoxicity of tested compounds towards SK-OV-3 cell lines. Fitting curves are shown as solid black lines. Dots and error bars represent the mean and the standard deviation from a minimum of nine values resulted from three biological replicates (i.e. cells split from three different passages); each biological replicate is calculated from three technical replicates (i.e. cells split from the same passage).

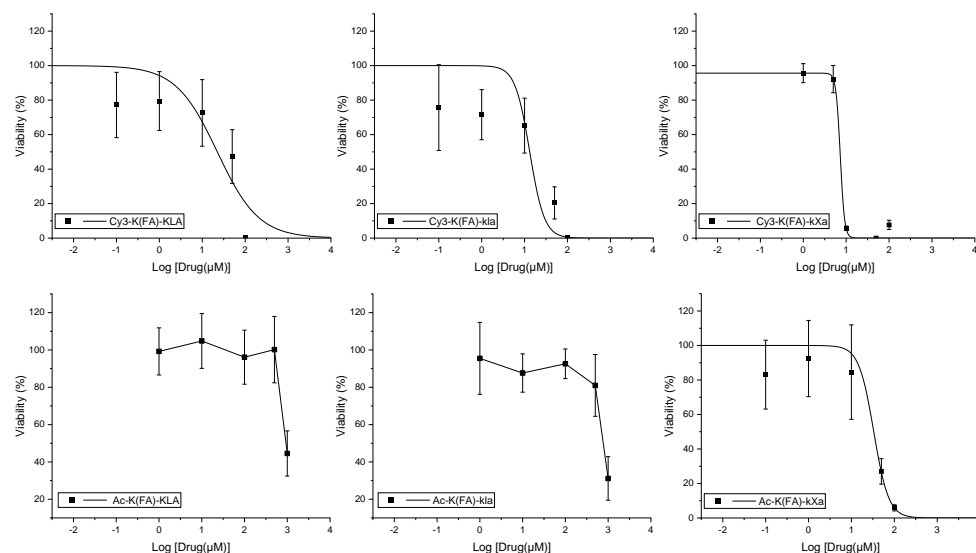


Figure 4.16. Cytotoxicity of tested compounds towards MCF7 cell lines. Fitting curves are shown as solid black lines. Data for **Ac-K(FA)-KLA** and **Ac-K(FA)-kIa** were not fitted. Dots and error bars represent the mean and the standard deviation from a minimum of nine values resulted from three biological replicates (i.e. cells split from three different passages); each biological replicate is calculated from three technical replicates (i.e. cells split from the same passage).

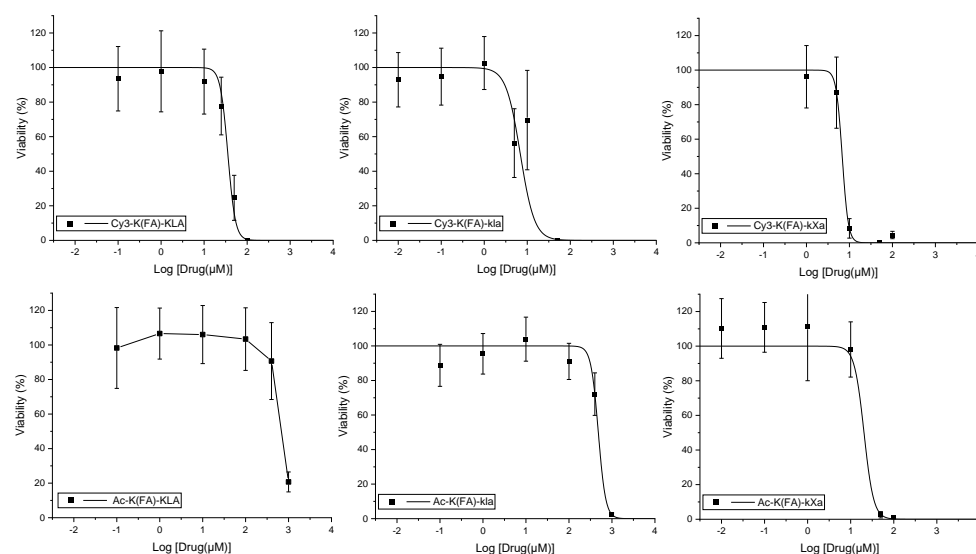


Figure 4.17. Cytotoxicity of tested compounds towards HEK293 cell lines. Fitting curves are shown as solid black lines. Data for **Ac-K(FA)-KLA** were not fitted. Dots and error bars represent the mean and the standard deviation from a minimum of nine values resulted from three biological replicates (i.e. cells split from three different passages); each biological replicate is calculated from three technical replicates (i.e. cells split from the same passage).

4.6.2.3 Confocal Microscopy

SK-OV-3 and MCF7 were seeded at a density of 1×10^6 cells per well in glass bottom culture dishes and grown at 37 °C in a 5% CO₂ atmosphere in medium supplemented with 10% (v/v) FBS for 24 h. Cells were washed once with the RPMI-1640 medium supplemented with 10% (v/v) FBS before staining. Folate conjugates were diluted into the RPMI-1640 medium supplemented with 10% (v/v) FBS to 10 µM and then add to the culture dishes respectively. After 10-min incubation at 37 °C, cells were washed with RPMI-1640 medium supplemented with 10% (v/v) FBS. Cells were then treated with 50 nM MitoTracker Green FM and 10 µg/ml Hoechst 33258 pre-formulated with RPMI-1640 medium supplemented with 10% (v/v) FBS, and then incubated for another 10 min at 37 °C before analysis on ZEISS LSM 900 with Airyscan 2. The results were analyzed using Image J software.

4.6.2.4 Flow cytometry

SK-OV-3 and MCF7 were seeded at a density of 2×10^5 cells per well in 24-well plate and grown at 37 °C in a 5% CO₂ atmosphere in DMEM medium supplemented with 10% (v/v) FBS for 24 h. Cells were washed once with the RPMI-1640 medium supplemented with 10% FBS before staining. Folate conjugates were diluted into the RPMI-1640 medium supplemented with 10% FBS to 10 µM and then add to the culture dishes. After 10-min incubation at 37 °C, cells were washed with RPMI-1640 medium supplemented with 10% FBS. Cells were then treated with 50 nM Mitotracker Green FM and 10 µg/ml Hoechst 33258 pre-formulated with RPMI-1640 medium supplemented with 10% FBS for another 10 min at 37 °C. Cells were washed once with PBS before trypsinization for flow cytometry analysis on Invitrogen Attune NxT. The results were analyzed using FlowJo™ v10 Software (BD Life Sciences).

4.6.2.5 Statistical analysis

Comparison of cytotoxicity fitting curves was achieved by applying the extra sum-of-squares F test, performed using GraphPad Prism version 9 for Windows, GraphPad Software, La Jolla California USA, www.graphpad.com. Statistical difference between cytotoxicity values was assumed when *p*-value, as

output of the extra sum-of-squares F test, was found to be below 0.05. Statistical analysis on the flow cytometry data was achieved by applying the unpaired two-tailed t-test test, performed using GraphPad Prism version 9 for Windows, GraphPad Software, La Jolla California USA, USA (<https://www.graphpad.com/>).

Chapter 5

Conclusions and future work

CHAPTER 5 - Conclusions and future work

In the presented work, I developed a new method for the cleavage of peptides and proteins from a solid support using mild conditions (chapter 2). Although further studies are required to fully explore the potential of the new cleavage technique, various constructs such as a short peptide, a polypeptide and a protein were successfully released from a PEG-based resin.

Furthermore, I evaluated the biological activity of newly synthesised proapoptotic peptides when conjugated to a mitochondria-targeting cyanine dye (chapter 3). The peptides, the mitochondria-targeting motif and their conjugates were successfully synthesised via SPPS. Cell viability assay results showed the increased cytotoxicity of the conjugates compared to the native sequences, and confocal microscopy experiments confirmed the mitochondrial localisation of the new constructs.

Finally, the cyanine dye-conjugated peptides were chemically labelled with a folate molecule, in an attempt to increase the selectivity towards cells overexpressing folate receptor α (chapter 4). While the new constructs were successfully obtained via SPPS, they did not show the expected selectivity in the cell viability assay; interestingly, flow cytometry experiments revealed decreased cellular uptake of the folate labelled compounds when compared to cyanine-dye conjugates without folate. Nonetheless, folate-conjugates retained the ability to localise within mitochondria.

Future efforts will focus on further exploring and optimising the projects examined in this work.

As already mentioned in section 2.4, the new cleavage technique requires additional investigations. A systematic evaluation of the cleavage conditions will be carried out, leading to the optimisation of crucial parameters such as temperature, pH, time, protein concentration, and salt concentrations of the cleavage buffer. Additionally, more case studies that encompass proteins of different size and bearing diverse modifications need to be carried out to obtain a solid cleavage protocol.

Despite the success of the preparation of the cyanine dye-labelled proapoptotic peptides and their increased cytotoxicity, the design of folate conjugates requires improvement (see section 4.5). Nonetheless, the pipeline for

the preparation and the evaluation of folate-conjugates has already been optimised. Therefore, I am positive that new constructs with improved selectivity towards cells overexpressing folate receptor α will be obtained soon. Next, the pharmacokinetics profile of the optimised conjugates will be studied and improved, thus laying the ground for their evaluation *in vivo*. This next phase of the project will provide opportunities for my research group to start new collaborations in the field of translational research.

Chapter 6

References

CHAPTER 6 - References

1. Henriksen JH, Schaffalitzky de Muckadell OB. Secretin, its discovery, and the introduction of the hormone concept. *Scand. J. Clin. Lab. Invest.* 2000; 60: 463-472.
2. Bayliss WM, Starling EH. The mechanism of pancreatic secretion. *J. Physiol.* (Oxford, U. K.). 1902; 28: 325-353.
3. Viero C, Shibuya I, Kitamura N, Verkhatsky A, Fujihara H, Katoh A, Ueta Y, Zingg HH, Chvatal A, Sykova E, Dayanithi G. Oxytocin: Crossing the Bridge between Basic Science and Pharmacotherapy. *CNS Neurosci. Ther.* 2010; 16: e138-e156.
4. Bakos J, Zatkova M, Bacova Z, Ostatnikova D. The Role of Hypothalamic Neuropeptides in Neurogenesis and Neuritogenesis. *Neural Plast.* 2016; 2016.
5. Merrifield RB. Solid Phase Peptide Synthesis. I. The Synthesis of a Tetrapeptide. *J. Am. Chem. Soc.* 1963; 85: 2149-2154.
6. Walsh CT, O'Brien RV, Khosla C. Nonproteinogenic Amino Acid Building Blocks for Nonribosomal Peptide and Hybrid Polyketide Scaffolds. *Angew. Chem. Int. Ed.* 2013; 52: 7098-7124.
7. Kang L, Han T, Cong H, Yu B, Shen Y. Recent research progress of biologically active peptides. *BioFactors.* 2022; 48: 575-596.
8. Boonen K, Creemers JW, Schoofs L. Bioactive peptides, networks and systems biology. *Bioessays.* 2009; 31: 300-314.
9. Knapen MFCM, Zusterzeel PLM, Peters WHM, Steegers EAP. Glutathione and glutathione-related enzymes in reproduction: A review. *European Journal of Obstetrics and Gynecology and Reproductive Biology.* 1999; 82: 171-184.
10. Avci FG, Sariyar Akbulut B, Ozkirimli E. Membrane Active Peptides and Their Biophysical Characterization. *Biomolecules.* 2018; 8: 77.
11. Assoni L, Milani B, Carvalho MR, Nepomuceno LN, Waz NT, Guerra MES, Converso TR, Darrieux M. Resistance Mechanisms to Antimicrobial Peptides in Gram-Positive Bacteria. *Front. Microbiol.* 2020; 11.
12. Kulkarni SS, Sayers J, Premdjee B, Payne RJ. Rapid and efficient protein synthesis through expansion of the native chemical ligation concept. *Nat. Rev. Chem.* 2018; 2.
13. Li H, Dong S. Recent advances in the preparation of Fmoc-SPPS-based peptide thioester and its surrogates for NCL-type reactions. *Sci. China Chem.* 2017; 60: 201-213.
14. Agouridas V, El Mahdi O, Diemer V, Cargoët M, Monbaliu J-CM, Melnyk O. Native Chemical Ligation and Extended Methods: Mechanisms, Catalysis, Scope, and Limitations. *Chem. Rev.* 2019; 119: 7328-7443.
15. Jaradat DMM. Thirteen decades of peptide synthesis: key developments in solid phase peptide synthesis and amide bond formation utilized in peptide ligation. *Amino Acids.* 2018; 50: 39-68.
16. Carpino LA. 1-Hydroxy-7-azabenzotriazole. An efficient peptide coupling additive. *J. Am. Chem. Soc.* 1993; 115: 4397-4398.
17. Yu RR, Mahto SK, Justus K, Alexander MM, Howard CJ, Ottesen JJ. Hybrid phase ligation for efficient synthesis of histone proteins. *Org. Biomol. Chem.* 2016; 14: 2603-2607.
18. Mäde V, Els-Heindl S, Beck-Sickinger AG. Automated solid-phase peptide synthesis to obtain therapeutic peptides. *Beilstein J. Org. Chem.* 2014; 10: 1197-1212.
19. Pedersen SL, Tofteng AP, Malik L, Jensen KJ. Microwave heating in solid-phase peptide synthesis. *Chem. Soc. Rev.* 2012; 41: 1826-1844.
20. Gordon CP. The renaissance of continuous-flow peptide synthesis – an abridged account of solid and solution-based approaches. *Org. Biomol. Chem.* 2018; 16: 180-196.
21. Ahmed N. Peptide Bond Formations through Flow Chemistry. *Chem. Biol. Drug Des.* 2018; 91: 647-650.
22. Hartrampf N, Saebi A, Poskus M, Gates ZP, Callahan AJ, Cowfer AE, Hanna S, Antilla S, Schissel CK, Quartararo AJ, Ye X, Mijalis AJ, Simon MD, Loas A, Liu S, Jessen C, Nielsen

- TE, Pentelute BL. Synthesis of proteins by automated flow chemistry. *Science*. 2020; 368: 980-987.
23. Wieland T, Bokelmann E, Bauer L, Lang H, Lau H, Schafer W. Polypeptide syntheses. VIII. Formation of sulfur containing peptides by the intramolecular migration of aminoacyl groups. *Liebigs Ann. Chem.* 1953; 583: 129-149.
 24. Dawson PE, Muir TW, Clark-Lewis I, Kent SB. Synthesis of proteins by native chemical ligation. *Science (Washington, DC, U. S.)*. 1994; 266: 776-779.
 25. Tam JP, Lu YA, Liu CF, Shao J. Peptide synthesis using unprotected peptides through orthogonal coupling methods. *Proc. Natl. Acad. Sci. U. S. A.* 1995; 92: 12485-12489.
 26. Sun H, Brik A. The Journey for the Total Chemical Synthesis of a 53 kDa Protein. *Acc. Chem. Res.* 2019; 52: 3361-3371.
 27. Dawson PE, Muir TW, Clark-Lewis I, Kent SB. Synthesis of proteins by native chemical ligation. *Science (Washington, DC, United States)*. 1994; 266: 776-779.
 28. Bang D, Kent SBH. A One-Pot Total Synthesis of Crambin. *Angew. Chem. Int. Ed.* 2004; 43: 2534-2538.
 29. Piontek C, Varón Silva D, Heinlein C, Pöhner C, Mezzato S, Ring P, Martin A, Schmid FX, Unverzagt C. Semisynthesis of a Homogeneous Glycoprotein Enzyme: Ribonuclease C: Part 2. *Angew. Chem. Int. Ed.* 2009; 48: 1941-1945.
 30. Tan Z, Shang S, Danishefsky SJ. Insights into the Finer Issues of Native Chemical Ligation: An Approach to Cascade Ligations. *Angew. Chem. Int. Ed.* 2010; 49: 9500-9503.
 31. Muir TW, Sondhi D, Cole PA. Expressed protein ligation: A general method for protein engineering. *Proc. Natl. Acad. Sci. U. S. A.* 1998; 95: 6705-6710.
 32. Bustin S. *Molecular Biology of the Cell*, Sixth Edition; ISBN: 9780815344643; and *Molecular Biology of the Cell*, Sixth Edition, The Problems Book; ISBN 9780815344537. *Int. J. Mol. Sci.* 16: MDPI; 2015. p. 28123-28125.
 33. Nödling AR, Spear LA, Williams TL, Luk LYP, Tsai Y-H. Using genetically incorporated unnatural amino acids to control protein functions in mammalian cells. *Essays Biochem.* 2019; 63: 237-266.
 34. Satakarni M, Curtis R. Production of recombinant peptides as fusions with SUMO. *Protein Expression Purif.* 2011; 78: 113-119.
 35. Raibaut L, Ollivier N, Melnyk O. Sequential native peptide ligation strategies for total chemical protein synthesis. *Chem. Soc. Rev.* 2012; 41: 7001-7015.
 36. Camarero JA, Cotton GJ, Adeva A, Muir TW. Chemical ligation of unprotected peptides directly from a solid support. *J. Pept. Res.* 1998; 51: 303-316.
 37. Canne LE, Botti P, Simon RJ, Chen Y, Dennis EA, Kent SBH. Chemical Protein Synthesis by Solid Phase Ligation of Unprotected Peptide Segments. *J. Am. Chem. Soc.* 1999; 121: 8720-8727.
 38. Raibaut L, Adihou H, Desmet R, Delmas AF, Aucagne V, Melnyk O. Highly efficient solid phase synthesis of large polypeptides by iterative ligations of bis(2-sulfanylethyl)amido (SEA) peptide segments. *Chem. Sci.* 2013; 4: 4061-4066.
 39. Ollivier N, Desmet R, Drobecq H, Blanpain A, Boll E, Leclercq B, Mougél A, Vicogne J, Melnyk O. A simple and traceless solid phase method simplifies the assembly of large peptides and the access to challenging proteins. *Chem. Sci.* 2017; 8: 5362-5370.
 40. Abboud SA, Amoura M, Madinier J-B, Renoux B, Papot S, Piller V, Aucagne V. Enzyme-Cleavable Linkers for Protein Chemical Synthesis through Solid-Phase Ligations. *Angew. Chem. Int. Ed.* 2021; 60: 18612-18618.
 41. Aucagne V, Valverde IE, Marceau P, Galibert M, Dendane N, Delmas AF. Towards the Simplification of Protein Synthesis: Iterative Solid-Supported Ligations with Concomitant Purifications. *Angew. Chem. Int. Ed.* 2012; 51: 11320-11324.
 42. Zheng J-S, Tang S, Qi Y-K, Wang Z-P, Liu L. Chemical synthesis of proteins using peptide hydrazides as thioester surrogates. *Nat. Protoc.* 2013; 8: 2483-2495.

43. Blanco-Canosa JB, Dawson PE. An Efficient Fmoc-SPPS Approach for the Generation of Thioester Peptide Precursors for Use in Native Chemical Ligation. *Angew. Chem. Int. Ed.* 2008; 47: 6851-6855.
44. Hong ZZ, Yu RR, Zhang X, Webb AM, Burge NL, Poirier MG, Ottesen JJ. Convergent Hybrid Phase Ligation Strategy for Efficient Total Synthesis of Large Proteins Demonstrated for 212-residue Linker Histone H1.2. *bioRxiv.* 2019; 661744.
45. Agouridas V, Diemer V, Melnyk O. Strategies and open questions in solid-phase protein chemical synthesis. *Curr. Opin. Chem. Biol.* 2020; 58: 1-9.
46. Jbara M, Seenayah M, Brik A. Solid phase chemical ligation employing a rink amide linker for the synthesis of histone H2B protein. *Chem. Commun.* 2014; 50: 12534-12537.
47. Brik A, Keinan E, Dawson PE. Protein Synthesis by Solid-Phase Chemical Ligation Using a Safety Catch Linker. *The Journal of Organic Chemistry.* 2000; 65: 3829-3835.
48. Vamiseti GB, Satish G, Sulkshane P, Mann G, Glickman MH, Brik A. On-Demand Detachment of Succinimides on Cysteine to Facilitate (Semi)Synthesis of Challenging Proteins. *J. Am. Chem. Soc.* 2020; 142: 19558-19569.
49. Reimann O, Smet-Nocca C, Hackenberger CPR. Traceless Purification and Desulfurization of Tau Protein Ligation Products. *Angew. Chem. Int. Ed.* 2015; 54: 306-310.
50. Bang D, Pentelute BL, Kent SBH. Kinetically Controlled Ligation for the Convergent Chemical Synthesis of Proteins. *Angew. Chem. Int. Ed.* 2006; 45: 3985-3988.
51. Kar A, Mannuthodikayil J, Singh S, Biswas A, Dubey P, Das A, Mandal K. Efficient Chemical Protein Synthesis using Fmoc-Masked N-Terminal Cysteine in Peptide Thioester Segments. *Angew. Chem. Int. Ed.* 2020; 59: 14796-14801.
52. Javadpour MM, Juban MM, Lo W-CJ, Bishop SM, Alberty JB, Cowell SM, Becker CL, McLaughlin ML. De Novo Antimicrobial Peptides with Low Mammalian Cell Toxicity. *J. Med. Chem.* 1996; 39: 3107-3113.
53. Lee S, Mihara H, Aoyagi H, Kato T, Izumiya N, Yamasaki N. Relationship between antimicrobial activity and amphiphilic property of basic model peptides. *Biochim. Biophys. Acta, Biomembr.* 1986; 862: 211-219.
54. DeGrado WF, Kezdy FJ, Kaiser ET. Design, synthesis, and characterization of a cytotoxic peptide with melittin-like activity. *J. Am. Chem. Soc.* 1981; 103: 679-681.
55. Cornut I, Büttner K, Dasseux J-L, Dufourcq J. The amphipathic α -helix concept: Application to the de novo design of ideally amphipathic Leu, Lys peptides with hemolytic activity higher than that of melittin. *FEBS Lett.* 1994; 349: 29-33.
56. Epand RM, Shai Y, Segrest JP, Anantharamaiah GM. Mechanisms for the modulation of membrane bilayer properties by amphipathic helical peptides. *Biopolymers.* 1995; 37: 319-338.
57. Saberwal G, Nagaraj R. Cell-lytic and antibacterial peptides that act by perturbing the barrier function of membranes: facets of their conformational features, structure-function correlations and membrane-perturbing abilities. *Biochim. Biophys. Acta.* 1994; 1197: 109-131.
58. Zhou NE, Kay CM, Hodges RS. Synthetic model proteins: the relative contribution of leucine residues at the nonequivalent positions of the 3-4 hydrophobic repeat to the stability of the two-stranded α -helical coiled-coil. *Biochemistry.* 1992; 31: 5739-5746.
59. Akerfeldt KS, Lear JD, Wasserman ZR, Chung LA, DeGrado WF. Synthetic peptides as models for ion channel proteins. *Acc. Chem. Res.* 1993; 26: 191-197.
60. Roth KG, Mambetsariev I, Kulkarni P, Salgia R. The Mitochondrion as an Emerging Therapeutic Target in Cancer. *Trends Mol. Med.* 2020; 26: 119-134.
61. Murphy MP, Hartley RC. Mitochondria as a therapeutic target for common pathologies. *Nat. Rev. Drug Discov.* 2018; 17: 865-886.
62. Ellerby HM, Arap W, Ellerby LM, Kain R, Andrusiak R, Rio GD, Krajewski S, Lombardo CR, Rao R, Ruoslahti E, Bredesen DE, Pasqualini R. Anti-cancer activity of targeted pro-apoptotic peptides. *Nat. Med.* 1999; 5: 1032-1038.

63. Horton KL, Kelley SO. Engineered Apoptosis-Inducing Peptides with Enhanced Mitochondrial Localization and Potency. *J. Med. Chem.* 2009; 52: 3293-3299.
64. Zielonka J, Joseph J, Sikora A, Hardy M, Ouari O, Vasquez-Vivar J, Cheng G, Lopez M, Kalyanaraman B. Mitochondria-Targeted Triphenylphosphonium-Based Compounds: Syntheses, Mechanisms of Action, and Therapeutic and Diagnostic Applications. *Chem. Rev.* 2017; 117: 10043-10120.
65. Dhanasekaran A, Kotamraju S, Karunakaran C, Kalivendi SV, Thomas S, Joseph J, Kalyanaraman B. Mitochondria superoxide dismutase mimetic inhibits peroxide-induced oxidative damage and apoptosis: Role of mitochondrial superoxide. *Free Radic. Biol. Med.* 2005; 39: 567-583.
66. Luo S, Tan X, Fang S, Wang Y, Liu T, Wang X, Yuan Y, Sun H, Qi Q, Shi C. Mitochondria-Targeted Small-Molecule Fluorophores for Dual Modal Cancer Phototherapy. *Adv. Funct. Mater.* 2016; 26: 2826-2835.
67. Liu Y, Zhou J, Wang L, Hu X, Liu X, Liu M, Cao Z, Shanguan D, Tan W. A Cyanine Dye to Probe Mitophagy: Simultaneous Detection of Mitochondria and Autolysosomes in Live Cells. *J. Am. Chem. Soc.* 2016; 138: 12368-12374.
68. Large DE, Soucy JR, Hebert J, Auguste DT. Advances in Receptor-Mediated, Tumor-Targeted Drug Delivery. *Adv. Ther. (Weinheim, Ger.)*. 2019; 2.
69. Bae YH, Park K. Targeted drug delivery to tumors: Myths, reality and possibility. *J. Controlled Release.* 2011; 153: 198-205.
70. Horton KL, Stewart KM, Fonseca SB, Guo Q, Kelley SO. Mitochondria-penetrating peptides. *ACS Chem. Biol.* 2008; 15: 375-382.
71. Leamon CP, Pastan I, Low PS. Cytotoxicity of folate-Pseudomonas exotoxin conjugates toward tumor cells. Contribution of translocation domain. *J. Biol. Chem.* 1993; 268: 24847-24854.
72. Fernández M, Javaid F, Chudasama V. Advances in targeting the folate receptor in the treatment/imaging of cancers. *Chem. Sci.* 2018; 9: 790-810.
73. Cheung A, Bax HJ, Josephs DH, Ilieva KM, Pellizzari G, Opzoomer J, Bloomfield J, Fittall M, Grigoriadis A, Figini M, Canevari S, Spicer JF, Tutt AN, Karagiannis SN. Targeting folate receptor alpha for cancer treatment. *Oncotarget.* 2016; 7: 52553-52574.
74. Sudimack J, Lee RJ. Targeted drug delivery via the folate receptor. *Adv. Drug Del. Rev.* 2000; 41: 147-162.
75. Vlahov IR, Leamon CP. Engineering Folate-Drug Conjugates to Target Cancer: From Chemistry to Clinic. *Bioconj. Chem.* 2012; 23: 1357-1369.
76. Kimple ME, Brill AL, Pasker RL. Overview of Affinity Tags for Protein Purification. *Curr. Protoc. Protein Sci.* 2013; 73: 9.9.1-9.9.23.
77. Waugh DS. An overview of enzymatic reagents for the removal of affinity tags. *Protein Expression Purif.* 2011; 80: 283-293.
78. Gross E, Witkop B. Selective cleavage of the methionyl peptide bonds in ribonuclease with cyanogen bromide. *J. Am. Chem. Soc.* 1961; 83: 1510-1511.
79. Parac TN, Kostić NM. Effects of Linkage Isomerism and of Acid-Base Equilibria on Reactivity and Catalytic Turnover in Hydrolytic Cleavage of Histidyl Peptides Coordinated to Palladium(II). Identification of the Active Complex between Palladium(II) and the Histidyl Residue. *J. Am. Chem. Soc.* 1996; 118: 5946-5951.
80. Dutca LM, Ko KS, Pohl NL, Kostić NM. Platinum(II) complex as an artificial peptidase: selective cleavage of peptides and a protein by *cis*-[Pt(en)(H₂O)₂]²⁺ ion under ultraviolet and microwave irradiation. *Inorg. Chem.* 2005; 44: 5141-5146.
81. Krężel A, Kopera E, Protas AM, Poznański J, Wysłouch-Cieszyńska A, Bal W. Sequence-Specific Ni(II)-Dependent Peptide Bond Hydrolysis for Protein Engineering. Combinatorial Library Determination of Optimal Sequences. *J. Am. Chem. Soc.* 2010; 132: 3355-3366.
82. Dang B, Mravic M, Hu H, Schmidt N, Mensa B, DeGrado WF. SNAC-tag for sequence-specific chemical protein cleavage. *Nat. Methods.* 2019; 16: 319-322.

83. Komander D, Rape M. The Ubiquitin Code. *Annu. Rev. Biochem.* 2012; 81: 203-229.
84. Yang R, Hou W, Zhang X, Liu C-F. N-to-C Sequential Ligation Using Peptidyl N,N-Bis(2-mercaptoethyl)amide Building Blocks. *Org. Lett.* 2012; 14: 374-377.
85. Moyal T, Hemantha HP, Siman P, Refua M, Brik A. Highly efficient one-pot ligation and desulfurization. *Chem. Sci.* 2013; 4: 2496-2501.
86. Neumann K, Farnung J, Baldauf S, Bode JW. Prevention of aspartimide formation during peptide synthesis using cyanosulfonylides as carboxylic acid-protecting groups. *Nat. Commun.* 2020; 11: 982.
87. Flood DT, Hintzen JCJ, Bird MJ, Cistrone PA, Chen JS, Dawson PE. Leveraging the Knorr Pyrazole Synthesis for the Facile Generation of Thioester Surrogates for use in Native Chemical Ligation. *Angew. Chem. Int. Ed.* 2018; 57: 11634-11639.
88. Kim S, Nam HY, Lee J, Seo J. Mitochondrion-Targeting Peptides and Peptidomimetics: Recent Progress and Design Principles. *Biochemistry.* 2020; 59: 270-284.
89. Law B, Quinti L, Choi Y, Weissleder R, Tung CH. A mitochondrial targeted fusion peptide exhibits remarkable cytotoxicity. *Mol. Cancer Ther.* 2006; 5: 1944-1949.
90. Singh R, Letai A, Sarosiek K. Regulation of apoptosis in health and disease: the balancing act of BCL-2 family proteins. *Nat. Rev. Mol. Cell Biol.* 2019; 20: 175-193.
91. Lopez J, Tait SWG. Mitochondrial apoptosis: killing cancer using the enemy within. *Br. J. Cancer.* 2015; 112: 957-962.
92. Jung HK, Kim S, Park RW, Park JY, Kim IS, Lee B. Bladder tumor-targeted delivery of pro-apoptotic peptide for cancer therapy. *J. Controlled Release.* 2016; 235: 259-267.
93. Qiao Z-Y, Lai W-J, Lin Y-X, Li D, Nan X-H, Wang Y, Wang H, Fang Q-J. Polymer-KLAK Peptide Conjugates Induce Cancer Cell Death through Synergistic Effects of Mitochondria Damage and Autophagy Blockage. *Bioconj. Chem.* 2017; 28: 1709-1721.
94. Smolarczyk R, Cichoń T, Graja K, Hucz J, Sochanik A, Szala S. Antitumor effect of RGD-4C-GG-D(KLAKLAK)₂ peptide in mouse B16(F10) melanoma model. *Acta Biochim. Pol.* 2006; 53: 801-805.
95. Mai JC, Mi Z, Kim SH, Ng B, Robbins PD. A proapoptotic peptide for the treatment of solid tumors. *Cancer Res.* 2001; 61: 7709-7712.
96. Kim HY, Kim S, Youn H, Chung J-K, Shin DH, Lee K. The cell penetrating ability of the proapoptotic peptide, KLAKLAKKLAKLAK fused to the N-terminal protein transduction domain of translationally controlled tumor protein, MIIYRDLISH. *Biomaterials.* 2011; 32: 5262-5268.
97. Chen W-H, Xu X-D, Luo G-F, Jia H-Z, Lei Q, Cheng S-X, Zhuo R-X, Zhang X-Z. Dual-Targeting Pro-apoptotic Peptide for Programmed Cancer Cell Death via Specific Mitochondria Damage. *Sci. Rep.* 2013; 3: 3468.
98. Kelkar SS, Reineke TM. Theranostics: Combining Imaging and Therapy. *Bioconj. Chem.* 2011; 22: 1879-1903.
99. Usama SM, Park GK, Nomura S, Baek Y, Choi HS, Burgess K. Role of Albumin in Accumulation and Persistence of Tumor-Seeking Cyanine Dyes. *Bioconj. Chem.* 2020; 31: 248-259.
100. Yang X, Shi C, Tong R, Qian W, Zhau HE, Wang R, Zhu G, Cheng J, Yang VW, Cheng T, Henary M, Strekowski L, Chung LW. Near IR heptamethine cyanine dye-mediated cancer imaging. *Clin. Cancer Res.* 2010; 16: 2833-2844.
101. Jiang Z, Pflug K, Usama SM, Kuai D, Yan X, Sitcheran R, Burgess K. Cyanine-Gemcitabine Conjugates as Targeted Theranostic Agents for Glioblastoma Tumor Cells. *J. Med. Chem.* 2019; 62: 9236-9245.
102. Kvach MV, Ustinov AV, Stepanova IA, Malakhov AD, Skorobogatyi MV, Shmanai VV, Korshun VA. A Convenient Synthesis of Cyanine Dyes: Reagents for the Labeling of Biomolecules. *Eur. J. Org. Chem.* 2008; 2008: 2107-2117.
103. Vanier GS. Microwave-assisted solid-phase peptide synthesis based on the Fmoc protecting group strategy (CEM). 2013/08/15 ed2013. 235-249 p.

104. Vaughan L, Glänzel W, Korch C, Capes-Davis A. Widespread Use of Misidentified Cell Line KB (HeLa): Incorrect Attribution and Its Impact Revealed through Mining the Scientific Literature. *Cancer Res.* 2017; 77: 2784-2788.
105. Zhang L, Hou S, Mao S, Wei D, Song X, Lu Y. Uptake of folate-conjugated albumin nanoparticles to the SKOV3 cells. *Int. J. Pharm.* 2004; 287: 155-162.
106. Xing L, Xu Y, Sun K, Wang H, Zhang F, Zhou Z, Zhang J, Zhang F, Caliskan B, Qiu Z, Wang M. Identification of a peptide for folate receptor alpha by phage display and its tumor targeting activity in ovary cancer xenograft. *Sci. Rep.* 2018; 8: 8426.
107. Elwood PC. Molecular cloning and characterization of the human folate-binding protein cDNA from placenta and malignant tissue culture (KB) cells. *J. Biol. Chem.* 1989; 264: 14893-14901.
108. Thakkar N, Lockhart AC, Lee W. Role of Organic Anion-Transporting Polypeptides (OATPs) in Cancer Therapy. *AAPS J.* 2015; 17: 535-545.
109. Shi C, Wu JB, Chu GC-Y, Li Q, Wang R, Zhang C, Zhang Y, Kim HL, Zhau HE, Pan D, Chung LWK. Heptamethine carbocyanine dye-mediated near-infrared imaging of canine and human cancers through the HIF-1 α /OATPs signaling axis. *Oncotarget.* 2014; 5: 10114-10126.
110. Xiao L, Zhang Y, Yue W, Xie X, Wang J-p, Chordia MD, Chung LWK, Pan D. Heptamethine cyanine based ⁶⁴Cu-PET probe PC-1001 for cancer imaging: Synthesis and in vivo evaluation. *Nucl. Med. Biol.* 2013; 40: 351-360.
111. Wu JB, Shao C, Li X, Shi C, Li Q, Hu P, Chen Y-T, Dou X, Sahu D, Li W, Harada H, Zhang Y, Wang R, Zhau HE, Chung LWK. Near-infrared fluorescence imaging of cancer mediated by tumor hypoxia and HIF1 α /OATPs signaling axis. *Biomaterials.* 2014; 35: 8175-8185.
112. Zhao N, Zhang C, Zhao Y, Bai B, An J, Zhang H, Wu JB, Shi C. Optical imaging of gastric cancer with near-infrared heptamethine carbocyanine fluorescence dyes. *Oncotarget.* 2016; 7: 57277-57289.
113. Yuan J, Yi X, Yan F, Wang F, Qin W, Wu G, Yang X, Shao C, Chung LW. Near-infrared fluorescence imaging of prostate cancer using heptamethine carbocyanine dyes. *Mol. Med. Report.* 2015; 11: 821-828.
114. Usama SM, Lin C-M, Burgess K. On the Mechanisms of Uptake of Tumor-Seeking Cyanine Dyes. *Bioconj. Chem.* 2018; 29: 3886-3895.
115. Horton KL, Pereira MP, Stewart KM, Fonseca SB, Kelley SO. Tuning the activity of mitochondria-penetrating peptides for delivery or disruption. *ChemBioChem.* 2012; 13: 476-485.
116. Chazotte B. Labeling Mitochondria with MitoTracker Dyes. *Cold Spring Harb. Protoc.* 2011; 2011: pdb.prot5648.
117. Latt SA, Stetten G, Juergens LA, Willard HF, Scher CD. Recent developments in the detection of deoxyribonucleic acid synthesis by 33258 Hoechst fluorescence. *J. Histochem. Cytochem.* 1975; 23: 493-505.
118. Vergel Galeano CF, Rivera Monroy ZJ, Rosas Pérez JE, García Castañeda JE. Efficient Synthesis of Peptides with 4-Methylpiperidine as Fmoc Removal Reagent by Solid Phase Synthesis. *J. Mex. Chem. Soc.* 2014; 58: 386-392.
119. Ducker GS, Rabinowitz JD. One-Carbon Metabolism in Health and Disease. *Cell Metab.* 2017; 25: 27-42.
120. Sabharanjak S, Mayor S. Folate receptor endocytosis and trafficking. *Adv. Drug Del. Rev.* 2004; 56: 1099-1109.
121. Nödling AR, Mills EM, Li X, Cardella D, Sayers EJ, Wu S-H, Jones AT, Luk LYP, Tsai Y-H. Cyanine dye mediated mitochondrial targeting enhances the anti-cancer activity of small-molecule cargoes. *Chem. Commun.* 2020; 4672-4675.
122. Aletras A, Barlos K, Gatos D, Koutsogianni S, Mamos P. Preparation of the very acid-sensitive Fmoc-Lys(Mtt)-OH. Application in the synthesis of side-chain to side-chain

cyclic peptides and oligolysine cores suitable for the solid-phase assembly of MAPs and TASP. *Int. J. Pept. Protein Res.* 1995; 45: 488-496.

123. Marverti G, Marraccini C, Martello A, D'Arca D, Pacifico S, Guerrini R, Spyraakis F, Gozzi G, Lauriola A, Santucci M, Cannazza G, Tagliazucchi L, Cazzato AS, Losi L, Ferrari S, Ponterini G, Costi MP. Folic Acid–Peptide Conjugates Combine Selective Cancer Cell Internalization with Thymidylate Synthase Dimer Interface Targeting. *J. Med. Chem.* 2021; 64: 3204-3221.

124. Kim WH, Kim CG, Kim MH, Kim D-W, Park CR, Park JY, Lee Y-S, Youn H, Kang KW, Jeong JM, Chung J-K. Preclinical evaluation of isostructural Tc-99m- and Re-188-folate-Gly-Gly-Cys-Glu for folate receptor-positive tumor targeting. *Ann. Nucl. Med.* 2016; 30: 369-379.

125. Leamon CP, Reddy JA, Vlahov IR, Westrick E, Dawson A, Dorton R, Vetzal M, Santhapuram HK, Wang Y. Preclinical Antitumor Activity of a Novel Folate-Targeted Dual Drug Conjugate. *Mol. Pharm.* 2007; 4: 659-667.

126. Dharmatti R, Miyatake H, Nandakumar A, Ueda M, Kobayashi K, Kiga D, Yamamura M, Ito Y. Enhancement of Binding Affinity of Folate to Its Receptor by Peptide Conjugation. *Int. J. Mol. Sci.* 2019; 20: 2152.

127. Leamon CP, Deprince RB, Hendren RW. Folate-mediated Drug Delivery: Effect of Alternative Conjugation Chemistry. *Journal of Drug Targeting.* 1999; 7: 157-169.

128. Wang S, Low PS. Folate-mediated targeting of antineoplastic drugs, imaging agents, and nucleic acids to cancer cells. *J. Controlled Release.* 1998; 53: 39-48.

129. Leamon CP, Low PS. Delivery of macromolecules into living cells: a method that exploits folate receptor endocytosis. *Proc. Natl. Acad. Sci. U. S. A.* 1991; 88: 5572-5576.

Chapter 7

Appendix

7.1 SPPS MW cycle and method descriptions of CEM Liberty Blue™ Automated Microwave Peptide Synthesizer

MW cycle 1

Temperature (°C)	Power (W)	Hold time (s)
25	0	300
50	35	600

MW cycle 2

Temperature (°C)	Power (W)	Hold time (s)
75	30	300

MW cycle 3

Temperature (°C)	Power (W)	Hold time (s)
25	0	5
80	115	20
86	70	10
90	30	120

MW cycle 4

Temperature (°C)	Power (W)	Hold time (s)
25	0	5
80	115	20
86	70	10
90	30	480

MW cycle 5

Temperature (°C)	Power (W)	Hold time (s)
25	0	120
50	35	600

MW cycle 6

Temperature (°C)	Power (W)	Hold time (s)
75	30	420

MW cycle 7

Temperature (°C)	Power (W)	Hold time (s)
50	30	30

MW cycle 8

Temperature (°C)	Power (W)	Hold time (s)
50	30	180

MW cycle 9

Temperature (°C)	Power (W)	Hold time (s)
25	0	300

MW cycle 10

Temperature (°C)	Power (W)	Hold time (s)
25	0	600

MW cycle 11

Temperature (°C)	Power (W)	Hold time (s)
20	0	5
78	100	20

88	60	10
-----------	----	----

MW cycle 12

Temperature (°C)	Power (W)	Hold time (s)
25	0	5
78	80	20
88	50	10
90	25	60

MW cycle 13

Temperature (°C)	Power (W)	Hold time (s)
50	60	270

Method 1

Step	Operation	Parameters	MW cycle
1	Wash	DMF volume: 4 mL	--
2	Deprotection (x2)	Deprotection cocktail volume: 2 mL	9+10
3	Wash (x4)	DMF volume: 4 mL	--
4	Coupling (x2)	AA volume: 1.5 mL, DIC volume: 1 mL, HOBt volume: 0.5 mL	5
5	Wash through synthesiser manifold	DMF volume: 4 mL	--

Method 2

Step	Operation	Parameters	MW cycle
1	Wash	DMF volume: 4 mL	--

2	Deprotection (x2)	Deprotection cocktail volume: 2 mL	9+10
3	Wash (x4)	DMF volume: 4 mL	--
4	Coupling	AA volume: 1.5 mL, DIC volume: 2 mL, HOBt volume: 1 mL	5
5	Wash through synthesiser manifold	DMF volume: 4 mL	--

Method 3

Step	Operation	Parameters	MW cycle
1	Wash	DMF volume: 4 mL	--
2	Deprotection (x2)	Deprotection cocktail volume: 2 mL	7+8
3	Wash (x4)	DMF volume: 4 mL	--
4	Coupling	AA volume: 1.5 mL, DIC volume: 2 mL, HOBt volume: 1 mL	5
5	Wash through synthesiser manifold	DMF volume: 4 mL	--

Method 4

Step	Operation	Parameters	MW cycle
1	Wash	DMF volume: 4 mL	--
2	Deprotection (x2)	Deprotection cocktail volume: 2 mL	7+8
3	Wash (x4)	DMF volume: 4 mL	--
4	Coupling (x2)	AA volume: 1.5 mL, DIC volume: 1 mL, HOBt volume: 0.5 mL	5
5	Wash through synthesiser manifold	DMF volume: 4 mL	--

Method 5

Step	Operation	Parameters	MW cycle
1	Wash	DMF volume: 4 mL	--
2	Coupling (x2)	AA volume: 1.5 mL, DIC volume: 1 mL, HOBt volume: 0.5 mL	5
3	Wash through synthesiser manifold	DMF volume: 4 mL	--

Method 6

Step	Operation	Parameters	MW cycle
1	Deprotection	Deprotection cocktail volume: 2 mL	12
3	Wash (x4)	DMF volume: 4 mL	
4	Coupling	AA volume: 2.5 mL, DIC volume: 2 mL, Oxyma pure volume: 0.5 mL	3
5	Wash through synthesiser manifold	DMF volume: 4 mL	

Method 7

Step	Operation	Parameters	MW cycle
1	Deprotection	Deprotection cocktail volume: 2 mL	12
3	Wash (x4)	DMF volume: 4 mL	
4	Coupling	AA volume: 2.5 mL, DIC volume: 2 mL, Oxyma pure volume: 0.5 mL	1
5	Wash through synthesiser manifold	DMF volume: 4 mL	

Method 8

Step	Operation	Parameters	MW cycle
------	-----------	------------	----------

1	Wash	DMF volume: 4 mL	--
2	Deprotection (x2)	Deprotection cocktail volume: 2 mL	9+10
3	Wash (x4)	DMF volume: 4 mL	--
4	Coupling (x2)	AA volume: 0.75 mL, HATU volume: 0.5 mL, DIPEA volume: 0.25 mL	6
5	Wash through synthesiser manifold	DMF volume: 4 mL	--

Method 9

Step	Operation	Parameters	MW cycle
1	Wash	DMF volume: 4 mL	--
2	Deprotection (x2)	Deprotection cocktail volume: 2 mL	9+10
3	Wash (x4)	DMF volume: 4 mL	--
4	Coupling (x3)	AA volume: 0.75 mL, HATU volume: 0.5 mL, DIPEA volume: 0.25 mL	6
5	Wash through synthesiser manifold	DMF volume: 4 mL	--

Method 10

Step	Operation	Parameters	MW cycle
1	Wash	DMF volume: 4 mL	--
2	Deprotection (x2)	Deprotection cocktail volume: 2 mL	9+10
3	Wash (x4)	DMF volume: 4 mL	--
4	Coupling (x3)	AA volume: 1.5 mL, HATU volume: 1 mL, DIPEA volume: 0.5 mL	6
5	Wash through synthesiser manifold	DMF volume: 4 mL	--

Method 11

Step	Operation	Parameters	MW cycle
1	Wash	DMF volume: 4 mL	--
2	Deprotection (x2)	Deprotection cocktail volume: 2 mL	9+10
3	Wash (x4)	DMF volume: 4 mL	--
4	Coupling	AA volume: 1.5 mL, HATU volume: 1 mL, DIPEA volume: 0.5 mL	6
5	Wash through synthesiser manifold	DMF volume: 4 mL	--

Method 12

Step	Operation	Parameters	MW cycle
1	Wash	DMF volume: 4 mL	--
2	Deprotection (x2)	Deprotection cocktail volume: 2 mL	11
3	Wash (x4)	DMF volume: 4 mL	--
4	Coupling (x2)	AA volume: 0.75 mL, HATU volume: 0.5 mL, DIPEA volume: 0.25 mL	6
5	Wash through synthesiser manifold	DMF volume: 4 mL	--

Method 13

Step	Operation	Parameters	MW cycle
1	Wash	DMF volume: 4 mL	--
2	Deprotection (x2)	Deprotection cocktail volume: 2 mL	11
3	Wash (x4)	DMF volume: 4 mL	--
4	Coupling	AA volume: 1.5 mL, HATU volume: 1 mL, DIPEA volume: 0.5 mL	6

5	Wash through synthesiser manifold	DMF volume: 4 mL	--
----------	-----------------------------------	------------------	----

Method 14

Step	Operation	Parameters	MW cycle
1	Deprotection (x2)	Deprotection cocktail volume: 2 mL	11
2	Wash (x4)	DMF volume: 4 mL	--
3	Coupling	AA volume: 1 mL, HATU volume: 0.2 mL, DIPEA volume: 0.25 mL	4
4	Wash through synthesiser manifold	DMF volume: 4 mL	--

Method 15

Step	Operation	Parameters	MW cycle
1	Deprotection (x2)	Deprotection cocktail volume: 2 mL	9+10
2	Wash (x4)	DMF volume: 4 mL	--
3	Coupling (x3)	AA volume: 1 mL, HATU volume: 0.15 mL, DIPEA volume: 0.25 mL, DMF volume: 2 mL	6
4	Wash through synthesiser manifold	DMF volume: 4 mL	--

Method 16

Step	Operation	Parameters	MW cycle
1	Wash	DMF volume: 4 mL	--
2	Deprotection (x2)	Deprotection cocktail volume: 2 mL	7+8
3	Wash (x4)	DMF volume: 4 mL	--

4	Coupling (x2)	AA volume: 0.75 mL, HATU volume: 0.5 mL, DIPEA volume: 0.25 mL	5
5	Wash through synthesiser manifold	DMF volume: 4 mL	--

Method 17

Step	Operation	Parameters	MW cycle
1	Wash	DMF volume: 4 mL	--
2	Deprotection (x2)	Deprotection cocktail volume: 2 mL	7+8
3	Wash (x4)	DMF volume: 4 mL	--
4	Coupling	AA volume: 0.75 mL, HATU volume: 0.5 mL, DIPEA volume: 0.25 mL	5
5	Wash through synthesiser manifold	DMF volume: 4 mL	--

Method 18

Step	Operation	Parameters	MW cycle
1	Wash	DMF volume: 4 mL	--
2	Deprotection (x2)	Deprotection cocktail volume: 2 mL	9+10
3	Wash (x4)	DMF volume: 4 mL	--
4	Coupling	AA volume: 0.75 mL, HATU volume: 0.5 mL, DIPEA volume: 0.25 mL	5
5	Wash through synthesiser manifold	DMF volume: 4 mL	--

Method 19

Step	Operation	Parameters	MW cycle
-------------	------------------	-------------------	---------------------

1	Wash	DMF volume: 4 mL	--
2	Deprotection (x2)	Deprotection cocktail volume: 2 mL	9+10
3	Wash (x4)	DMF volume: 4 mL	--
4	Coupling (x2)	AA volume: 0.75 mL, HATU volume: 0.5 mL, DIPEA volume: 0.25 mL	5
5	Wash through synthesiser manifold	DMF volume: 4 mL	--

Method 20

Step	Operation	Parameters	MW cycle
1	Wash	DMF volume: 4 mL	--
2	Deprotection (x2)	Deprotection cocktail volume: 2 mL	12
3	Wash (x4)	DMF volume: 4 mL	--
4	Coupling (x2)	AA volume: 0.75 mL, HATU volume: 0.5 mL, DIPEA volume: 0.25 mL	5
5	Wash through synthesiser manifold	DMF volume: 4 mL	--

Method 21

Step	Operation	Parameters	MW cycle
1	Wash	DMF volume: 4 mL	--
2	Deprotection (x2)	Deprotection cocktail volume: 2 mL	11
3	Wash (x4)	DMF volume: 4 mL	--
4	Coupling	AA volume: 0.75 mL, HATU volume: 0.5 mL, DIPEA volume: 0.25 mL	5
5	Wash through synthesiser manifold	DMF volume: 4 mL	--

Method 22

Step	Operation	Parameters	MW cycle
1	Wash	DMF volume: 4 mL	--
2	Deprotection (x2)	Deprotection cocktail volume: 2 mL	11
3	Wash (x4)	DMF volume: 4 mL	--
4	Coupling (x2)	AA volume: 0.75 mL, DIC volume: 0.5 mL, HOBt volume: 0.25 mL	3
5	Wash through synthesiser manifold	DMF volume: 4 mL	--

Method 23

Step	Operation	Parameters	MW cycle
1	Wash	DMF volume: 4 mL	--
2	Deprotection (x2)	Deprotection cocktail volume: 2 mL	7+8
3	Wash (x4)	DMF volume: 4 mL	--
4	Coupling	AA volume: 1.5 mL, DIC volume: 1 mL, HOBt volume: 0.5 mL	3
5	Wash through synthesiser manifold	DMF volume: 4 mL	--

Method 24

Step	Operation	Parameters	MW cycle
1	Wash	DMF volume: 4 mL	--
2	Deprotection (x2)	Deprotection cocktail volume: 2 mL	7+8
3	Wash (x4)	DMF volume: 4 mL	--
4	Coupling (x2)	AA volume: 0.75 mL, DIC volume: 0.5 mL, HOBt volume: 0.25 mL	3

5	Wash through synthesiser manifold	DMF volume: 4 mL	--
---	-----------------------------------	------------------	----

7.2 Publications in peer-reviewed journals

Effect of Trimethine Cyanine Dye- and Folate-Conjugation on the In Vitro Biological Activity of Proapoptotic Peptides

D. Cardella, L. Y. P. Luk, and Y.-H. Tsai, ***Biomolecules***, 2022, 12, 725. DOI: 10.3390/biom12050725

Cyanine dye mediated mitochondrial targeting enhanced the anti-cancer activity of small-molecule cargos

A. R. Nödling, E. M. Mills, X. Li, **D. Cardella**, E. J. Sayers, S.-H. Wu, A. T. Jones, L. Y. P. Luk, and Y.-H. Tsai, ***Chem. Commun.***, 2020, 56, 4672-4675. DOI: 10.1039/C9CC07931A

Use of an Asparaginyl Endopeptidase for Chemo-enzymatic Peptide and Protein Labeling

S. T. M. Tang, **D. Cardella**, A. Lander, X. Li, J. Sánchez; Y.-H. Tsai, L. Y. P. Luk, ***Chem. Sci.***, 2020, 11, 5881-5888. DOI: 10.1039/D0SC02023K